METHODS FOR IDENTIFYING SUBCELLULAR TARGETING LIGANDS AND SELECTED APPLICATIONS

APPROVED BY SUPERVISORY COMMITTEE

Kathlynn Brown, Ph.D. (Mentor)

Joseph Albanesi, Ph.D. (Chairman)

Sandra Schmid, Ph.D.

Jennifer Kohler, Ph.D.

DEDICATION

I would like to thank the members of my Graduate Committee, my family, and laboratory co-workers without whom this work would not be possible.

METHODS FOR IDENTIFYING SUBCELLULAR TARGETING LIGANDS AND SELECTED APPLICATIONS

by

BENJAMIN J. UMLAUF

DISSERTATION

Presented to the Faculty of the Graduate School of Biomedical Sciences

The University of Texas Southwestern Medical Center at Dallas

In Partial Fulfillment of the Requirements

For the Degree of

DOCTOR OF PHILOSOPHY

The University of Texas Southwestern Medical Center at Dallas

Dallas, Texas

December, 2015

METHODS FOR IDENTIFYING SUBCELLULAR TARGETING LIGANDS AND SELECTED APPLICATIONS

Benjamin J. Umlauf

The University of Texas Southwestern Medical Center at Dallas, 2015

Supervising Professor: Kathlynn C. Brown, Ph.D.

Subcellular localization plays an essential role in targeting drug therapies as generally the pro-drug or linker relies on physical conditions of a particular subcellular compartment to function. We developed two methods that allow for selecting targeting ligands that both internalize specifically in cancer cells as well as accumulate in a defined subcellular location. The first method utilizes endocytic selection pressure to identify targeting peptides from a phage displayed peptide library that internalize specifically in cancer cells via a defined mechanism of endocytosis while the second couples together a traditional biopanning selection protocol with a secondary immunofluorescent screen to directly identify functional

targeting peptides. In addition we also present a method for reducing amplification bias during phage display experiments. Finally, we demonstrate the utility of a novel peptide, termed H1299.3 selected via the endocytic pressure method, to serve as targeting ligand for a novel immunotherapy. H1299.3 targeted liposomes facilitate delivery of antigenic peptide specifically in MHC class 1 molecules of cancer cells resulting in activation of secondary immune response against the cancer cells. Thus, we present two novel methods for identify targeting ligands with selective internalization that accumulate in defined subcellular localizations as well as a novel application for a newly identified targeting ligand.

TABLE OF CONTENTS

PRIOR PUBLICATIONS

Umlauf BJ, Chung CY, Brown KC. Modular Three-Component Delivery System Facilitates HLA Class I Antigen Presentation and CD8+ T cell Activation Against Tumors. Mol Ther. 2015 Jun;23(6):1092-102

Umlauf BJ, McGuire MJ, Brown KC. Introduction of plasmid encoding for rare tRNAs reduces amplification bias in phage display biopanning. Biotechniques. 2015 Feb 1;58(2):81-4.

Umlauf BJ, Mercedes JS, Chung CY, Brown KC. Identification of a Novel Lysosomal Trafficking Peptide using Phage Display Biopanning Coupled with Endocytic Selection Pressure. Bioconjug Chem. 2014 Oct 15;25(10):1829-37.

Umlauf BJ, Haralambieva IH, Ovsyannikova IG, Kennedy RB, Pankratz VS, Jacobson RM, Poland GA: Associations between Demographic Variables and Multiple Measles-Specific Innate and Cell-Mediated Immune Responses Following Measles Vaccination, Viral Immunol. 2012 Feb;25(1):29-36

Umlauf BJ, Pinsky NP, Ovsyannikova IG, Poland GA: Detection of vaccinia virus-specific IFNγ and IL-10 secretion from human PBMCs and $CD8^+$ T cells by ELISPOT, Methods Mol Biol. 2012;792:199-218.

Haralambieva IH, Ovsyannikova IG, **Umlauf BJ**, Vierkant RA, Shane Pankratz V, Jacobson RM, Poland GA: Genetic polymorphisms in host antiviral genes: Associations with humoral and cellular immunity to measles vaccine, Vaccine. 2011 Nov 8;29(48):8988-97.

Umlauf BJ, Ovsyannikova IG, Haralambieva IH, Kennedy RB, Vierkant RA, Pankratz VS, Jacobson RM, Poland GA: Correlations between vaccinia-specific immune responses within a cohort of armed forces members, Viral Immunol. 2011 Oct;24(5):415-20.

LIST OF FIGURES

LIST OF TABLES

LIST OF ABBREVIATIONS

NSCLC – Non-Small Cell Lung Cancer

rpHPLC – reverse phase High Pressure Liquid Chromatography

MALDI TOF – Matrix-Assisted Laser Desorption Ionization, Time Of Flight

CHC – Clathrin Heavy Chain

SA-PE – Streptavidin Phycoerythrin

Ab – Antibody

GFP – Green Fluorescent Protein

HBEC – Human Bronchial Epithelial Cells

AFU – Arbitrary Fluorescence Units

BMPH – N-β-maleimidopropionic acid hydrazide

CM – Cell Mediated

HLA – Human Leukocyte Antigen

MHC – Major Histocompatibility Complex

PBMC – Peripheral Blood Mononuclear Cell

APC – Antigen Presenting Cell

ELISA – Enzyme Linked Immunosorbant Assay

mAb – Monoclonal Antibody

EPR – Enhanced Permeability and Retention

AST – Aspartate Aminotransferase

ALT – Alanine Aminotransferase

ECM – Extra-Cellular Matrix

CHAPTER ONE
Introduction

Subcellular Localization of Targeting Ligands

Subcellular localization of targeting ligands is emerging as a key feature in the successful design of a pro-drug based therapy.[33,96,120,130,141,165] For the terms of this study subcellular localization refers to the accumulation pattern of a given targeting ligand post-internalization into a cell. Generally this is quantified using either co-localization of the targeting ligand with a given organelle marker or by indirect measurement of the physical properties associated with a given organelle.[12,35,56,137,167] For example, co-localization with cytosolic marker would indicate accumulation in the cytosol, or conjugation of an oxidative sensor to determine exposure to reducing environment of the cytosol both provide an indication of subcellular localization of the targeting ligand.

The subcellular localization of a targeting ligand is an important feature of the targeting ligand because it mediates exposure of the conjugate to physical properties and organelles. Exposure to unique physical properties underlies the entire theory of targeting ligand directed pro-drugs (Figure 1). In this class of pro-drug, the drug is inactivated by conjugation of a targeting ligand to the drug via a linker. The linker or drug is then inactive during circulation; however, when the linker or drug is exposed to certain physical environments the linker is cleaved or the drug becomes active.[83,139,156] Thus, if the targeted pro-drug does not encounter this environment it remains inactive and the treatment exhibits

reduced efficacy. Knowledge of the subcellular accumulation patterns of a targeting ligand may mitigate this problem as well as allow for rational design of pro-drug conjugates.

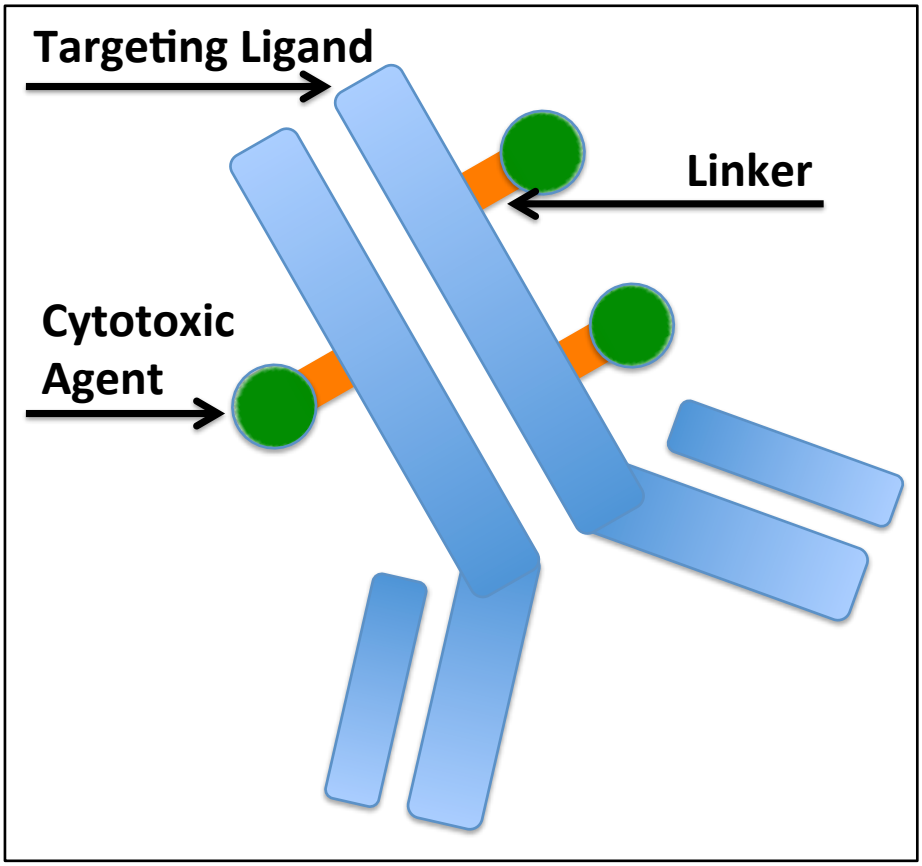

Figure 1. Three component Targeted Drug Conjugate. *Modified from Genetech.* The standard targeted drug conjugate consists of three components: 1. Targeting Ligand which is pictured as an antibody 2. Linker to link the cytotoxic agent to the antibody 3. Cytotoxic Agent to destroy cells that internalize the targeting ligand

Targeted Drug Conjugates

One class of pro-drugs are targeted drug conjugates. This class of pro-drug generally consists of three components: 1. targeting ligand, 2. linker, and 3. drug (Figure 1).[18,43,66,89,111,120]

1. Targeting Ligand – The targeting ligand has two functions for this class of drug. The first function is to restrict the activity of the drug.[66,70,89,111,122,139] By restricting the activity, the targeting ligand alters the functionality of the drug with the attempt to reduce adverse events associated with the drug. For example, conjugation of a targeting ligand to doxorubicin negates the cell permeability property of this drug.[9,25,31,38,67,89,120,166] Thus the functionality of doxorubicin is substantially reduced because it can no longer freely diffuse through cells to intercalate DNA and induce cytotoxicity. The second function of the targeting ligand is to alter the therapeutic window of the drug.[9,38,72,90,133,136] This is accomplished through targeting aspect of the ligand. By selectively binding to and/or internalizing into a subset of cells the therapeutic window is altered relative to the subset of targeted cells. Again using doxorubicin as an example, selective binding and internalization into cancer cells allows for increased cytotoxicity in the cancer cells compared to endothelial and clearance organ cytotoxicity.[8,55,67,73,107]

Targeting ligands can take many forms. Three common examples include antibodies, aptamers, and peptides. Antibodies are the most commonly utilized targeting ligand.[5,8,66,70,89,111,122,129,133] Antibodies demonstrate high specificity and affinity toward a cellular receptor and have previously been demonstrated to distinguish between diseased and normal tissue.[2,8,9,19,25,26,38,69,78,89,112,113,120] Further, multiple means of selection and generation

of cell and tissue specific antibodies exist making this class of molecules attractive as targeting ligands. In addition, recent widespread acceptance of antibodies by the FDA for treatment of a variety of disease states allows for easy transfer of these approved ligands into drug conjugate applications.[9,75,90,136,159] Finally, chemical studies of linkers have resulted in the development of linkers that allow for conjugation of antibodies to a wide range of cargo from small molecules to liposomes.[8,31,55,73,107,166] In addition second generation traceless linkers have been developed for conjugation of antibodies to biological cargo including cytokines as well as traditional small molecules. [8,15,30,34,44,78,82,89,159] Currently there are 3 FDA approved antibody drug conjugates (ADC), Brentuximab vedotin for treatment of relapsed Hodgkin Lymphoma and relapsed systemic anaplastic large cell lymphoma (Seattle Genetics), Trastuzumab emtansine for treatment of HER2-positive metastatic breast cancer (Genentech and Roche), and Gemtuzumab ozogamicin for treatment of acute myelogenous leukemia (Pfizer/Wyeth). However, Gemtuzumab ozogamicin was removed from the market in 2010 despite being the first approved ADC. Currently there are more than 30 ADC in differing stages of clinical trials.

Antibodies are the most widely utilized targeting moiety for a wide number of reasons. Particularly antibodies have gained wide clinical acceptance, they have excellent PK and PD properties, and exhibit naturally high affinity for binding partners. However, in comparison to aptamers and peptides they cannot be synthesized using synthetic methods, are more difficult to modify using chemical and biochemical techniques, and post translational modifications that occur during antibody manufacture can effect efficacy and adverse events profile associated with antibody treatment.

Aptamers are a nucleic acid based targeting ligand in which the secondary structure of a nucleic acid sequence provides specific binding to a cellular receptor.[8,15,44,82,137,155,156] Aptamers are commonly identified utilizing the SELEX method that involves iterative rounds of binding to a target, washing, elution, and amplification.[24,33,39,125,126,130,141,162,165] Aptamers can bind and discriminate between a large variety of targets including dyes, proteins, inorganic compounds, and whole cells similar to peptide or antibody ligands.[35,71,72,99,121,137,167] Also similar to other targeting ligands aptamers can mediate targeting of a large range of cargos including small molecules, liposomes, and other nanoparticles.[14,156] An interesting application for aptamers involves generating chimeric aptamers containing a targeting region and RNAi silencing region.[18,43,83] As both regions are derived from nucleic acid this approach allows for rapid synthesis and manufacture of drug conjugate.

Aptamers are made of both DNA or RNA; however, RNA apatmers are difficult to synthesize and are more sensitive to degradation than other targeting ligands. Also, in comparison to antibodies and peptides, aptamers require a unique binding pocket for recognition as the secondary structure of the nucleic acid is utilized for generating specificity rather than using the unique chemical properties of amino acid sequence to generate specificity. Additionally aptamers often exhibit poorer PK and PD properties compared to antibodies as nucleic acid is quickly degraded in serum. Incorporation of un-natural nucleic acids is often used to mitigate this issue.

Finally, peptides are the final type of targeting ligand discussed in this manuscript. Previous studies from our group and others demonstrate peptides ranging from 5-20 amino acids display the ability to bind specifically to unique cellular populations and proteins.

[9,24,39,77,96,107,111,112,118,125,126,133,162] In addition, multimerization of targeting peptides results in similar affinities to antibodies (pM-nM affinity).[67,71,72,99,121] Peptides can be selected against whole cells, tissues, or purified proteins using a variety of section and screening methods. Thus, peptide targeting ligands display similar benefits to using antibody targeting ligands but can be manufactured synthetically in high quantities and yields.[14,30,55,60,70,139] In addition, chemical synthesis allows for ease of conjugation through selected motifs. Cysteine or Lysine can be incorporated into the synthesis to allow for thiol and amine conjugation strategies, including conjugation through traceless linkers. In addition amino acids and PEG (Polyethylene Glycol) based spacers are readily incorporated during targeting ligand synthesis to allow for freedom of the targeting ligand to interact with the receptor without steric hindrance of the cargo. Peptides do not have as desirable PK and PD properties as antibodies but incorporation of non-natural amino acids or capping of peptides enhances serum stability and overall serum half-life. Additionally, conjugation of peptides to larger entities allows peptides to evade initial clearance by the renal system further extending half-life. Synthetic synthesis, ease of modification, and high affinity make peptides a desirable choice for use as a targeting ligand.

2. Linkers – The second component of a typical drug conjugate is the linker region. As the name implies the linker serves to link the targeting ligand to the drug.[9,61,77,83,103,118,119,132,158,161] Large amounts of work and effort have gone into identification and characterization of linkers suitable for use as drug conjugates. The first generation of linkers utilized non-cleavable linkers.[5,8,34,111,120,122,129,133] The targeting ligand is covalently

bound to the drug to prevent separation of the drug from the targeting ligand. While this strategy successfully accomplished the goal of reducing adverse events associated with a treatment, this strategy was only effective with a small number of conjugates. This is thought to be due to the inability of active drug to be released from the targeting ligand. In a qualitative sense the drug is effectively limited to the accumulation pattern of the targeting ligand such that the ligand must accumulate at the site of drug action for these conjugates to be effective. However, second generation linkers have emerged that attempt to address this problem.[2,8,19,26,60,64,69,75,78,89,112,113,127] The first method developed to address this problem employs a labile linker that is stable in serum but is cleaved upon exposure to selective physical properties.[75,89,158,159] Two of the best known examples of this class of linkers are protease sensitive linkers, such as cathepsin B cleavage linkers, and acid labile linkers, such as linkages which degrade upon exposure to low pH[31,48,81,107,108,131,160,166]Interestingly, both of these strategies depend on internalization into a cell as well as trafficking to a lysosome where the conjugate is exposed to cathepsin B or low pH environment. Finally, in addition to liable linkers, chemical modification of the drug with traceless linkers, which leave the drug in its unaltered state following degradation of the linker, have also enhanced the efficacy and release properties of second generation linkers.[30,34,65,78,89,119,159] Figure 2 outlines several major types of cleavable linkers and defines two traceless, self-immolative release strategies, Electronic cascade linker and Cyclization linker.

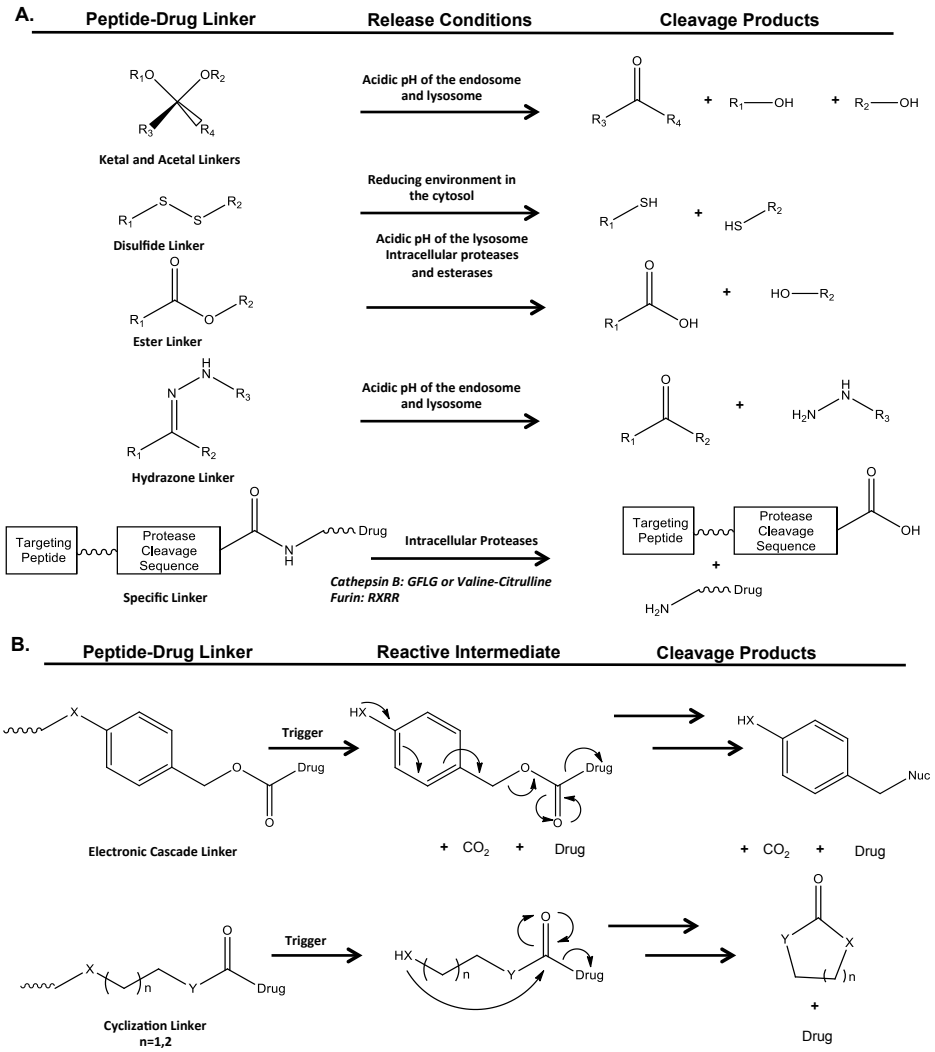

Figure 2. Schematic of Second Generation Targeted Direct Conjugate Linkers. A) Schematic outlining different types of cleavable linker, release conditions required for linker cleavage, and the cleavage products. **B)** Schematic of self-immolative linkers utilized for traceless release of drug from linker moiety

3. Drugs – The final component of a drug conjugate is the drug itself. In theory, any class of drug may be useful in a drug conjugate. A literature search demonstrates that everything from standard of care chemotherapeutics to small plant toxins have been utilized as the drug component in a drug conjugate strategy.[9,77,96,106,107,111,112,118,133] However, several common trends are emerging relative to drugs utilized in drug conjugates. The first trend is to utilize drugs that have undesirable adverse events associated with systemic administration. A classic example of this is doxorubicin. Given as free drug, doxorubicin is associated with cardiotoxicity however upon conjugation with targeting ligands, the adverse events profile at the same dose shifts from cardiac death to a rash on the palms and feet.[1,6,14,22,47,53,67,87,95,100,102,125,126,164] Similarly, drugs that are too toxic for systemic administration such as Auristatin E are widely used, as conjugation of the targeting ligand prevents systemic toxicity while the low ratio of free drug to cytotoxicity minimizes need for 100% release of drug to observe clinical benefit.[30,55,60,62,70,74,95,116,139] The final class of drugs widely utilized in drug conjugates are non-cell permeable toxins that require internalization for cytotoxic effect.[9,14,61,77,87,103,118,119,132,158,161] For example, the plant toxin Gelonin is non-cell permeable if the signal sequence is removed, therefore only cells that internalize the entire conjugate are killed. The type of drug utilized in the conjugate should be paired with the targeting ligand to observe maximal efficacy. For example, utilizing a lysosomal trafficking targeting ligand with Gelonin may result in degradation of the toxin before it can function. Thus, the drug selection as well as the linker selection could be guided by subcellular trafficking patterns of the targeting ligand to rationally design drug conjugates.

The three part drug conjugate is a simple tool that can be applied in many applications to create a diverse number of therapies. However, while large amounts of effort have gone into development of linkers and optimization of drugs for drug conjugate strategies relatively less effort has gone into developing targeting ligands. In fact all approved drug conjugates utilize only three targeting ligands.[22,24,28,34,41,47,89,100,111,120,126-128,154] Thus this proposal focuses on development of methods and targeting ligands which preferentially accumulate in a given cell subset and traffic to defined subcellular locations to expand the number of targeting ligands suitable for drug conjugate strategies.

Role of Receptor-Mediated Endocytosis in Drug Conjugates

As outlined above most second generation drug conjugates rely on some type of change in physical properties to activate the drug. One simple method is to generate a labile linker that is sensitive to changes in physical properties that occur during endocytosis of the conjugate. This strategy is attractive because of the dramatic change in physical conditions that occur during endocytosis such as reduction in pH.[39,60,64,75,89,127] In addition by utilizing endocytosis as a trigger for activation, the drug is then theoretically only released intracellularly in a targeted cell population thereby potentially widening the therapeutic window of the drug by preventing systemic circulation of free drug.[6,47,89,102,158] This then begs the question of how should the conjugate enter the cell in order to achieve maximum therapeutic benefit. Due to the size of drug conjugates two methods are widely utilized. The first is a classical receptor-mediated endocytosis strategy. [14,48,81,108,131,160] In this strategy, a targeting ligand first binds to a receptor on the target cell. Binding either triggers internalization of the receptor as well as

the drug conjugate bound to it, or the receptor is constitutively recycled and the conjugate is internalized when the receptor is internalized back into the cell, independent of whether a drug conjugate is bound. Alternatively, cell penetrating ligands may be used to drive internalization of the conjugate into cells. Cell penetrating ligands probably also utilize a receptor mediated strategy but for purposes of this manuscript we consider them separately as these ligands internalize indiscriminately into multiple cellular populations. These ligands are widely studied, with the hallmark being the Tat peptide derived from HIV. Tat and other highly charged ligands mediate internalization into a cell via a non-specific manner.[65,106,119] While these ligands do allow for exposure of the conjugate to a variety intracellular compartment using for example the iPhage system which allows for selection of Tat fused targeting peptides that accumulate in a desired organelle, it is doubtful whether these targeting ligands widen the therapeutic window of the drug conjugate.[106,108] In particular for small molecule application where the drug is cell permeable in the non-conjugated state these ligands can alter the PK and PD of the drug but have little effect on the therapeutic window as these ligands demonstrate minimal preferential internalization into a given cell population. Thus, methods that identify targeting ligands that internalize via a receptor mediated fashion may offer addition benefit to cell permeable ligands as these ligands can both alter the PK and PD as well as widen the therapeutic window of the drug.

Utilizing Phage Display to identify targeting ligands

Phage display is a powerful technique that is often applied to the identification of targeting ligands.[1,6,14,22,47,50,53,56,87,92,95,100,102,125,126,147,157,164] In this method a targeting ligand is

genetically fused into a coat protein of a bacteriophage. The fusion construct generally contains variable regions that are used to create libraries of diverse targeting ligands displayed from the coat protein.[29,62,64,65,74,95,106,116,131,132,149] A typical phage display experiment starts by incubating the phage library with bait. Non-bound phage is removed and the phage that bind the bait are recovered and amplified. This process is repeated iteratively to enrich for phage displayed targeting ligands that bind to the bait. Finally, as the targeting ligand is genetically fused into the phage clone, individual clones are sequenced to generate punitive hits.[14,41,87,134,135,140] This powerful technique has been applied to a wide variety of targeting ligands including peptides, antibodies, and scaffold proteins.[22,24,28,40,41,47,86,89,100,121,126-128,154] This study will focus on utilizing phage display methods to identify targeting peptides.

In addition to supporting a wide range of targeting ligands, the bait utilized in phage display experiments is also highly adaptable.[39,120] Phage display can be performed on purified receptors, organic/inorganic compounds, whole cells, or tissues.[6,47,102,111] Whole cell panning or phage display biopanning is particularly powerful as this application is a non-biased selection in which multiple types of putative targeting ligands hits can be generated.[14,38,120] For example, both phage that bind to the surface of the cell or phage that internalize into the cell can be identified using this technique by simple modification of the selection pressures applied during the panning experiment (Figure 3). If the target cells are lysed and the intracellular fraction is amplified, the assay will identify phage (and targeting ligands) that internalize into cells. The studies presented in this manuscript utilize additional selection criteria such as inhibiting endocytosis to further select targeting ligands that display

desired properties such as selective accumulation as well as defined subcellular trafficking. Thus, phage display is a powerful tool to identify targeting ligands for use in drug conjugate applications.

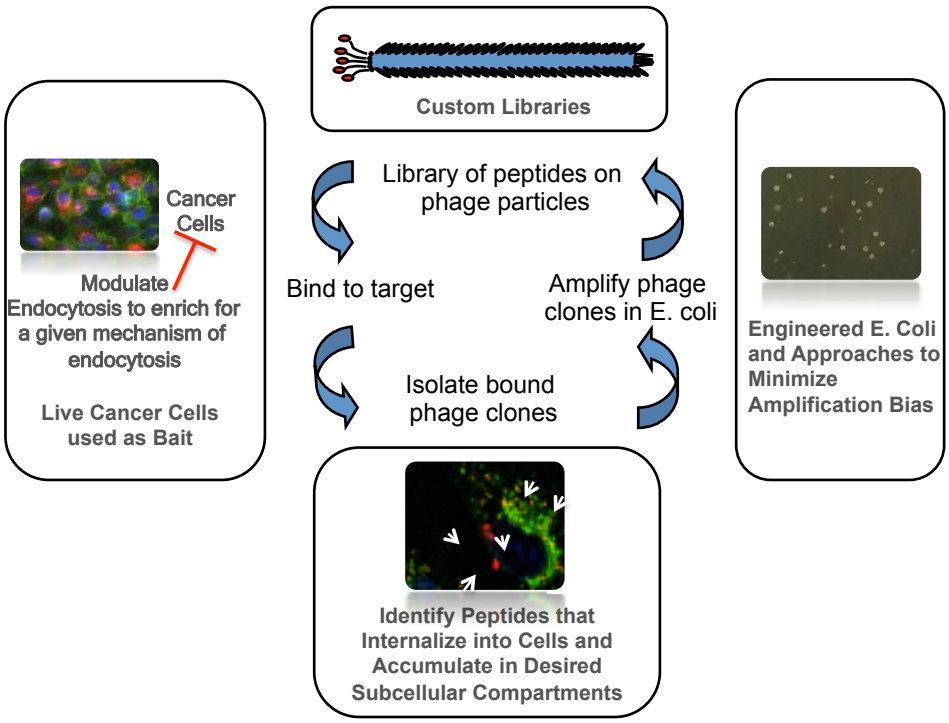

Figure 3. Diagram Outlining Phage Display Schemes Utilized in this Manuscript. M13 derived phage library displaying unique peptides on the pIII protein is incubated with live cancer cells. Chapter 2 describes methods to perturb the endocytic machinery of the bait cells to enrich for phage clones that internalize via a defined set of pathways. Bait cells are then subjected to differential washing to isolate the desired phage population. In experiments presented in chapter 3 we describe selection of phage that accumulate in a desired subcellular location. Recovered phage are then incubated with E. coli and amplified. Chapter 4 describes a method to reduce amplification bias during this step. Amplified phage are then purified and used for the next round of panning. 5 rounds of panning are generally performed. Phage are sequenced starting in round 3 to identify hits.

An alternative to this approach is utilizing the iPhage system developed by Pasqualini et al. that utilizes a cell penetrating ligand genetically encoded into the pVIII protein of M13 and a random library displayed on the pIII coat protein.[106,111] Thus, the M13 phage readily penetrates the cellular membrane then accumulates in a subcellular location based on the ligand displayed on the pIII protein. This system was originally designed as an alternative to two-hybrid systems to identify intracellular receptors, however it is now being utilized to identify targeting ligands that accumulate in a desired subcellular location. This presents a particular conundrum when translating these ligands to in vivo applications as the ligand demonstrates no-selectivity for cell type accumulation. So while this approach works for in vitro identification peptides that accumulate in a desired subcellular accumulation it has been difficult to translate these ligands into pharmacological applications in comparison to the non-cell penetrating ligands identified using the methods outlined above.

Alternative Methods for Controlling Subcellular Localization

Targeting ligands offer a powerful tool to identify a single motif that can both preferentially internalize into cellular population as well as accumulate in a defined cellular location, but targeting ligands represents only one strategy for controlling subcellular localization of drug. Data indicate that shape and size of drug delivery vehicle can affect the subcellular accumulation.[14,39,108] Further signaling and functional peptides can be fused to a targeting ligand to alter the subcellular acclamation of the drug. For example, addition of a Nuclear Localization Sequence or ER retention sequence (KDEL) may dramatically alter the subcellular localization of the targeting sequence. [50,56,92,131,147,157] Finally addition of

endosomal bursting peptides or Tat peptides may alter the subcellular localization of the drug by allowing access to the cytosol. [29,38,64,65,106,111,131,132,149] Thus, while direct selection of targeting ligands that accumulate in a defined subcellular location is preferable from a manufacturing and synthesis standpoint, modification to the delivery vehicle is an alternative strategy that maybe useful to alter the subcellular trafficking patterns of the drug conjugate.

Subcellular Targeting Outside the Drug Conjugate Context

Subcellular trafficking is important to both the design and efficacy of drug conjugate therapies. However, controlling subcellular localization of cargo may also be useful outside the traditional three-component drug conjugate system. For example targeting ligands could be utilized in larger scale drug delivery vehicles such as micelles or liposomes.[41,49,81,134,135,140] Data from our lab and others indicate targeting ligands may be able to control the subcellular localization of larger nanoparticles.[31,40,78,86,121,166] Controlling the subcellular localization of these types of vehicles maybe equally important. For example, delivery of siRNA should avoid lysosomes while promoting access to cytosol. Attachment of targeting ligands to the delivery vehicle may enhance these desired effects. In addition delivery of immunogenic peptides to different organelles may alter the presentation of these peptides in HLA class 1 molecules thereby acting as an adjuvant to enhance the immune response against the antigen. Thus, controlling subcellular patterns of accumulation maybe useful outside the typical targeted drug conjugate application. Chapter five of this manuscript will describe an application where a liposomal based immunotherapy is designed around ability of a targeting

ligand to promote presentation of an immunogenic peptide in HLA class I molecules of cancer cells.

Aims of this study

The goals of this study are two-fold. First, generation of methods that identify targeting ligands that preferentially internalize into NSCLC cell lines as well as accumulate in a defined subcellular location. I will present two methods: first a method utilizing endocytic selection pressure during panning to identify targeting ligands which preferentially internalize into NSCLC cell lines via defined mechanism of endocytosis and second, coupling together a phage display selection protocol with secondary immunofluorescent screen to directly identify targeting ligands that preferentially internalize in NSCLC cells and accumulate in a defined subcellular location. In addition to describing these methods, I will present two proof-of-concept targeting ligands, each identified using one of the methods described above, that preferentially internalize into a panel of NSCLC cells lines compared to normal bronchial epithelial control and accumulate in lysosomes. Also I will present a method that uses knock in of rare tRNAs into E. coli used for phage amplification to reduce amplification bias during phage display panning experiments. Finally, I will present a novel immunotherapy application of one of these targeting peptides based on subcellular accumulation of the targeting ligand allowing for presentation of antigen in HLA class I molecules specifically in NSCLC cells and tumors. Thus, this study provides both methods for identifying targeting ligands that both preferentially internalize into cancer cells and

accumulate in a defined subcellular location as well as applications to demonstrate the utility of the targeting ligands selected using these methods.

CHAPTER TWO

Identifying Cancer Specific Targeting Ligands with Defined Mechanism of Endocytosis

INTRODUCTION:

Direct drug conjugates generally consist of three distinct parts: the targeting ligand, linker region, and the drug.[29,77,120] The idea, simply put, is to conjugate a highly toxic and non-specific drug to a cell-specific targeting ligand using a chemical linker region. This process has the potential to alter the pharmacodynamics and kinetics of the original drug with the goal of enhancing therapeutic efficacy while minimizing adverse event associated with the treatment.[86,111] In terms of cancer therapies, the goal is to enhance accumulation or internalization of the conjugate within the tumor while minimizing toxic, non-specific interactions with healthy cells and clearance organs.[38,81,120,131]

One of the major hurtles in developing efficacious direct drug conjugates is releasing active drug from the targeting agent. Most drug conjugates are inactive, existing as pro-drugs. Thus, the conjugate is designed to be stable while traveling in the blood system but able to release active drug within the tumor or directly within cancer cells. Typically this is performed using physiological properties associated with either the tumor environment or endocytic pathways.[51,111] Endocytic pathways are particularly advantageous as the drug is released intracellularly to directly exert cytotoxic effects and is not free to circulate through the blood stream in an active form.[14,39,51]

Many endocytic release strategies focus on internalization via the canonical clathrin-mediated endocytic pathway that includes internalization into coated pits that mature into

endosomes and eventually the ligand accumulates in low pH lysosomes.[86,131] This well-defined pathway has multiple physical properties which can be used for releasing the drug including decreasing pH as the ligand progresses from endosomal to lysosomal compartments as well as exposure to lysosomal specific proteases, such as cathespins.[38,86,111] However, recent advances from studying endocytosis have highlighted that this pathway is one of many endocytic pathways that cells utilize to internalize extracellular ligands including raft-mediated, Arf6, Clic/Geec (clathrin-independent carriers/GPI-enriched early endosomal compartments), and macropinocytosis to mention a few.[14,49,81,86,87] Many of these internalization pathways do not share the same trafficking route as the canonical clathrin-mediated pathway and can result in delivery of the cargo through different physiological environments and alternative subcellular locations. As such, release of free drug from the conjugate may be suboptimal. For example, certain raft-mediated endocytic mechanisms do not proceed through low pH endosomes thus impairing release by pH sensitive linkers.[24,31,78,87,166] However, this type of trafficking pattern may be useful for delivering pH sensitive cargo such as nucleic acids or protein toxins.[29,77,87] Thus, knowledge of endocytic trafficking patterns has the potential to allow for better pairing of both linkers and cargo with a given targeting ligand.

Our previous studies have identified multiple peptide targeting ligands that demonstrate selective accumulation in cancer cells. In depth studies of the flagship ligand H2009.1, which binds to αvβ6, reveal that this ligand accumulates in cells in a clathrin and caveolae -independent mechanism. The ligand does not traffic through a compartment with a pH lower that 6.5 implying this ligand does not accumulate or traffic through lysosomes.

Further, EM images of the peptide caring gold nanoparticles indicates the targeting ligand accumulates in a peri-nuclear space that consists of multi-vesicular bodies. Other peptide targeting ligands identified in our laboratory using similar methods to those used to identify H2009.1 appear to have similar trafficking patterns.[86,87]

This study sought to develop a method that identifies cell-targeting ligands that are specifically internalized by cancer cells and utilize a defined endocytic pathway using phage display biopanning. Current phage biopanning methods focus on identifying peptides that bind to and/or mediate cellular uptake. Little attention has been given to identifying peptides that have the added level of specificity for delivery to a subcellular location. Understanding the mechanism of endocytosis may allow for better pairing of a targeting ligand with a linker that is cleavable based on the anticipated subcellular trafficking which is associated with a given mechanism of endocytosis.[81,87,131]

This proof of concept study utilizes phage display biopanning coupled with specific inhibitors of endocytosis to identify peptides that both selectively accumulate in cancer cells and are biased toward the non-inhibited mechanism of endocytosis.[51,87] H1299 non-small cell lung cancer (NSCLC) cells were treated with chlorpromazine to inhibit clathrin-mediated endocytosis,[14,51,72,87] then subjected to side-by-side phage display biopanning on cells in the presence and absence of the inhibitor allowing us to identify phage clones that are group specific and clones that are enriched in both conditions. Using this method, we identified two potential targeting peptides. The first peptide (ATEPRKQYATPRVFWTDAPG, named 15.1) appeared in both the chlorpromazine treated and non-treated group. Our group previously identified this peptide from a panning on HCC15 NSCLC cells and demonstrated

this peptide accumulates in a perinuclear subcellular location in H1299 cells.[40,71,86] This study demonstrates that HCC15.1 primarily internalizes via a cholesterol dependent mechanism of endocytosis. The second peptide is a novel peptide here termed H1299.3 (LQWRRDDNVHNFGVWARYRL). H1299.3 was present only in the non-chlorpromazine treated group, and appears to internalize primarily through a clathrin-dependent mechanism of endocytosis. Further, the peptide demonstrates selective accumulation in cancers cells and co-localizes with Lamp-1, a marker for lysosomes, indicating that H1299.3 may utilize the canonical clathrin-mediated endocytic pathway to selectively accumulate in cancer cells. Thus, we present a proof of concept phage display method that may allow for identification of cancer specific peptides that internalize via a known mechanism of endocytosis. This method may facilitate rapid discovery of efficacious direct drug conjugates by allowing informed selection of linkers and cargo based on endocytic trafficking.

MATERIALS AND METHODS:

Cell Culture: Non-small cell lung cancer (NSCLC) cell lines were graciously provided by the Hamon Center for Therapeutic Research (UT Southwestern) and cultured according to previously reported conditions.[71,86] All cell lines were DNA fingerprinted and routinely tested for *Mycoplasma* contamination.

Phage Display Biopanning: Phage display was performed with slight modification from established protocols.[14,86,87] The library for this study consisted of an M13 phage displaying a random 20-mer peptide fused to the pIII protein.[24,87,123,151] Phage display was performed using established protocols with the exception of adding a 15 minute pre-incubation with 100

μM chloroquine prior to addition of library.[86,87,123] Chloroquine is used in this scheme to neutralize lysosomal pH with the idea that neutralizing the low pH environment of the lysosome will enhance recovery of intact phage which traffic to the lysosome. As outlined in figure 4, the phage output from round 1 was split and side-by-side biopanning was performed in the presence of 125 μM chlorpromazine or without inhibitor. In round 1, 1 x 10^{10} phage articles were added to H1299 cells. The library has an approximate diversity of 1 x 10^{8} unique phage clones thus this represents 100 library equivalents i.e.100 copies of every unique phage present in the library. For rounds 2-5 chlorpromazine was preincubated with H1299 cells for 15 minutes prior to addition of phage. The cells from each group were then incubated with phage for 1 hour then washed 2-times with PBS^{+}+0.1%BSA (10 minutes total), washed 3-times with acid wash pH=2.2 (10 minutes total) to remove extra-cellular bound phage, and finally washed 2-times with PBS^{+}+0.1%BSA (2 minutes total). Cells from each group were lysed using 30 mM Tris + 0.05% Triton-X-100, pH=8, according to standard protocol.[86,87] Lysates were mixed with K91 *E. coli* to amplify internalized phage after each round. A total of 6-12 phage clones were sequenced from the output of each group in rounds 3-5 using established colony PCR-based protocol.[51,87] Phage selectivity was measured by calculating the fold increase in internalization of the selected phage compared to a control phage in H1299 cells using previously established methods.[3,87,91,115]

Peptide Synthesis: All peptides were synthesized using standard FMOC solid phase synthesis techniques and purified to >95% purity using reverse phase HPLC as previously reported.[14,21,72,87] Peptides were synthesized on NovaPeg Rink amide resin (NovaBiochem) and had a 10mer Polyethylene Glycol (PEG_{10}) spacer (Polypure) between the c-terminus of

the peptide identified from the phage and the cysteine used to multimerize the peptides (HCC15.1 – ATEPRKQYATPRVFWTDAPG-(PEG_{10})-C-NH_2, H1299.3 – LQWRRDDNVHNFGVWARYRL-(PEG_{10})-C- NH_2). The expected/observed mass for HCC15.1 and H1299.3 is 2,991.52/2,991.32 and 3,305.06/3,305.07, respectively. The peptides were multimerized using tri and mono -lysine cores functionalized with maleimide, as previously described, to create tetrameric and dimeric presented peptides, respectively.[40,71] Biotinylated-glutamate or cysteine (NovaBioChem) was synthesized into the core in order to conjugate dyes and cargos to the peptides using streptavidin or cysteine-maleimide chemistry, respectively, as previously reported.[12,71,86] H1299.3 dimeric peptide was conjugated to C5-maleimide AF546 for imaging studies. H1299.3 and C5-maleimide AF546 were dissolved in phosphate buffer (13 mM KH_2PO_4, 54 mM $NaHPO_4$, pH 7.4.) then shaken for 1 hr. at RT. The precipitate was washed 3 times in phosphate buffer then dried in a desiccator O.N. The purity of the dimeric dye labeled peptide was >95% as measured by rpHPLC with the expected/observed mass found to be 8,265.68/8,265.12. The peptide was suspended in DMSO then culture media for imaging studies. H1299.3 peptide solutions were made fresh from lyophilized, stock stored at -20°C, for each assay due to poor stability in neutral pH solutions.

Flow Cytometry Assays: Established flow cytometry protocols were used to determine the specificity of endocytic pathway inhibition, demonstrate peptide internalization, and determine primary mechanism of endocytosis.[86] To determine specificity of endocytosis, human Transferrin-AF488 (Life Technologies) was used to measure clathrin-mediated endocytosis according to manufacturer's protocol and LacCer-BODIPY (Life Technologies)

to monitor raft-mediated endocytosis as previously reported.[28,123,151] Nysatin (10-50 nM) and Chlorpromazine (50-150 μM) were titrated on H1299 cells and internalization of fluorescent markers of endocytosis were used to determine selective inhibition of endocytosis. Inhibitors were pre-incubated with cells for 15 minutes at 37°C, 5%CO_2 then fluorescent markers were added in the presence of inhibitor and incubated for 30 minutes at 37°C, 5%CO_2. Cells were washed 2x in PBS^++0.1%BSA then fluorescent markers were removed from the cell surface using acid wash (3-times 10 min, pH=2.2) or washing with defatted BSA (Sigma) as previously described.[71,86,123] Internalization was detected using flow cytometry to measure level of florescence in a single cell. Treatment with 125 μM chlorpromazine resulted in 63% reduction in clathrin specific internalization with minimal cytotoxicity (Figure 5, data not shown).

For peptide internalization assays, peptides were conjugated to streptavidin-phycoerythrin (SA-PE) via the multimerization core using previously established protocols.[86] For assays using HCC15.1, 10 nM of tetrameric peptide was incubated with 1:1 molar ratio SA-PE for 30 minutes in PBS with gentle agitation. Excess Streptavidin binding sites were quenched by the addition of RPMI 1640 that contains 0.2 mg/L D-biotin. For assay using H1299.3 10-50nM of dimeric or tetrameric peptide was incubated at 1:1 molar ratio of SA-PE for 30 minutes in phosphate buffer (13mM KH_2PO_4, 54mM $NaHPO_4$, pH7.4) with gentle agitation and then quenched with RPMI 1640. Peptide SA-PE conjugates were incubated with cells for 60 minutes at 37°C, 5%CO_2 to allow for peptide internalization. Surface bound extra-cellular peptide was removed using acid wash (pH=2.2) then cell fluorescence was analyzed via flow cytometry. As determined by titration of peptide, 50 nM of H1299.3

fluorescence conjugate resulted in sufficient signal to noise ratio for detecting internalization by the flow cytometry assay and thus this concentration is used for subsequent internalization assays.

For inhibitor studies cells were pre-incubated with 125 μM chlorpromazine or 30 nM nystatin for 15 or 60 minutes, respectively, as previously described[51,71,72] then treated with either 10 nM of HCC15.1 or 50 nM of H1299.3 peptide SA-PE conjugate in the presence of inhibitor for 30 minutes at 37°C, 5%CO_2. Surface bound extra-cellular peptide was removed using either acid wash (pH=2.2) or trypsinization (0.25% Trypsin with 2.21 mM EDTA, Corning) then cells were analyzed for internal fluorescence using flow cytometry.

Time Course Study: To measure internalization of H1299.3 over time H1299.3 dimer was conjugated to IRDye800CW (Li-Cor) using cysteine –maleimide chemistry as outlined above. The purity of the dimeric dye labeled peptide was >95% as measured by rpHPLC with the expected/observed mass found to be 8,422.31/8,421.12. 50 nM of dye was incubated with H1299 cells in black walled, clear bottom 96 well plate for the indicated time; surface bound dye was removed using an acid wash. Fluorescence was read using an Odyssey CLx imager (Li-Cor).

Clathrin siRNA Assays: H1299 cells were treated with siRNA oligos against clathrin heavy chain (CHC) or control siRNA oligo using previously established protocols.[3,4,13,91,115] Briefly, H1299 cells were seeded in 12 well plate at a density that allowed >72 hrs. of growth before confluence. Cells were treated with 5.5 μL of 20 μM oligo solution and 6.5 μL of RNAiMax (Invitrogen) in total of 200 μL of RPMI 1640. Cells were washed with RPMI 1640 then treated with 100uL of siRNA oligo solution for 4 hr. at 37°C, 5%CO_2. Cells were

washed once then placed back in complete media. This procedure was repeated again the following day. At 72 hours post initial treatment with siRNA oligos, cells were treated with peptide SA-PE conjugates, described above, to measure peptide internalization or utilized for western blot assays to measure relative protein levels. CHC knock down was confirmed by western blot using monoclonal antibody against CHC (TD.1, Santa Cruz-12734) as primary and goat anti-mouse-HRP secondary antibody using established protocols.[21,86]

Fluorescent Confocal Microscopy: Laser scanning confocal microscopy was used to monitor live cell accumulation of peptide as well as identify subcellular localization of peptide accumulation using established protocols.[40,57,75] A549 cells were transfected with Golgi, ER, or Lysotracker GFP fusion constructs using Bacman 2.0 (Life Technologies) system, according to manufactures protocol. Briefly 200 μL of trypsinized and washed A549 were incubated with 1:10 dilution of baculovirus encoding for the fusion protein at 37°C 5% CO_2 for 10 minutes with gentle mixing. The cell/virus mixture was plated in poly-lysine coated glass bottom dishes containing 1 mL of complete media. A549 cells were incubated overnight at 37°C, 5% CO_2 to allow for cells to adhere to the dish. The next day cells were washed and treated with 100 nM of H1299.3 dimeric peptide, directly conjugated to Alexa Fluor 546 (Life Technologies) via cysteine-maleimide chemistry according to manufacturer's protocol, for 1 hr. at 37°C, 5% CO_2. Cells were washed twice with complete media then stained for 10 minutes with Hoechst 33342 (Molecular Probes) according to manufacturer's protocol. Live cells were imaged using a Nikon TE200-E laser scanning confocal microscope, through a 30μm pinhole visualizing the blue, green, and red channels using 408 nm, 488 nm, and 543 nm lasers for excitation, respectively.

Statistics: Statistical analysis were performed using GraphPad Prism software or Microsoft Excel. Flow cytometry values are presented as mean with standard deviation or as percentage of mean with standard deviation. In vitro experiments were performed a minimum of 3 independent times using multiple replicates per experiment. Reported p-values are paired or unpaired, two tailed t-tests (where appropriate). A p-value ≤ 0.05 was considered statistically significant. Non-significant results are indicated throughout the text as N.S. Co-localization studies were analyzed for Mander's coefficient using ImageJ software with the JaCoP plugin[11,12,38,111,120]

RESULTS:

Novel Panning Scheme: We developed the phage display scheme outlined in Figure 4 to select peptides that both accumulate specifically in a given cell type and internalize via a known mechanism of endocytosis. Phage display biopanning in Round 1 is performed using established protocols with cell binding and internalization as the selection criteria. The amplified phage recovered from Round 1 is then split into two groups. One group is treated with a specific inhibitor of endocytosis and one group remains untreated. The remaining rounds of panning are then carried out in parallel with each group, sequencing selected clones at each round. Clones enriched in one or both group are then further characterized as targeting ligands for drug conjugates.

Paramount to this protocol is utilizing inhibitors that are specific to a mechanism of endocytosis. Chlorpromazine at 125 μM specifically inhibited 63% of clathrin-mediated endocytosis in H1299 cells as determined by reduction of transferrin uptake. At this concentration minimal cytotoxicity and no effect on raft-mediated endocytosis was observed (Figure 5, data not shown). Unfortunately, consistent inhibition of raft-mediated endocytosis in H1299 cells using pharmacological inhibitors proved difficult in our hands. Therefore it was necessary to compare between the chlorpromazine and non- treated cells to identify clones that internalize via clathrin-mediated endocytosis.

After verifying inhibition of clathrin-mediated endocytosis, biopanning was performed on H1299 cells according to the scheme outlined in Figure 4 using chlorpromazine as the endocytic inhibitor. Starting at Round 3, 6-12 phage clones per group were sequenced (Table 1). We identified a novel phage clone

LQWRRDDNVHNFGVWARYRL, termed H1299.3 by observing repeat sequences in the non-treated group (Figure 4b, Table 1). H1299.3 phage clone was observed twice in round 3 and again in round 4. This clone was not observed the chlorpromazine treated cells. Further, the peptide was not listed in existing peptide databases, and blast searches indicated the peptide did not align to a known protein or contain punitive domains/motifs.

However, at later rounds of biopanning both the chlorpromazine and non–treated groups converged on the phage clone ATEPRKQYATPRVFWTDAPG previously identified in our lab as HCC15.1 (6 for 6 clones in round 5 for both groups). This phage clone was selected on the HCC15 NSCLC cell line and has affinity for H1299 cells as reported.[29,77,86] As such, it is not surprising that this clone was isolated again. No other repeat sequences were observed in this panning experiment nor were consensus sequences observed amongst phage clones (Table 1).

Both phage clones accumulate in H1299 cells above the background internalization of the library. The selectivity values of each clone were calculated by measured the difference in accumulation between the selected phage and a control, random phage, in H1299 cells using the following formula [(Phage Clone[Output Titer/Input Titer])/(Control Phage[Output Titer/Input Titer])]. HCC15.1 and H1299.3 accumulated 18 and 11 -fold above control phage in H1299 cells (Figure 4). Thus, both HCC15.1 and H1299.3 phage clones accumulate in H1299 cells and the binding is mediated by the displayed peptide. However, HCC15.1 was the convergent clone probably both due to slightly higher internalization as well as unintended selection pressures which are inherent to all phage panning protocols.[28] Early sequencing, starting in round 3, allowed for partial mitigation of amplification bias and other

unintended selection pressure by allowing the observation of enriched clones that accumulate in H1299 cells that might be lost in later rounds. It is important to note that these clones were isolated without a negative selection step. Thus, highly selective clone can be identified using this technique without the use of a negative selection step.

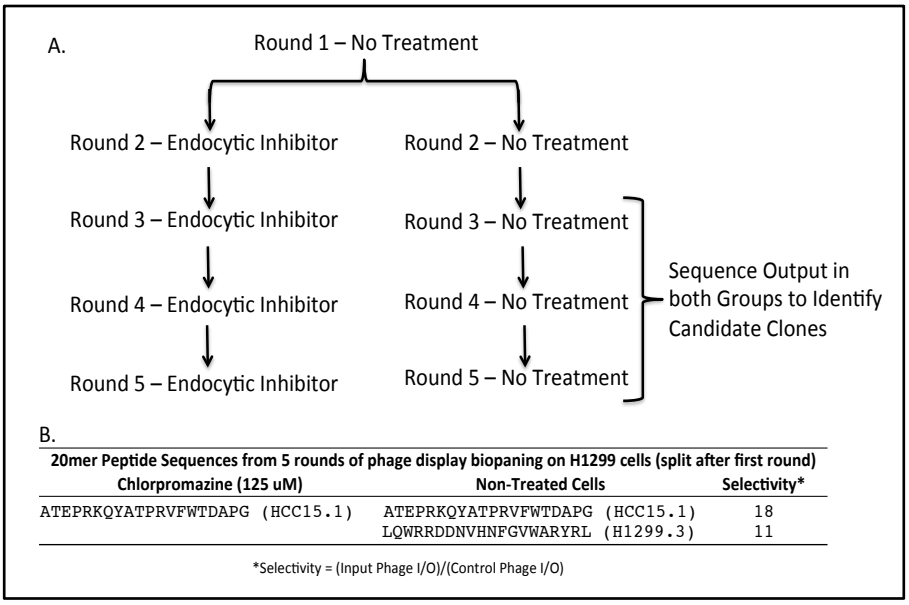

B.

20mer Peptide Sequences from 5 rounds of phage display biopaning on H1299 cells (split after first round)		
Chlorpromazine (125 uM)	**Non-Treated Cells**	**Selectivity***
ATEPRKQYATPRVFWTDAPG (HCC15.1)	ATEPRKQYATPRVFWTDAPG (HCC15.1)	18
	LQWRRDDNVHNFGVWARYRL (H1299.3)	11

*Selectivity = (Input Phage I/O)/(Control Phage I/O)

Figure 4. Phage Display Biopanning Selection to Identify Cancer Specific Peptides that Accumulate via Known Mechanism of Endocytosis. A) In this scheme phage display biopanning techniques are used to isolate peptides that are specific for cancer cells as well as internalize via a known mechanism of endocytosis. Round 1 of panning is performed according to standard protocols. The output of round 1 is then split into two groups. One group is treated with a specific inhibitor of endocytosis while the second group remains untreated. Panning proceeds in parallel between both groups. Phage clones are sequenced in both groups starting in round 3 to identify potential hits between groups. **B)** Results from H1299 biopanning experiment using chlorpromazine as endocytic inhibitor. One clone, HCC15.1 is present in both the treated and non-treated group while H1299.3 is present only in the non-treated group. HCC15.1 and H1299.3 selectively internalize into H1299 cells 18 and 11 -fold greater than control phage, respectively.

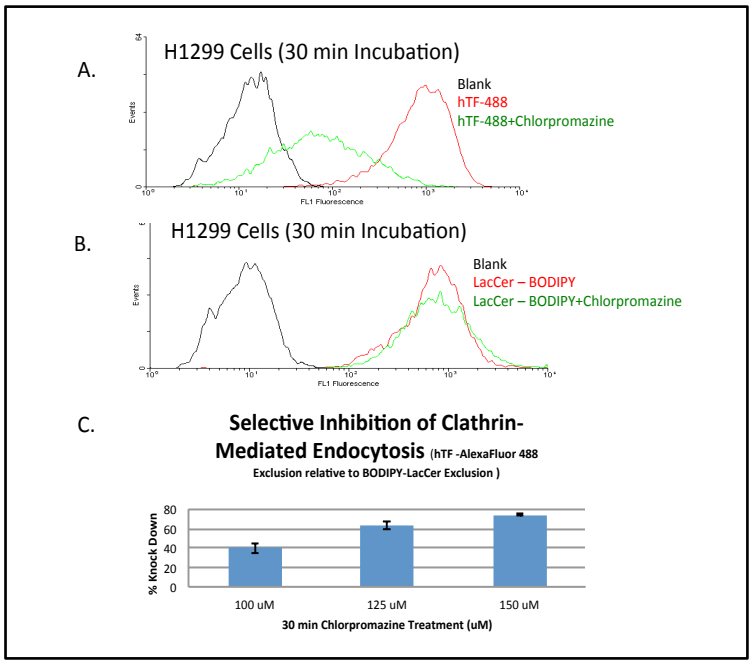

Figure 5. Set up and Results of Biopanning with Endocytic Pressure. A) Representative histogram of H1299 cells stained with Transferrin-AF488 +/- treatment with 125 uM Chlorpromzine (green and red traces respectively). The black trace is H1299 cells not stained with Transferrin-AF488. **B)** Representative histogram of H1299 cells stained with LacCer-BODIPY +/- treatment with 125 uM Chlorpromzine (green and red traces respectively). The black trace is unstained cells. **C)** Quantification of selective Clathrin inhibition in chlorpromazine treated H1299 cells. Value represents difference between levels of transferrin and LacCer internalization in the presence of chlorpromazine.

Table 1. List of all Phage Clones Identified During Biopanning

H1299 Round 3 20mer Sequences

No Treat	Chlorpromazine (125 uM)
EEHTHRWPFWGHQERWGKQS	AARPPTAPTEMHGAEMKGMT
EHGDGPGGKMRWWWHGGGTR	EEGGEVKGSAHASTDDTTRF
GAFWKNNGSTQPWNPEDSSL	GDMVPWAHPWEPWLGNKVEA
GDATAKEMRSTQDTPQERGA	GTYASVTRSHDRSGERIGDH
LQWRRDDNVHNFGVWARYRL	KVQVERKEALGIQKIAVSRR
LQWRRDDNVHNFGVWARYRL	LAGRQGPERSTVENNLSGTK
LSLGRGADRIIPWELRRPGG	NATWGKALRDYHRGVWSRVS
MEGRSIGGRFRHTADMMVEA	SKSFALDGTPERYSRTLVRR
RVSGDNQAPTQRNNQGAEWT	VVSIPSTVGKGYPDSWAVRR
SQTLKGWRTGKLQPETLRWS	WEGSEGTVESDNLQNKKGGK
SSEFAGENGGSTRGHKFDGY	WGANQNRFAMAWAGATGASS
VAPLLRSESAIARSLVSYPQ	

H1299 Round 4 20mer Sequences

No Treat	Chlorpromazine (125 uM)
ATEPRKQYATPRVFWTDAPG	AAPRLGGTQIKSESTKMGSD
ATEPRKQYATPRVFWTDAPG	ATEPRKQYATPRVFWTDAPG
ATEPRKQYATPRVFWTDAPG	ATEPRKQYATPRVFWTDAPG
ATEPRKQYATPRVFWTDAPG	ATEPRKQYATPRVFWTDAPG
ATEPRKQYATPRVFWTDAPG	ATEPRKQYATPRVFWTDAPG
ATEPRKQYATPRVFWTDAPG	ATEPRKQYATPRVFWTDAPG
ATEPRKQYATPRVFWTDAPG	ATEPRKQYATPRVFWTDAPG
ATEPRKQYATPRVFWTDAPG	ATEPRKQYATPRVFWTDAPG
ATEPRKQYATPRVFWTDAPG	ATEPRKQYATPRVFWTDAPG
ATEPRKQYATPRVFWTDAPG	ATEPRKQYATPRVFWTDAPG
LQWRRDDNVHNFGVWARYRL	GAWEAVRDRIAEWGSWGIPS
FGSWPTGWKARAYNDLPPAR	TWDGNEAERSPGSTGEDAAR

H1299 Round 5 20mer Sequences

No Treat	Chlorpromazine (125 uM)
ATEPRKQYATPRVFWTDAPG	ATEPRKQYATPRVFWTDAPG
ATEPRKQYATPRVFWTDAPG	ATEPRKQYATPRVFWTDAPG
ATEPRKQYATPRVFWTDAPG	ATEPRKQYATPRVFWTDAPG
ATEPRKQYATPRVFWTDAPG	ATEPRKQYATPRVFWTDAPG
ATEPRKQYATPRVFWTDAPG	ATEPRKQYATPRVFWTDAPG
ATEPRKQYATPRVFWTDAPG	ATEPRKQYATPRVFWTDAPG

Tables list of phage clones identified by PCR based sequencing in rounds 3-5. The tables are divided into groups based on treatment with endocytic inhibitor.

The Free Peptides Mediate Cellular Internalization: Previous studies by our group demonstrated that multimeric presentation of peptides on lysine cores is an effective method for retaining specificity and affinity of peptides selected from pIII displayed libraries.[28,71] We therefore synthesized dimeric and tetrameric H1299.3 peptide with a PEG_{10} spacer on each peptide monomer between a biotinylated mono- or tri -lysine core respectively (Figure 6). The peptides are conjugated to streptavidin -Phycoerythrin (SA-PE) and incubated with cells of interest. Surface bound extra-cellular peptide was removed using an acid wash prior to flow cytometry analysis allowing for measurement of internalized peptide. As shown in Figure 7, the free peptides are able to bind and internalize into H1299 cells, again indicating that this process is peptide mediated and not dependent on the phage particle. A negligible difference in internalization was observed between dimeric and tetrameric forms of H1299.3 by flow cytometry (Figure 7a). Thus, increasing valency past the dimeric format does not improve cell binding or internalization. This is particularly fortunate as the tetrameric peptide has limited solubility in aqueous solution. Monomeric peptide was not tested in this study. Uptake of the H1299.3 dimeric peptide is concentration dependent over a 10 nM- 50 nM range as predicted for a peptide that internalizes via receptor-mediated endocytosis. In addition, we also performed a time course to monitor H1299.3 accumulation in H1299 cells (Figure 7c). 50 nM of dimeric H1299.3 internalized in an exponential fashion, saturating after 30 minutes further implying the peptide internalizes via receptor mediated endocytosis. Similar to the selectivity data, H1299.3 accumulated less than tetrameric HCC15.1 in H1299 cells (mean afu H1299.3= 138.3 +/- 33.7, and HCC15.1 = 844.9 +/- 50.8).

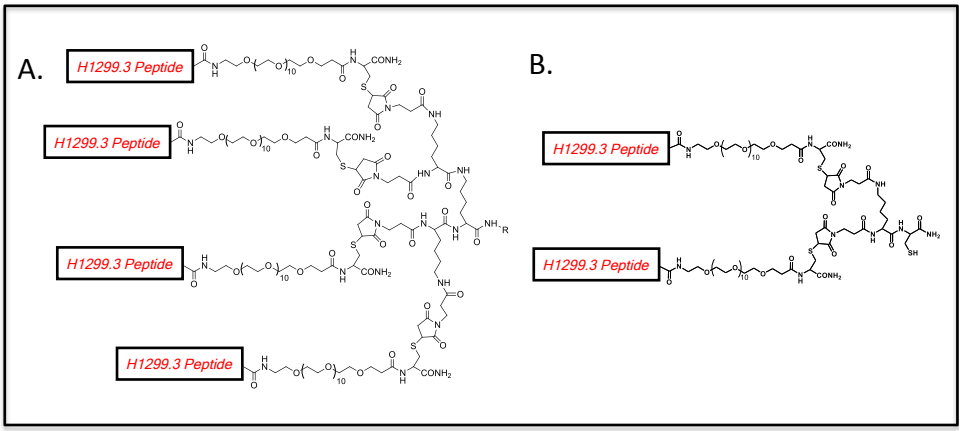

Figure 6. Targeting Peptide Multimerization strategy. A) A tri-lysine core is utilized to facilitate binding of 4 peptides to the core using a convergent synthesis scheme. Targeting peptide monomers are conjugated using thiol-ester chemistry to the core to generate tetrameric peptides. **B)** Similar scheme as in A; however a mono-lysine core is utilized to generate dimeric targeting peptides.

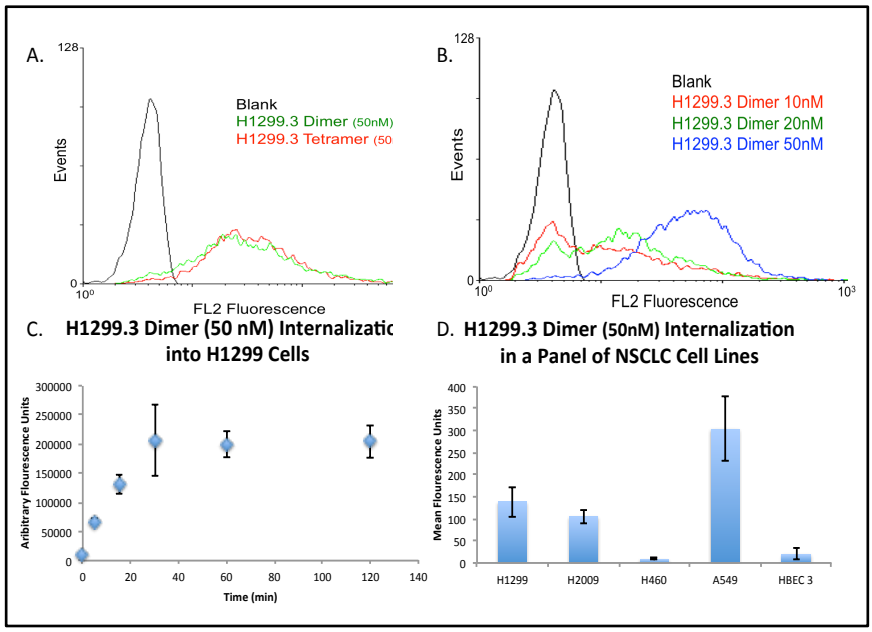

Figure 7. H1299.3 Peptide Mediates Cellular Internalization. **A)** Representative histogram generated from treating H1299 cells with 50 nM of dimeric and tetrameric forms H1299.3 conjugated to PE (green and red traces respectively). The black trace is H1299 cells not treated with peptide. **B)** H1299.3 dimeric peptide titration demonstrates dose dependent internalization. **C)** Time course of H1299.3 dimeric peptide accumulation in H1299 cells. **D)** Internalization of H1299.3 in a panel of NSCLC cell lines. Internalization values ranged from 8.6 +/- 1.9 to 303.3 +/-72.2 mean A.F.U. Importantly, H1299.3 demonstrated minimal accumulation in HBEC3 cells, a model of normal lung epithelial cells, compared to all NSCLC cell excluding H460 ($p<0.01$).

H1299.3 Differentially Accumulates in NSCLC Cell Lines: Internalization of H1299.3 was determined on a panel of NSCLC cell lines (Figure 7d). H1299.3 displays significantly lower internalization in Human Bronchial Epithelial Cells (HBEC3) a model for normal lung epithelium compared to most NSCLC cell lines (5-10 fold increase). Thus, the peptide has a window for selective accumulation into lung cancer cells. In addition, H1299.3 internalized into multiple histological subtypes of NSCLC including Large Cell (H1299 mean afu=138.3 +/- 33.8) and Adenocarcinoma (H2009 mean afu=104.9 +/- 15.5 and A549, mean afu=303.3 ± 72.2). However, the peptide does not accumulate in all NSCLC cells; no significant uptake is seen in the large cell line, H460 (mean afu=8.6 +/- 1.9). Our previous studies demonstrate that HCC15.1 differentially accumulates in these cell lines.[33,86,96,120,130,141,149,165] However, H1299.3 and HCC15.1 display differential pattern of accumulation across NSCLC lines. Most striking is HCC15.1 has no affinity for A549 cells. The differential cell-specificity may indicate that these peptides internalize via different mechanisms and/or bind to different cellular receptors.

H1299.3 and HCC15.1 Utilize Different Types of Receptor-Mediated Endocytosis: We sought to determine the primary mechanism of endocytosis of H1299.3 and HCC15.1 peptides in H1299 cells. H1299 cells were pre-incubated with pharmacological inhibitors before addition of the H1299.3 dimer and internalization of the peptide was quantitated. A significant 83% ($p<0.01$) reduction in H1299.3 internalization is observed in the presence of chlorpromazine while treatment with nystatin to block raft mediated endocytosis resulted in only an 18% reduction in internalization (N.S.) compared to non-treated H1299 cells (Figure

8a). Incubation of H1299.3 with H1299 cells at 4°C also resulted in a significant loss of peptide internalization ($p<0.01$). Finally, a 76% and 77% reduction in internalization is observed in H1299 cells treated with either of two different siRNA oligos targeting clathrin heavy chain (CHC) ($p<0.01$). Minimal perturbation is observed in H1299.3 uptake in H1299 cells treated with control siRNA (7% reduction, N.S.). CHC protein knock down in H1299 cells treated with siRNA oligos was confirmed using western blot to measure relative CHC protein levels (Figure 8c,d). The 78% and 86% reduction in CHC protein levels in H1299 cells treated with one of two siRNA oligos against CHC, respectively, is consistent with the decrease in peptide uptake. In comparison, treatment with control siRNA oligo resulted in a 17% decrease in CHC expression levels compared to control. In sum, these data support that the H1299.3 peptide undergoes clathrin-mediated endocytosis.

The mechanism of endocytosis of HCC15.1 in H1299 cells was determined by repeating the above assays (Figure 8b). Nystatin treatment significantly decreased HCC15.1 internalization (82%, $p<0.01$) while chlorpromazine treatment had minimal effect on internalization of HCC15.1 (2% reduction, N.S.). Incubating HCC15.1 with H1299 cells at 4°C resulted in loss of peptide internalization ($p<0.01$). Finally, treatment with either of two siRNAs targeting CHC or a control siRNA had minimal effect on HCC15.1 internalization (12%, 1%, and 4% reduction, respectively N.S.). Unlike the H1299.3 peptide, HCC15.1 does not utilize a clathrin-mediated pathway for internalization but most likely utilizes a raft-dependent mechanism.

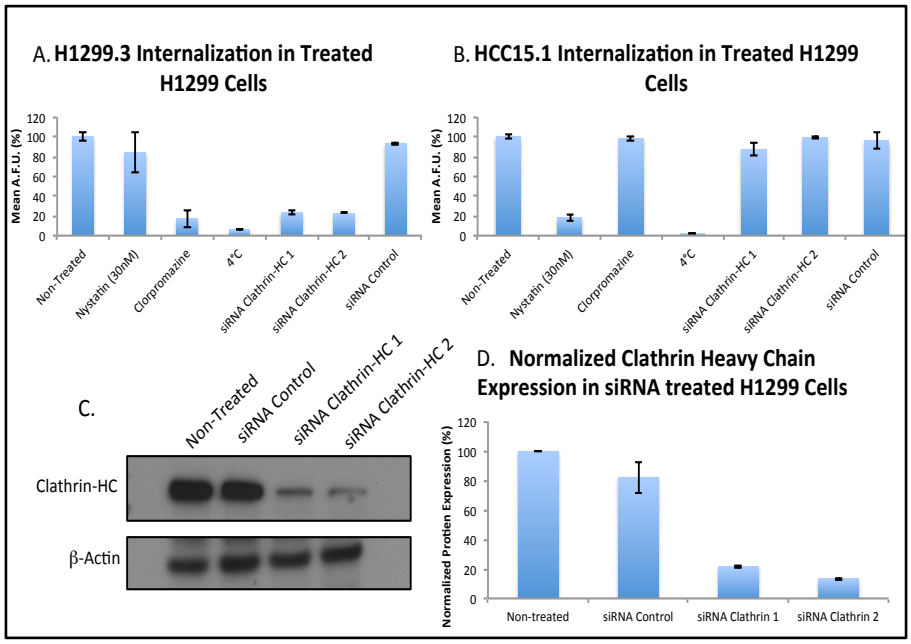

Figure 8. Peptides H1299.3 and HCC15.1 Primarily Internalize via Different Mechanisms. A) Internalization of H1299.3 in H1299 cells treated with selective inhibitors of endocytosis. Treatment of H1299 cells with inhibitors to clathrin-mediated endocytosis including chlorpromazine and siRNA toward CHC significantly reduced internalization ($p<0.01$). Membrane fluidity was also a significant factor for internalization ($p<0.01$). **B)** Internalization of HCC15.1 in H1299 cells treated with selective inhibitor of endocytosis. Only treatment with Nystatin and 4°C resulted in significant reduction in HCC15.1 internalization ($p<0.01$) indicating the necessity of cholesterol and membrane fluidity for internalization of HCC15.1. **C)** Western blot demonstrating Clathrin Heavy Chain (CHC) knockdown using targeted siRNA in H1299 cells. **D)** Quantification of CHC knockdown in H1299 cells, normalized for loading, using β-actin as loading control.

H1299.3 Co-localizes with Lamp-1: Live cell, confocal fluorescent microscopy was used to determine subcellular accumulation of these peptides. H1299.3 subcellular localization was determined by conjugating the H1299.3 dimeric peptide directly to AF546 using cysteine maleimide chemistry.[12,35,56,71,72,86,137,167] A549 cells, transfected with GFP-fusion constructs to mark organelles using the Bacmam 2.0 system purchased from Life Technologies,[4,13,83,105,106,139,156] were treated with H1299.3-AF546 (Figure 9). A549 cells were used because they internalize the most H1299.3 peptide of the cell lines assayed thus allowing for the greatest observable signal with the lowest concentration of H1299.3 to avoid false positive data. H1299.3 appears subcellularly as multiple distinguished puncta. The puncti co-localized well with Lamp 1-GFP fusion and localized poorly with both Endoplasmic Reticulum and Golgi markers. The Mander's coefficient for these groups are 0.608, 0.368, and 0.107 for Lamp 1, ER, and Golgi, respectively indicating strongest co-location is with lysosomes. In addition, the matching puntcal shapes further supports co-localization with lysosomes rather than ER. These data further supports the model that the H1299.3 peptide binds to an extracellular receptor and is internalized by a canonical clathrin-mediated process which results in accumulation of ligand in lysosomes. By comparison, previous studies demonstrated that HCC15.1 accumulates in a perinuclear location and results in a distinctively different staining pattern than the H1299.3 peptide (Figure 10).[18,43,66,86,89,111,120]

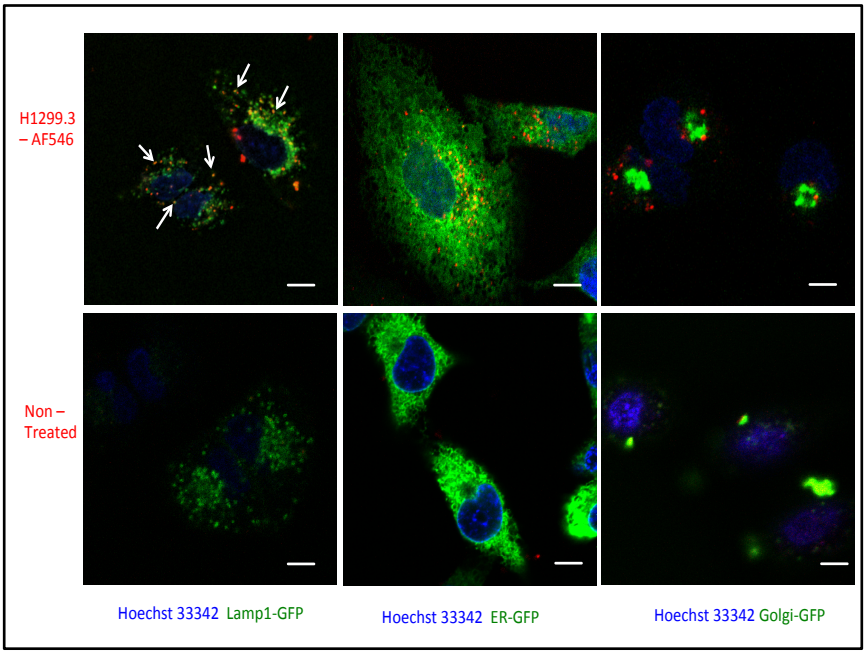

Figure 9. H1299.3 Co-localizes with Lamp-1 in A549 Cells. A549 cells treated with H1299.3 peptide and an organelle tracking GFP fusion construct. The top three panel are A549 cell treated with 100 nM of H1299.3 dimer conjugated to AF546, while the bottom three panel are negative control A549 cells not treated with peptide but imaged in the red channel. H1299.3 displays a distinct puncti type staining in all treated wells while no red signal is observed in control groups. A549 cells were treated 24 h prior to imaging with BacMam 2.0 live imaging constructs to stain organelles with GFP. A549 cells were stained from left to right with Lamp 1-GFP as a lysosomal marker, KDEL-GFP as endoplasmic reticulum marker, and N-acetylgalactosaminyltransferase 2-GFP as Golgi marker. White arrows indicate co-staining between Lamp-1-GFP and H1299.3 peptide. Minimal co-localization is observed with other organelle markers. Scale bar = 10 µm.

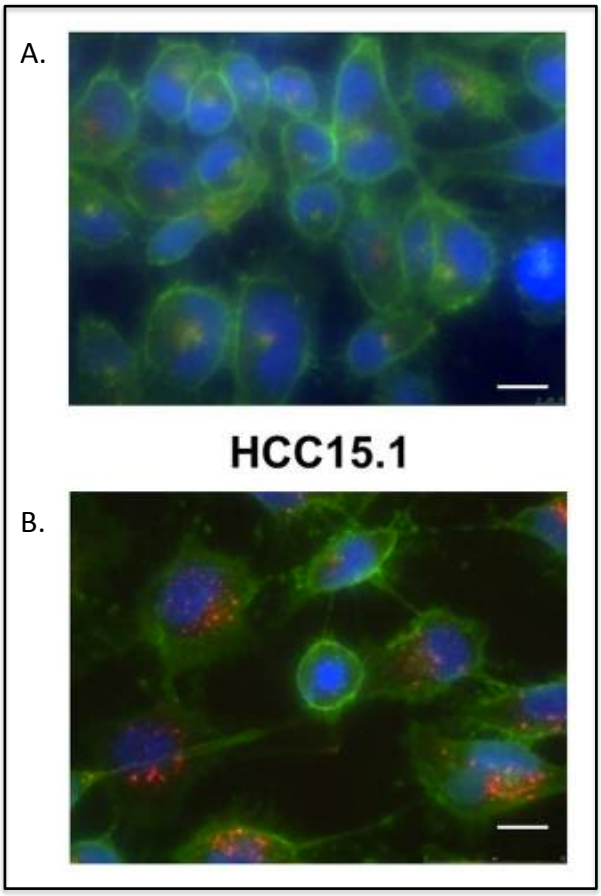

Figure 10. Subcellular Localization of HCC15.1 Targeting Peptide. *Modified from McGuire et al. Sci Rep. 2014 Mar 27;4:4480* **A)** H2009 NSCLC treated with scrHCC15.1 (10nM) conjugated to 605 Qdots (red) cells are fixed and stained with Wheat Germ Agglutinin (Green) and DAPI (Blue). **B)** H2009 cells treated as in A with HCC15.1 (10nM) conjugated 605 Qdots. Scale bars indicate 20 μm

DISSCUSION:

Phage biopanning has proven to be an effective method for identifying cell-targeting ligands. However, little emphasis has been placed on identifying cell-specific ligands that not only internalize into a specific cell type but also can deliver cargo to a desired subcellular. Furthermore, only a few studies have actually determined the subcellular localization of cell-targeting peptides after they have been isolated from a combinatorial library.[57,66,70,75,86,89,111,122,139] This study sought to develop a method that can identify targeting peptides that both accumulate significantly in cancer cells and internalize via a known mechanism of endocytosis. The overall goal is to enhance selection of peptides that traffic to a desirable subcellular localization of ligand accumulation. Recent literature has highlighted the need for matching subcellular localization with drug release strategies for both drug conjugate as well as nanoparticle platforms.[9,11,17,25,31,38,51,67,89,111,120,166] Phage display techniques are well suited to perform this task as it is a nonbiased technique to identifying targeting ligands and allows for wide versatility of selection pressures to tune the output ligand to the desired specifications.

In addition, facilitating the ability to match a targeting ligand with a linker understanding primary endocytic mechanism of a targeting ligand may also guide cargo attachment. For example, small molecule drugs may be delivered through the lysosomal pathway; however, trafficking nucleic acid for RNAi therapies or protein toxins through a lysosomal compartment is demonstrated to degrade cargo resulting in suboptimal delivery.[9,29,38,72,77,90,111,120,133,136] Thus, utilizing protocols that allow for selection of major endocytic mechanisms and subsequent subcellular localization have the potential to guide

selection of both linker and cargo resulting in more rapid creation of effective drug conjugates of multiple subclasses.

This study capitalized on the multitude of endocytic pathways and the differential subcellular accumulation of ligands known to traffic through these endocytic methods. Here we utilized chlorpromazine to specifically inhibit clathrin-mediated endocytosis as a model to demonstrate proof of principle. Our model relies on the specificity of endocytic inhibition as well as consistency of inhibition across panning rounds. As demonstrated in Figure 5 chlorpromazine specifically inhibits clathrin-mediated endocytosis. In our hands we could not specifically and consistently knockdown of raft-mediated endocytosis using pharmacological inhibitors in H1299 cells. Thus, this study used a comparison between chlorpromazine treated and non-treated cells to identify peptides internalized via clathrin-mediated endocytosis. By comparing side-by-side biopanning experiments and sequencing clones at early rounds of enrichment, peptides specific for raft-mediated and clathrin-mediated endocytosis were identified.

During the panning, it was necessary to perform one round of panning before splitting the output into two groups to achieve consistency in convergent sequences (data not shown). This step is probably necessary due to the large loss of clonal diversity that occurs during the first round of selection.[8,11,28,55,67,73,96,107] Interestingly both groups converged on a single phage clone HCC15.1. However, both HCC15.1 and H1299.3 had high selectivity values on H1299 cells. This result may be due in part to amplification bias, which is known to occur during phage selections.[8,14,15,28,44,82,102,137,155,156] Additionally, phage amplification is inherently dependent on the ability to isolate viable phage clones able to infect bacteria. It is

possible that phage clones localized within particular subcellular compartments are more difficult to identify as they are degraded or difficult to isolate from the cells. Early sequencing, starting in round 3, appears to partially mitigate this problem by identifying clones enriched in the selection population but which are not the convergent sequence due to amplification bias and other factors that influence clonal selection outside of the desired selection pressure. Interestingly, both isolated clones exhibited high selectivity for H1299 cells without using a negative selection step. Thus, this protocol generates highly selective phage clones for the target cells without the need for an additional negative selection step.

This panning scheme does not allow for determining if a phage can undergo endosomal escape after internalization, and our data do not address the ability of the peptide to be eventually released into the cytoplasm. Endosomal escape is considered an important step in delivery biologically active cargo to cells.[24,33,39,86,102,125,126,130,141,149,162,165] This scheme is focused on initial internalization of the phage and selection of the internalization pathway. This may limit the applications of phage/peptide selected using this protocol. However, layering of addition selection criteria may be possible to select for phage that internalize a defined mechanism and escape from endosomes. Additionally, many endosomal escape agents have been reported to improve endosomal release of biologics and can be incorporated into the targeting peptide if necessary.

The data from the panning experiments indicate that HCC15.1 and H1299.3 may use different mechanisms of endocytosis because H1299.3 is present only in the non-treated group whereas HCC15.1 was present in both the non-treated and chlorpromazine treated groups. Subsequent studies to confirm this observation indicated that HCC15.1 primarily

uses a cholesterol dependent mechanism of endocytosis implying a raft-mediated mechanism of endocytosis (Figure 8b). On the other hand H1299.3 is dependent on clathrin for endocytosis (Figure 8a). In addition, HCC15.1 accumulates in a perinuclear location[35,71,72,86,87,99,121,137,167] whereas H1299.3 accumulation co-localizes with Lamp-1 in the periphery of the cell. Therefore only H1299.3 is internalized via clathrin-mediated mechanism and subsequently in trafficked into lysosomes.

This study outlines a selection scheme that is fundamentally different than the recent papers published by Pasqualini et al. which also describe a technique to identify peptides which accumulate in organelles.[14,86,105,106,143,156] Pasqualini et al. selections rely on penetrin to mediate receptor-independent internalization of the phage prior to accumulation in a given organelle. Our technique differs in that internalization is driven by receptor-mediated internalization process then the phage accumulates in an organelle via intracellular trafficking pathways. This important difference allows selection of ligands that maintain specificity for cancer cells by preventing non-selective membrane penetration. This difference may enhance the therapeutic window of drug conjugates targeted using peptides selected by the method presented in this study by reducing off-target effects resulting from cytotoxicity of non-targeted, healthy cells.

Both peptides identified from this panning scheme internalize into NSCLC cell lines (Figure 7).[18,24,43,83,86,87] Also both HCC15.1 and H1299.3 demonstrate minimal internalization into a normal bronchial epithelial cells line, HBEC3 implying a potential therapeutic window for both peptides to be used as targeting ligands. However, despite both HCC15.1 and H1299.3 internalizing into a similar panel of NSCLC cell lines the peptide

differentially accumulate into these lines (Figure 7,[5,8,66,70,86,87,89,111,122,129,133]). For example, minimal HCC15.1 accumulation is observed in A549 while these cells internalized the greatest amount of H1299.3. These data imply that these peptides may use different forms of endocytosis, as predicted by the phage panning protocol, and/or the peptides may bind to different receptors to mediate internalization. Currently, the identities of receptors that bind HCC15.1 or H1299.3 are unknown. Further, BLAST searches of H1299.3 did not reveal any strong leads as to the receptor(s) that mediate binding and subsequent internalization into cells. Despite lacking this data, these ligands still exhibit differential trafficking patterns that may be beneficial for designing drug conjugates. For example, HCC15.1 is potentially better suited to delivering sensitive cargo as it appears to avoid organelles known to degrade biologic molecules where as H1299.3 is potentially better suited to delivering toxic chemotherapeutic pro-drugs due to the availability of multiple lysosomal cleavable linkers that will release active drug only intracellularly.

In conclusion, we developed a phage display biopanning scheme to identify peptides that both accumulate specifically in cancer cells as well as internalize via a defined mechanism of endocytosis. We demonstrate proof of principle for this approach by identifying two peptides that were both specific for cancer cells but internalized via different mechanisms of endocytosis. In the future we plan to expand the phage display biopanning methodology to additional cell lines as well as endocytic inhibitors in order to identify additional targeting ligands and expand the utility of the method. Clearly, other specific inhibitors, such as nystatin, filipin or siRNA toward endocytic machinery for example, could be readily applied into the panning scheme potentially resulting in the ability to tune this

method to select peptides specific for any type of endocytosis.[2,8,9,17,19,25,26,38,51,69,78,87,89,112,113,120] Future studies using H1299.3 as a targeting ligand in direct drug conjugate constructs will determine the efficacy of H1299.3 as a targeting ligand. Finally, further characterizing the details of H1299.3 subcellular trafficking and identify the receptor H1299.3 uses for internalization may enhance the utility of H1299.3 as a targeting ligand.

CHAPTER THREE

Direct Identification of Cancer-Specific Targeting Ligands that Accumulate in Defined Subcellular Locations

INTRODUCTION:

Drug conjugates generally utilize one of two strategies to generate a prodrug; either the drug is inactivated using a labile linker or the drug is only active in a distinct subcellular compartment.[9,38,40,75,87,90,111,120,136,159] Both of these strategies rely on the conjugate accumulating in defined subcellular compartments for optimal drug activity.[8,11,31,55,73,86,96,107,143,166] While there is substantial research on drug-conjugates that deliver their cargo to a particular cell type, there has been less effort on designing drug conjugates that exhibit both cellular and subcellular specificity. As such, drug conjugates with excellent cell-specificity can display minimal efficacy if the conjugate is trafficked to the wrong location within the cell.

Phage display is a useful tool for selecting peptide and antibody targeting ligands for use in drug conjugates.[8,14,15,30,34,44,78,82,89,102,143,159] Targeting ligands are generally selected by panning the phage-displayed library against a known, purified target or in an unbiased fashion, for example biopanning on whole cancer cells or tissues.[9,24,39,77,86,96,102,107,111,112,118,125,126,133,162] In this study, we coupled together an unbiased biopanning selection protocol that selects peptides that preferentially internalize into cancer cells with a secondary immunoflourescent screen to identify the subcellular location of phage accumulation.[67,71,72,87,99,121,143]

We utilized this protocol to identify a targeting peptide termed H1993.1 (GAAPSGQDANVQSTIQKDHY) that specifically internalizes into a subset of Non-Small Cell Lung (NSCLC) cell lines. Importantly, H1993.1 exhibits minimal binding to a normal human bronchial epithelial (HBEC) control cell line; the peptide internalizes into NSCLC cell lines 100–fold greater than the HBEC control. Microscopy data demonstrate that the peptide accumulates in lysosomes. Increased intracellular fluorescence is observed when treating H2009 cells with a low pH dye indicator conjugated to H1993.1 corroborating accumulation of the conjugate in an acidic subcellular compartment. Treatment of cells that internalize the H1993.1 peptide with this conjugate results in a 2-fold decrease in IC_{50} compared to free doxorubicin. By contrast, treatment of a cell line that has significant reduction in H1993.1 peptide internalization increases the IC50 9-fold compared to free drug. Thus the conjugate improves efficacy while widening the therapeutic window. This study demonstrates a novel method for identifying targeting peptides that specifically internalize into cancer cells and accumulate in defined subcellular localization.

MATERIALS AND METHODS:

Cell Lines: All cell lines used in this study were provided through the Hamon Center for therapeutic research (UTSW) and cultured using previously reported conditions.[14,30,41,55,60,70,86,139,143] Cell lines were DNA fingerprinted and regularly tested for Mycoplasma contamination.

Phage Display Selection: A previously described M13 derived pIII displayed 20mer peptide library was used for all phage display experiments.[9,24,41,61,77,83,87,103,118,119,132,158,161] Phage

were amplified and extracted using standard protocol.[5,8,34,87,111,120,122,129,133,163] Five rounds of selection using previously published protocols was performed on H1993 cells using acid wash to remove any surface bound phage. In addition 0.05% Triton-X-100 was used to permeabilize cells in order to enhance recovery of internalized phage. The output samples used for titer were plated and used as a source for individual phage clones for the secondary screen. The output used for the secondary screen can be plated without interfering with a traditional phage panning protocol.

Secondary Microscopy Screening: Output colonies from Round 2 of traditional biopanning were picked and suspended in 25 μL of PBS. Three colonies (corresponding to 3 unique phage clones) were pooled into each well in a 96 well PCR plate. The picked colonies were incubated for 20 minutes at RT, spun down and the supernatant was harvested. The supernatant was then heated to 65°C for 15 minutes to inactive residual *E. coli*. The plate was spun again and supernatant was harvested.

H1993 cells were plated at a density of 10,000 cells/well (approximately a MOI of 25-50 phage/cell) in glass bottom 96 well poly-lysine coated plate (MatTek). The cells were pre-treated with chloroquine and protease inhibitors in PBS+0.1% BSA for 15 minutes then 12.5 μL of phage extract were added to each well and allowed to incubate for 1 hr. at 37°C 5%CO_2. Chloroquine and protease inhibitor are used because treatment with these compounds enhanced phage recovery (Data not shown); however, proteases and low pH environment are utilized for subcellular trafficking therefore the plate was then washed 1 time in PBS+0.1% BSA then incubated at 37°C 5%CO_2 for an additional hour to allow for intracellular trafficking of the phage. The cells were then fixed in 3.7% formaldehyde,

permeabilized with 0.1% Triton-X-100, blocked with 5% goat serum blocking buffer, and incubated with murine anti-phage antibodies (1:100 see below) O.N. at 4°C. The cells were then stained using the AF546 Tyramide staining kit according to manufactures protocol (Life Technologies). Finally, cells were mounted in fluoromount containing DAPI for imaging. HCC15.1 phage was utilized as a positive control.

Wells were imaged using laser scanning confocal microscopy (Nikon TE200-E) with 20x objective. To analyze patterns of subcellular phage accumulation, 3 fields/well were captured for all 96 wells. Each well was scored for staining patterns based on three different subcellular patterns: peripheral, tight perinuclear, and diffuse perinuclear. These subcellular location were defined as: Punctate-having multiple points of staining in the periphery of the cell, Tight Perinuclear- staining touching the nucleus which doesn't cover the entire face of the nucleus and is continuous in its staining pattern, and Diffuse Perinuclear- staining touching the nucleus that covers an entire face of the nucleus or demonstrates a non-continuous staining pattern i.e. staining contains holes or has button pattern. Wells could contain multiple types of staining patterns. After establishing a base pattern of subcellular accumulation wells were scored from 1-3 for degree of pattern based on number of cells expressing the pattern and clarity of the observed pattern. The highest scoring diffuse perinuclear well was carried forward in this study.

For top scoring wells the second 12.5 µL of phage were amplified and sequenced to identify potential clones. Clones were subjected to selectivity assays to measure accumulation in H1993 cells compared to a control phage as well as imaged in a single phage context to identify single phage of interest.[2,8,19,26,60,64,69,75,78,87,89,112,113,127]

Phage antibody: Anti-phage antibody was manufactured by vaccinating Balb/c mice with 4 mg/mL of double purified M13 phage, not displaying any peptide, suspended in Alum according to standard protocol (Imject Alum Adjuvant, Pierce). Animals were vaccinated subcutaneously every two weeks and serum was collected via submandibular bleeds in collection tubes. Sera was pooled and then further purified using M13 phage bound to agarose beads. Sera was incubated with beads O.N. at 4°C washed and antibodies were eluted using acid wash (pH=2.2). The antibody solution was neutralized and then concentrated with a 100,000 Dalton molecular weight cut-off filter. The final antibody solution was used at 1:100 ratio for imaging experiments. This experiments were performed in accordance with institutional guides for animal care and welfare with IACUC approval (IACUC # 2010-0282)

Peptide: H1993.1 (GAAPSGQDANVQSTIQKDHY) was synthesized via standard FMOC synthesis and purified to >95% purity via HPLC.[28,40,75,87,89,158,159] The expected/observed mass for the monomer is 2,789.35/2,789.12. The peptide was then dimerized using one of two previously described multimerization cores.[31,48,81,86,107,108,131,143,145,160,166] First a mono-lysine core containing a cysteine used for cysteine maleimide labeling and mono-lysine core containing a biotinylated glutamate for Streptavidin-dye labeling protocols.

Peptide Internalization Assays: For peptide internalization assays H1993.1 biotinylated dimer was incubated streptavidin labeled phycoerythrin (SAPE, 50nM). This conjugate was then incubated for 1 hr at 37°C 5%CO_2 with a given cell type to allow for internalization. The cells are then washed with RPMI and trypsinized to remove any surface bound peptide.

Internalization is quantified via flow cytometry as previously described.[30,34,65,78,86,87,89,119,121,143,159] Flow cytometry assays are presented as mean AFU score with standard deviation with a minimum of three independent replicates.[9,71,72,77,86,96,106,107,111,112,118,133]

For time course of internalization assays H1993.1 biotinylated dimer was incubated with SA-IR800cw dye and incubated with H1993 cells (50 nM) for 0, 5, 15, 30, 60, or 120 minutes in a 96 well black, clear bottom plate. The cells were then washed with PBS and acid wash (pH=2.2) before internalization was measured using a LiCOR Odyssey system.[1,6,14,22,47,53,67,87,95,100,102,125,126,143,164]

Co-localization microscopy: To measure co-localization H1993 cells were incubated with Bacmam 2.0 Lamp1-GFP fusion construct for 10 minutes, plated in glass bottom dishes then incubated O.N. at 37°C 5%CO_2. The next day H1993.1 biotinylated dimer was incubated with SA-605 Qdots (100 nM) then incubated with H1993 cells containing Lamp1 GFP construct for 1 hr. Cells were washed incubated with Hoechst 33342 for 10 minutes, washed then imaged alive using a Ziess LSM 700 laser scanning confocal microscope.

H1993.1 Microscopy using pH RodoRed conjugate: For pH sensitive microscopy H1993.1 biotinylated dimer was incubated with SA-pHrodoRed (Life Technologies) dye (100nM) then the conjugate was incubated with H2009 cells plated in a glass bottom dish (MatTek). The cells were washed and imaged as above. Chloroquine treated H2009 cells (0.1 mM) were used as a control.

H1993.1 Doxorubicin Acid-labile conjugate: Doxorubicin BMPH conjugate was generated as previously described.[30,41,55,60,62,70,74,87,95,116,139] This construct was then incubated with

H1993.1 dimer containing a cysteine to facilitate conjugation or quenched using 10-fold molar excess of BME for 2 hrs. at room temperature. The H1993.1 construct was purified via gel filtration (PD-10 columns) to remove excess BME. These constructs as well as free doxorubicin were then utilized in a standard killing assay as previously described.[9,12,14,41,61,77,87,103,118,119,132,158,161] Cells were incubated 3-fold dilutions of conjugate or controls (1uM-~1nM) for 1 hr. washed 2 times with RPMI+5% FBS then incubated for 96 hrs. The concentration of the conjugates and free doxorubicin was measured using the absorbance of doxorubicin at 480 nm (extinction coefficient = 11,500 $M^{-1} \cdot cm^{-1}$).[22,24,28,34,41,47,89,100,111,120,126-128,143,154,163] Surviving cell fraction was then quantified using Cell Titer Glo (Promega). IC_{50} values were calculated using Prism 6 software package with a minimum of four replicates per concentration. Values are presented as mean percentage of surviving cells based on non-treated wells with standard deviation.

RESULTS:

Coupling Phage Display Biopanning Selections with a Secondary Screen. One goal of this study is to develop a protocol that maintains the specificity enrichment that occurs during phage display selection protocols while allowing for rapid identification of phage that accumulate in a desired subcellular location. Therefore we designed a hybrid selection and immunofluorescent screen protocol to meet both these goals.

In this study we utilized H1993 NSCLC cells as bait and a phage display library displaying a 20-mer peptide from the pIII coat protein as a source for targeting ligands. We first performed five rounds of phage display biopanning according to standard protocol; we

sequencing phage clones to identify 20-mer targeting peptide following round three.[39,60,64,75,87,89,106,127] Starting in round three we observed a convergent clone sequence RGDLATLRQLAQEDGVVGVR, previously identified in our lab as H2009.1 (Table 2).

Using the above data as well as the phage output/input ratios to define library diversity (Table 3) we decided to perform the secondary screen using phage clones derived from round two of the panning experiment. By round 2 theoretically the complexity of the library is reduced but not collapsed.[6,28,31,41,47,89,102,158,166] Therefore 285 phage clones were harvested from round two output plates (derived from the plates utilized for titering the library). The phage is crudely purified, pooled into groups of three, and split into two aliquots. Phage were amplified prior to pooling to reduce amplification bias as well as easy integration into existing phage protocols. Two hundred and eight five phage represent only 0.2% of the output population assuming no repeat sequences, however in this proof of concept study sample size was sacrificed for methods development.

Table 2. Sequences Derived from Tradition Phage Display Biopanning on H1993 Cells by Round using 20mer Library

H1993 R3 Sequences	H1993 R4 Sequences	H1993 R5 Sequences
GSDMQRNLNQHGFQETSIDW	RGDLATLRQLAQEDGVVGVR	RGDLATLRQLAQEDGVVGVR
RGDLATLRQLAQEDGVVGVR	RGDLATLRQLAQEDGVVGVR	RGDLATLRQLAQEDGVVGVR
ARPYGTETGPKPAVSSASVF	RGDLATLRQLAQEDGVVGVR	RGDLATLRQLAQEDGVVGVR
VATSFKQVTFGGPFPKLVRS	RGDLATLRQLAQEDGVVGVR	RGDLATLRQLAQEDGVVGVR
GEEKEHGETNLERTRTEGKE	RGDLATLRQLAQEDGVVGVR	RGDLATLRQLAQEDGVVGVR
LAGTSITAETQSKEQASLVD	RGDLATLRQLAQEDGVVGVR	RGDLATLRQLAQEDGVVGVR
RGDLATLRQLAQEDGVVGVR	RGDLATLRQLAQEDGVVGVR	RGDLATLRQLAQEDGVVGVR
ELVSQKGQDYKGGHSKDGWM	MQVTGRGDAERQSAPEMPAE	RGDLATLRQLAQEDGVVGVR

*Blue indicates previously identified phage clone H2009.1

Table 3. Titer of Input and Output Phage during H1993 Phage Display Biopanning by Round

H1993	Input	Output	O/I
Round 2	1.37E+08	1.19E+04	8.72E-05
Round 3	3.68E+08	1.31E+05	3.55E-04
Round 4	3.15E+07	6.09E+04	1.93E-03
Round 5	5.88E+06	3.61E+04	6.13E-03

We plated 10,000 H1993 cells/well in a 96 well glass bottom, allowed cells to adhere overnight, then added pooled phage clones, isolated above, to each well at a MOI of 25-50 phage/cell. This MOI was chosen based on preliminary studies to observe phage staining in a large proportion of cells without saturating the signal (data not shown). We utilized the average phage recovered from an individual colony to estimate the number of phage in each aliquot for this measurement (please see chapter 4, figure 18).[14,31,48,81,108,131,145,160] Phage and cells were incubated together at 37°C, 5% CO_2 for 60 minutes. The plate is then washed to remove non-bound phage and further incubated for 60 minutes to allow for subcellular trafficking. Finally the cells were washed with acid to remove surface bound phage then fixed in 3.7% paraformaldehyde, permeabilized, and finally stained using immunofluorescent techniques with anti-phage antibody. The plate was imaged at 20x power using laser scanning confocal microscopy. Three fields from each well were counted to determine patterns of phage accumulation. We were unable to observe any signal using traditional fluorescently labeled antibodies to illuminate phage therefore tyramide amplification is used to boast the anti-phage signal. However the downside of this approach is it also resulted in reduced crispness of staining pattern resulting in blurred and blending of individual subcellular phage clusters (Figure 11b-d).

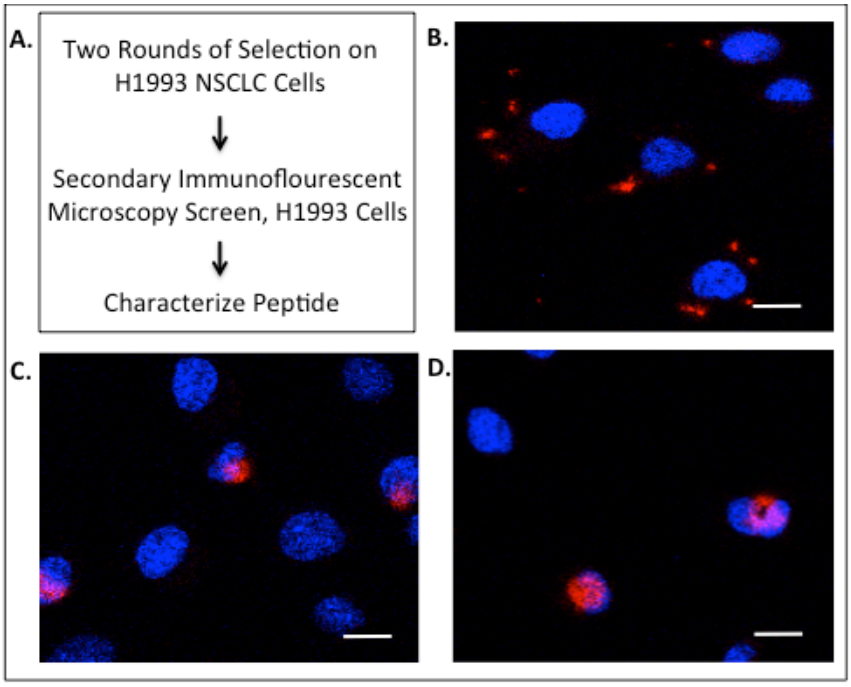

Figure 11. Design of Secondary Screen Experiment. A) Flow chart of strategy to couple a secondary screen to phage display selection protocol. Phage staining (Immunofluorescence staining amplified using Tyramide) is classified into three subcellular accumulation patterns, B-C. **B)** Representative image of H1993 cells demonstrating phage accumulation in a Puncate pattern. Phage is imaged in red channel; Nuclei stained in blue channel **C)** Representative image of phage accumulating in a Tight Perinuclear pattern. **D)** Representative image of phage accumulating in a Diffuse Perinuclear pattern. Scale bars = 20 µm

As this is a proof of concept study we decided to quantify wells using subcellular staining patterns rather than co-localization with an organelle marker. This simplified the experiment as it eliminated variability in staining of the organelle marker across all 96 wells of the plate, but also prevented direct mathematical quantification of the wells using co-localization of pixels. In addition, this prevents direct identification of the precise organelle of accumulation as wells are scored by staining pattern rather than co-localization with defined markers. None-the-less, this experimental design will allow us to test the feasibility of incorporating an imaging screen to the peptide selection protocol and will define parameters for future experiments. In this study we first identified three patterns of subcellular phage staining: punctate, tight perinuclear, and diffuse perinuclear. These were defined as: Punctate-having multiple points of staining in the periphery of the cell (Figure 11b), Tight Perinuclear- staining touching the nucleus which doesn't cover the entire face of the nucleus and is continuous in its staining pattern (Figure 11c), and Diffuse Perinuclear- staining touching the nucleus that covers an entire face of the nucleus or demonstrates a non-continuous staining pattern i.e. staining contains holes or has a button pattern (Figure 11d). Using these definitions wells were classified into these groups as well as degree of each type of staining pattern existing in each well to generate a score based on weight given to staining pattern and degree of staining. Of the 95 wells scored, 75% of wells demonstrated a quantifiable phage staining pattern, and 13% of wells demonstrated multiple subcellular staining patterns. Thirty two percent of wells in this experiment displayed punctate, 33% displayed tight perinuclear, and 15% displayed diffuse perinuclear staining pattern. We sequenced the top two wells in each group demonstrating puncate or diffuse staining patterns. Characteristics of these wells

are outlined in Table 4. We did not observe nuclear or cytoplasmic staining in this particular screen.

Table 4. Clones Identified using Secondary Immunofluorescence Screen on H1993 Cells

Peptide Sequence	Group	e-value*	Selectivity**
RGGPGEAAAERFGTAKLIGG	Punctate (1)	0.34	7
YAGENPVDKGVVTRIPGRGE	Punctate (1)	0.95	8
TGDAAGKGGQGRSLMGSGKR	Punctate (1)	7.40	2
RQTSGVQLTAITDQGRYYAL	Punctate (2)	2.50	4
ASLQQGEDEEDSSRHWRARA	Punctate (2)	0.64	1
TGMFRGTSEQVIYDNLVGWP	Punctate (2)	2.60	1
RHGEYASAQRGMLARSAPTL	Diffuse (1)	3.00	2
RWKDMTAQSPATWMEGVPQR	Diffuse (1)	0.67	3
GAAPSGQDANVQSTIQKDHY	Diffuse (1)	0.97	13
AVGVAGGSDVTRTRTESLLL	Diffuse (2)	0.05	8
SLEEEMKRTGGKPVSVGGVA	Diffuse (2)	0.66	5
MNTRGGATATGSEAHWRYTL	Diffuse (2)	8.50	1

*e-value is generated from performing protein blast using Homo sapiens database on 3/21/14 and 4/23/14 for punctate and diffuse groups, respectively
**Selectivity=(Input/Output titer of phage)/(Input/Output titer of control phage) a value ≥ 10 was used as a cut off for studies presented in this manuscript

For this study we decided to move forward with the highest scoring diffuse perinuclear well. Two organelles that are known to be involved in the receptor-mediated endocytosis system stain in a diffuse perinuclear pattern, Golgi and Lysosomes. Therefore we amplified the phage in the second aliquot of phage for the highest scoring diffuse perinuclear well (Figure 12a) and identified the three phage clones present in that well: RHGEYASAQRGMLARSAPTL, RWKDMTAQSPATWMEGVPQR, and GAAPSGQDANVQSTIQKDHY (Table 4, Figure 12). To deconvolute the well and identify single phage of interest we performed side by side immunofluorescent staining and selectivity assays. First, we repeated the immunofluorescent microscopy assay outlined above to determine subcellular staining pattern of each phage. RHGEYASAQRGMLARSAPTL (Figure 12c) and RWKDMTAQSPATWMEGVPQR (Figure 12d) demonstrated punctate or no staining while the GAAPSGQDANVQSTIQKDHY (Figure 12b) clone demonstrated a diffuse perinuclear staining pattern as well as some punctate staining. In addition, selectivity assays to determine internalization of each phage clone compared to a control phage demonstrated the GAAPSGQDANVQSTIQKDHY clone internalized significantly more than the other clones which is consistent with the microscopy data (10-fold increase, $p<0.05$, Figure 12b,e). These data imply the GAAPSGQDANVQSTIQKDHY clone is the clone of interest in this particular well. For the remainder of the manuscript the GAAPSGQDANVQSTIQKDHY sequence will be termed H1993.1.

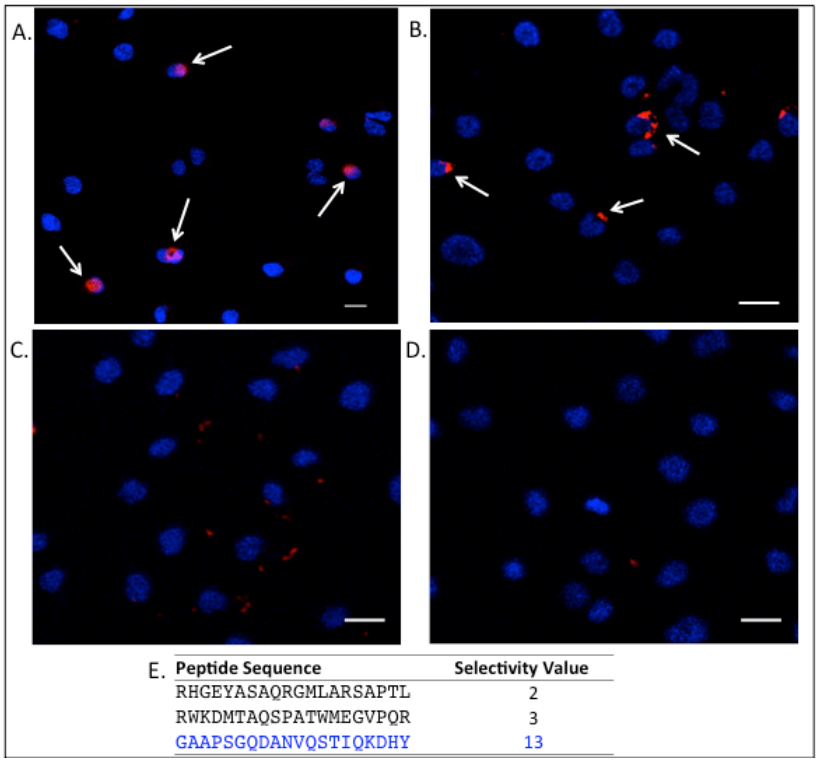

E.

Peptide Sequence	Selectivity Value
RHGEYASAQRGMLARSAPTL	2
RWKDMTAQSPATWMEGVPQR	3
GAAPSGQDANVQSTIQKDHY	13

Figure 12. Result from Screening for Diffuse Perinuclear Accumulation Pattern. A) H1993 cells treated with phage pool then imaged using immunofluorescence techniques. Image from Highest scoring Diffuse perinuclear well. Blue indicates nuclei, Red indicates phage. Arrows depict cells displaying phage accumulation in diffuse perinculear location as called in this study. The three phage from well in A. were identified and imaged individually, B-D, to identify single clone of interest. **B)** GAAPSGQDANVQSTIQKDHY phage alone imaged as in A. This phage clone exhibits primarily diffuse perinuclear staining. **C)** RHGEYASAQRGMLARSAPTL phage alone imaged as in A. This phage clone exhibits punctate staining pattern. **D)** RWKDMTAQSPATWMEGVPQR phage alone imaged as in A. This phage clone does not exhibit a quantifiable staining pattern. **E)** Table demonstrating selectivity value of each phage clone (Selectivity = [Input titer/Output titer of Selected Phage]/[Input titer/Output titer of Control Phage]). GAAPSGQDANVQSTIQKDHY phage demonstrated similar staining pattern to initial hit (A) as well as selectivity >10 and therefore termed H1993.1 and carried forward. Scale bars = 20 µm

H1993.1 Peptide Internalizes using a receptor mediated process. We synthesized the H1993.1 targeting peptide in order to determine effect of phage on peptide internalization and accumulation. H1993.1 was synthesized by FMOC solid phase peptide synthesis (SPPS), dimerized on a lysine core, and labeled using standard protocols.[41,65,71,86,87,106,119,121] The peptide was dimerized as the peptide is displayed in multiple copies on the phage and this technique is known to increase affinity.[71,72,106,108,120] We utilized a previously described flow cytometry based assay to measure peptide internalization (Figure 13).[1,6,14,22,47,50,53,56,87,92,95,100,102,125,126,143,147,157,164] Briefly, fluorescently labeled peptide is incubated with cells at 37°C, 5% CO_2 for 1 hr. then cells are washed and trypsinized to remove and free or surface bound peptide. Peptide internalization is then quantified using flow cytometry. Streptavidin-phycoerythrin (SA-PE) labeled H1993.1 at 50 nM internalized into H1993 as expected from the phage display data. We also observed that H1993.1 internalization saturates between 30-60 minutes and requires membrane fluidity for internalization (Figure 13b,c). Thus these data imply the peptide internalizes into mammalian cells outside the phage context and utilizes a receptor-mediated mechanism of endocytosis.

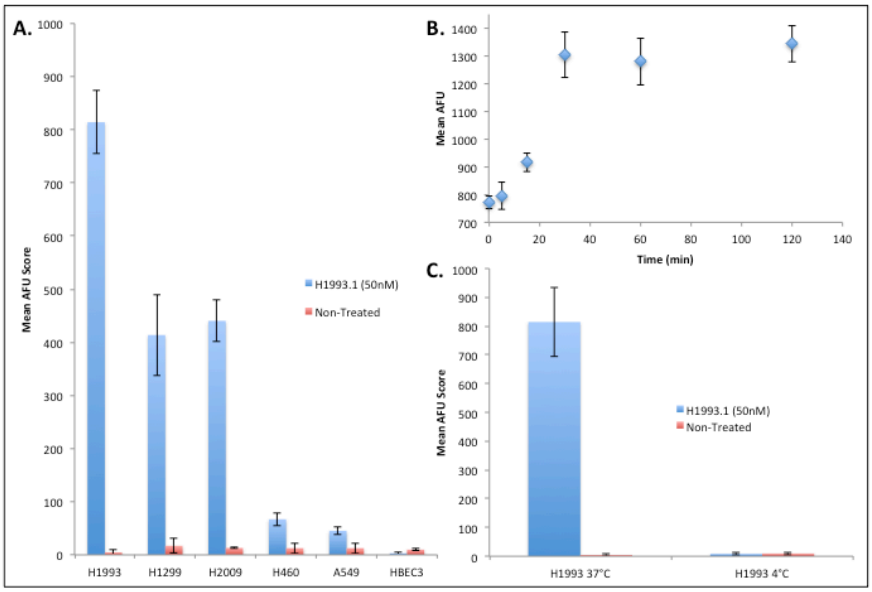

Figure 13. H1993.1 Peptide Internalizes Preferentially in a Panel of NSCLC Cell Lines using a Receptor-Mediated Mechanism. A) H1993.1 dimeric peptide (50 nM) differentially accumulates in a panel of NSCLC cell lines using a flow cytometry based assay (Blue, range: 814.2 – 2.9 mean AFU). Fluorescent values of Non-treated control cells are depicted in red. H1993.1 demonstrates minimal internalization in HBEC3 a normal epithelial control cell line. **B)** Time course of H1993.1 dimeric peptide (50 nM) internalization in H1993 cells. **C)** H1993.1 dimeric peptide (50 nM) internalization in H1993 cells at 37°C and 4°C. Non-Treated indicates cells not treated with labeled peptide. Error bars represent Standard Deviation.

H1993.1 Peptide internalizes into panel of NSCLC cell lines. We next measured the internalization of H1993.1 SA-PE labeled peptide in a panel of 5 NSCLC cell lines that includes both adenocarcinoma and large cell histology using the assay presented (Figure 13a). We observed differential endocytosis of the peptide ranging from 814.2 to 45.3 mean AFU in H1993 to A549 cell respectively. Fluorescence of non-peptide treated control cells (Non-Treated) are also plotted on the X-axis in red. Minimums of three independent flow cytometry assays were quantified to generate the values presented in figure 13a.

H1993.1 targeting peptide demonstrated low internalization in HBEC3 cells (3.0 mean AFU), which are model for normal human bronchial epithelium. H1993.1 accumulated 250-fold greater in H1993 cells and 100-fold greater than the panel of NSCLC cell lines compared to HBEC3 potentially indicating a large therapeutic window in which the peptide preferentially accumulates in cancer cells compared to normal tissue.

H1993.1 Accumulates in Lysosomes. H1993.1 was selected because it accumulated in a diffuse perinuclear pattern, however multiple organelles including Lysosomes and Golgi occupy this subcellular space. Therefore we performed co-localization studies to determine location of subcellular accumulation. As demonstrated, in Figure 14a and b, 100 nM of H1993.1 peptide dimer labeled with 605Qdots co-localized with Lamp1 (green) in H1993 cells using live cell laser scanning confocal microscopy. The peptide did not co-localize with Golgi (Figure 14c,d) potentially indicating the peptide accumulates in lysosomes. To further confirm that H1993.1 accumulates in lysosomes, we performed a series of assays based on lowering of pH that is known to occur during intracellular trafficking to lysosomes. We first

conjugated H1993.1 dimeric peptide to pHrodoRed dye that increases in fluorescence upon lowering of pH (Figure 15c,d). This dye has minimal fluorescence emission at pH=7 however, as the pH drops the probe increases in fluorescence (see BIOPROBES®70, Life Technologies). The response is reversible i.e. the probe is reflective of the environment it presently experiences rather than indicating that it has passed through a low pH compartment. In addition, chloroquine can be used as a control for these assays as it prevents acidification of vesicles (particularly lysosomes) resulting in a reduction in fluorescence emission from the probe. We observed a red signal indicating that the conjugate is trafficked to a low pH compartment (Figure 10c). As a control, chloroquine treated H2009 cells incubated with H1993.1 conjugated to pHrodoRed results in a loss of red signal (Figure 15d) indicating the H1993.1 conjugate is trafficked to a low pH subcellular compartment.

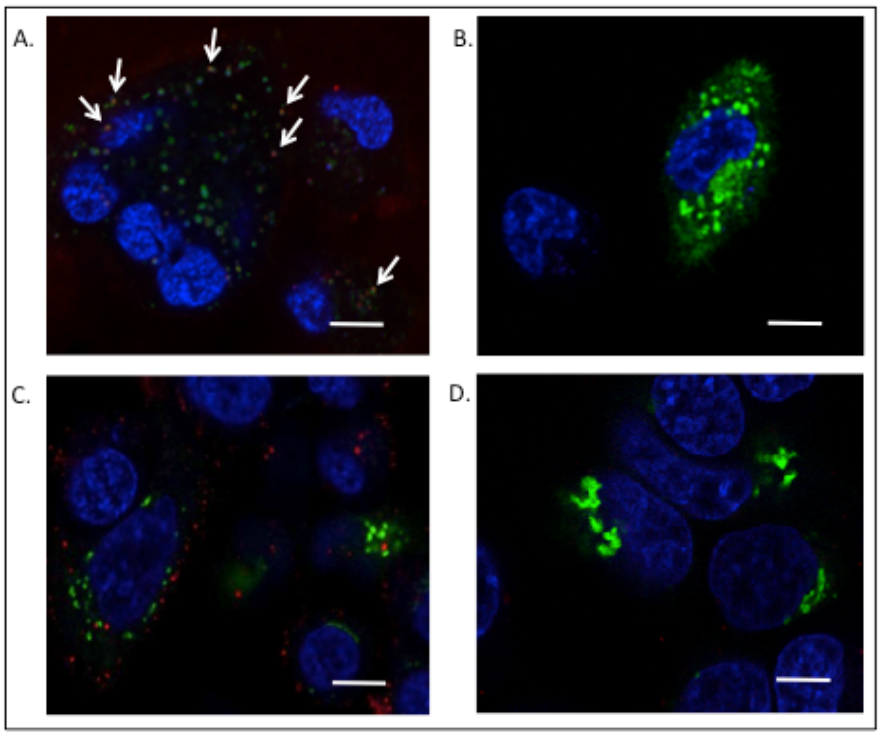

Figure 14. H1993.1 Peptide Co-localizes with Lamp1. A) Live cell, laser scanning confocal image of H1993 cells expressing Lamp1-GFP (Green) treated with 100 nM of H1993.1 dimeric peptide conjugated to 605Qdots (Red) and Hoechst 33342 (Blue). Arrows indicate co-localization. **B)** H1993 cells imaged as in A, but cells were not treated with labeled H1993.1 Dimeric peptide. **C)** H1993 cells expressing Golgi-GFP marker (green) treated as in A. **D)** H1993 cells imaged as in C, but cells were not treated with labeled H1993.1 Dimeric peptide. Scale bars = 20 µm.

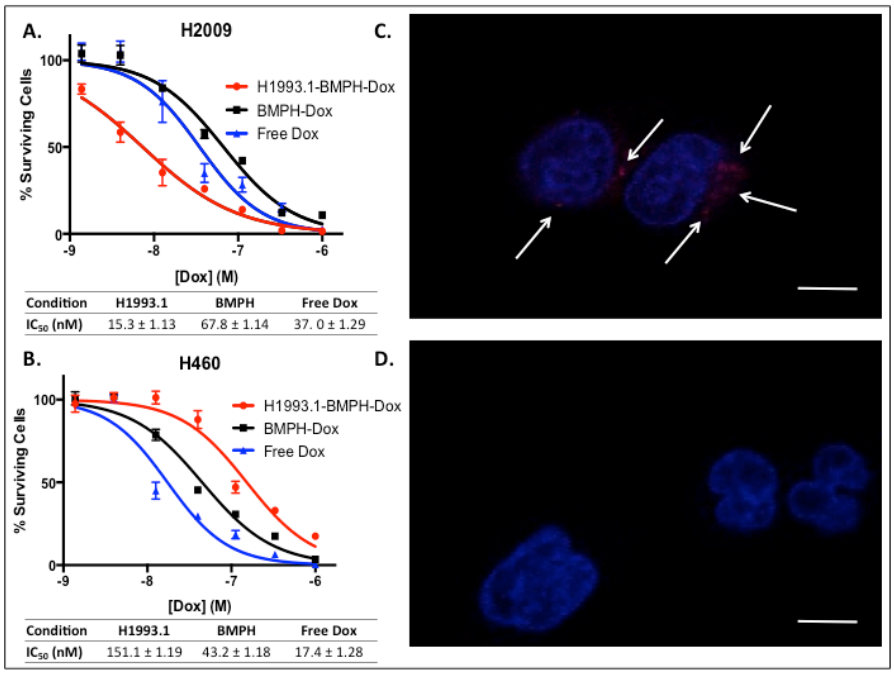

Figure 15. H1993.1 Peptide Traffics Through Low pH Compartment. **A)** H2009 cells were treated with: H1993.1 conjugated to Doxorubicin via an acid-labile linker (H1993.1-BMPH-Dox), Doxorubicin with quenched acid-labile linker (BMPH-Dox), or free Doxorubicin (Free Dox) for 1 hr. then washed and incubated for 96 hrs. Surviving cells were measured using Cell Titer Glo to generate IC_{50} values for each condition. Numeric IC_{50} values are indicated below the chart. **B)** H460 cells were treated as in A. **C)** H2009 cells incubated with H1993.1 conjugated to pHrodoRed dye that fluoresces in low pH conditions. Live cells were imaged using confocal microscopy. Blue is Hoechst 33342 while red indicates peptide conjugate. Arrows indicate visible conjugate. **D)** H2009 cells treated as in C with the addition of 0.1 mM chloroquine to neutralize pH. Scale bars = 20 µm.

Rationally Designed Drug Conjugate for Low pH Accumulating Targeting Ligand. As final proof of concept for this study we utilized information derived from the phage identification assay to rationally design a drug conjugate to test in vitro. We synthesized a doxorubicin conjugate consisting of H1993.1 dimeric peptide conjugated to doxorubicin using an acid-labile, hydrazone BMPH linker (Figure 15a,b, Figure 16). The hydrazone linkage is designed to break upon exposure to low pH environment, allowing doxorubicin to diffuse through membranes and accumulate in the nucleus. However, when we measured the cytotoxicity of this conjugate in H2009 cells, we observed a significant reduction in IC_{50} in H1993.1 targeted conjugate (15.3 ± 1.13 nM) compared to free doxorubicin (37.0 ± 1.29 nM, 2.4-fold reduction) or BMPH-doxorubicin that is treated with beta-mercaptoethanol to quench the free maleimide utilized to attach the peptide to the drug and linker (67.8 ± 1.14 nM, 4.4-fold reduction). H2009 cells were used in this assay as they are more sensitive than H1993 cells to Doxorubicin cytotoxicity. In addition we repeated these assays on the H460 cell line that has similar sensitivity to doxorubicin but demonstrates 10-fold decrease in H1993.1 peptide internalization. The IC_{50} for the H1993.1-BMPH-doxorubicin conjugate (151.1 ± 1.19 nM) was significantly greater compared to free doxorubicin (17.4 ± 1.28, 8.7-fold increase) and quenched BMPH-doxorubicin (43.2 ± 1.18 nM, 3.5-fold increase) in H460 cells. These data also further imply that H1993.1 may traffic through low pH compartments.

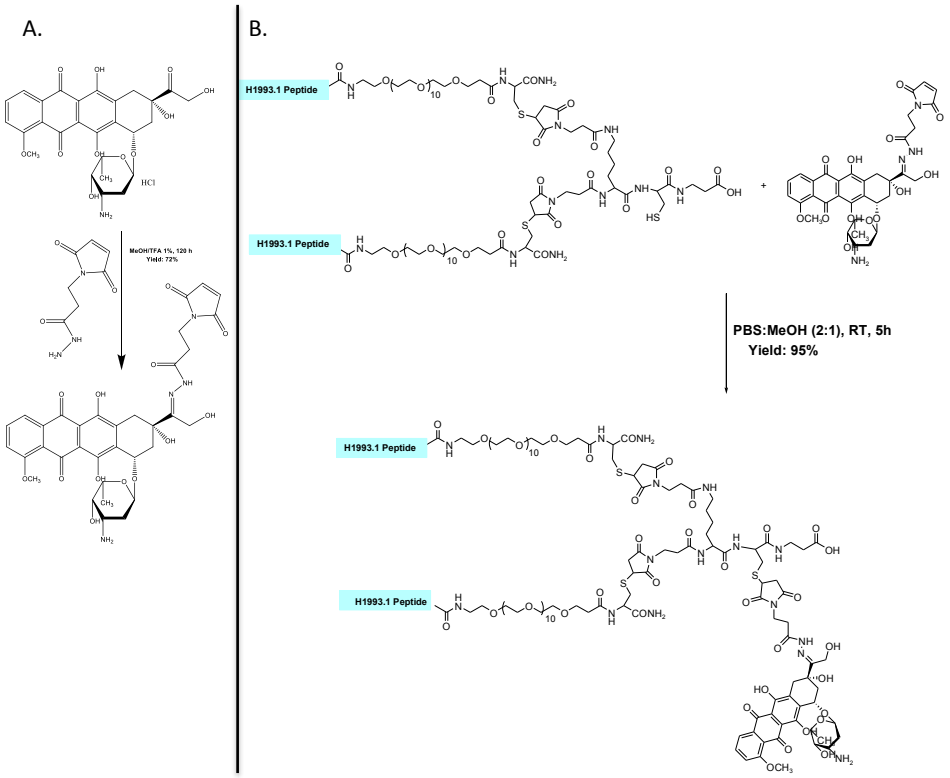

Figure 16. Schematic of H1993.1 BMPH Doxorubicin synthesis. A) synthesis of doxorubicin BMPH. **B)** Conjugation of Doxorubicin BMPH to H1993.1 dimeric peptide. Conjugation occurs through maleimide on the BMPH and a cysteine present on the dimeric core.

FUTURE DIRECTIONS:

Development of Live Cell Imaging Reagent. We identified a promising peptide hit using the secondary immunofluorescent screen. However, we were unable to utilize co-localization screening reliably and phage resolution was suboptimal with this protocol. In addition, fixation impaired our ability to reliably detect phage or organelle markers. For example, GFP fluorescence from transfected organelle markers was impaired by formaldehyde fixation. Therefore we sought to develop a reagent that allows for quantification of phage accumulation in live cells using existing phage display libraries. Other strategies to incorporate GFP or tags directly into the phage coat have been successful but they require either manufacture of new library or phagemid amplification that induces amplification bias of the original library. Thus, a reagent to stain non-modified phage would be very useful for performing live cell imaging of phage internalized into mammalian cells. To this end we performed a phage display panning experiment using an M13 derived library displaying a random 20mer peptide off the pIII coat protein, on blank M13 phage, (i.e. not displaying peptide off pIII coat protein) immobilized on Nunc Maxisorp plates. The blank, immobilized phage were fixed using either methanol or formaldehyde to prevent contamination of the library with truncated blank phage. We preformed 5 rounds of panning sequencing 8 phage from each group starting in round 2. We identified 2 phage hits by duplicate sequences (Table 5). Blank Phage Peptide 1 (BPP1), DWAPWWLTGTYGGKVEELRS, was identified in only the formaldehyde fixed group while Blank Phage Peptide 2 (BPP2), QDVRNWSQWMSTPSVWGRLS was identified in each group implying it may bind independent of fixation condition. BPP1 has a PI of pH = 4.44, net charge of -1 at pH-7.0 and

is hydrophilic. BPP2 has a PI of pH = 10.89, net charge of 1 at pH-7.0 and exhibits greater hydrophobicity compared to BPP1. We next synthesized both peptides using standard FMOC, and dimerized the peptide using previously reported lysine scaffold. The dimeric peptides were conjugated to SA-CW800 dye and analyzed for binding to blank phage via ELISA read on LiCOR Odyssey. Both peptides bound blank phage significantly above background and BPP2 exhibited significantly greater binding to blank phage that BPP1 (Figure 17a). Interestingly both phage did bind formaldehyde fixed BSA immobilized to Nunc plates, although to a significantly lower extent compared to phage coated wells.

We next sought to use this agent as a live imaging dye. We generated BPP2 dimer directly conjugated to AF546 using thiol-ester chemistry. 15.2 phage was then mixed with 1:200 with a 4.3 μM solution of BPP2-AF546 in DMSO. This phage was rocked for 45 minute at RT then mixed with chloroquine and protease inhibitor before being added to H1993 cells seeded in glass bottom plates. Plates was incubated for 1 hr. at 37°C then washed and incubated for an addition 1 hr. at 37°C to allow for internal phage trafficking. The cells are then acid washed, stained with Hoechst 33342, and then imaged live using laser scanning confocal microscopy. We observe multiple discrete puncta in these cells similar to 15.2 peptide stained H1993 cells (Figure 17b,c). In addition we observed high overall percentage of H1993 cells staining positive for phage. Additionally we observe a quantifiable signal from both in both the red and green channel indicating robust phage staining in H1993 cells as well as expression and detection of LCB3-GFP puncta (Figure 17c). These data demonstrate the feasibility of moving a secondary fluorescent screening protocol into a live setting with robust staining protocols.

Table 5. Identification of Clones from Blank Phage Panning Experiment

Formaldehyde Colonies	Methanol Colonies
*GDEGVAAAACSY*SVCVF*	*AAGLGGASFF**SCSAGAV
AASERPEGKGSVTVPTVKPV	*DVVS*AAECAEYVDVSAVC
DMNWTKNRPKAGNMWWGRPV	AGWMKPGAFKSPRLFWEPPE
DWAPWWLTGTYGGKVEELRS	AKNKVICAGLSELAGRGGSC
DWAPWWLTGTYGGKVEELRS	AWDWQWWNPKMAKVGAERAG
EEARGGKWLWPGWMYSRTGM	DWWPSSWSGWVQGYQTSGLG
FKGYPKWTETLTTYWFRDGR	EDAARDEKESSAIMAKLVLS
GGTAWATFWQANPWGDFSVG	EPRLGHPNKVPFFRVTERSG
GLGKAAELWPSQKDMMPIFF	FRHDAQQSYAKVPNWLGGRW
GTIRNWARRLNPXYY*WDSA	GMWDFVQREKFRRNDPKVLT
GTRRAPDSQGELSFWARYDP	GVPRLMWRMATTNNAELASA
LRPGEQRQEPHKAWYARTPV	GVXGEWWSHHWRRSQNQYRA
MPREITRTLWRLQPNTTXMV	GWRWPPRADGGIAQAEAGPN
MWESGAWGMAGRTLQKLGWT	GWSGPRWQLKSWETEYLRAR
NEMLSSPWGWPNLRSGPWWT	IWDMGRSGWQMALLQRLGQG
NQWWATTRYGYQAIMRAGWP	KANPTGGREWPRHPSWPGPR
NTNGSGGEVRRHVEMGHRPG	LGGDKWKDWPRGWWQDLDRG
QDVRNWSQWMSTPSVWGRLS	MEGQRYKAARELGSNGGGVA
QRGCRRNGSGPPKGYRAPML	NWWGLGYQTKMARVGVSTIT
RDWSPQASYPKWLDRQMASW	QDVRNWSQWMSTPSVWGRLS
RGISDNWYQGAMVERDWILP	QGTFWDRPGWPTLPRERVRD
SGV*GEGSVGGEEEWAEALC	RDARLKELYTAGSREVASRG
SLGWGLTWFSVPWQERGSLQ	SLLNVESCLAKPHTENSFTN
SVWDMWRGKTDNRLFNPASL	SLLNVESCLAKPHTENSFTN
SWRQXNEGLVKYMAFKPTSX	SMVQWLVSPKLGRLQATLHR
VEGWRTGVLAWRPRAYLAGG	STMGEMWGEESDRVGRTXIL
WGEPGWWDMHRMFSAKTLRE	TYASKVRMEEFMSRVACWVP
WMGSKVMGTQGWRTVKGLAF	VREGGGEKRPMTKKTSYGPV
WSERTWEKLMWNGPRELVAP	VTFAEWKAPDRWRNLPTWNQ
WYTGEPRWWGSRFTVADFRP	WGWGWTARPTDYTTSGLRDL
XDWPRGIPAPGLERWLPVGH	WGYSPLKSRTPWSHSRSAET
YRWNRWWEKNPRLITVSXRL	YGLNWRPPKVREMSPTPRVK

Two repeat clones were identified by sequencing 8 colonies from rounds 2-5 of panning on blank phage fixed with either methanol or formaldehyde using a 20mer pIII displayed M13 derived phage library. The first clone termed BPP1 (DWAPWWLTGTYGGKVEELRS) was observed only in formaldehyde group while the second termed BPP2 (QDVRNWSQWMSTPSVWGRLS) was observed once in each group.

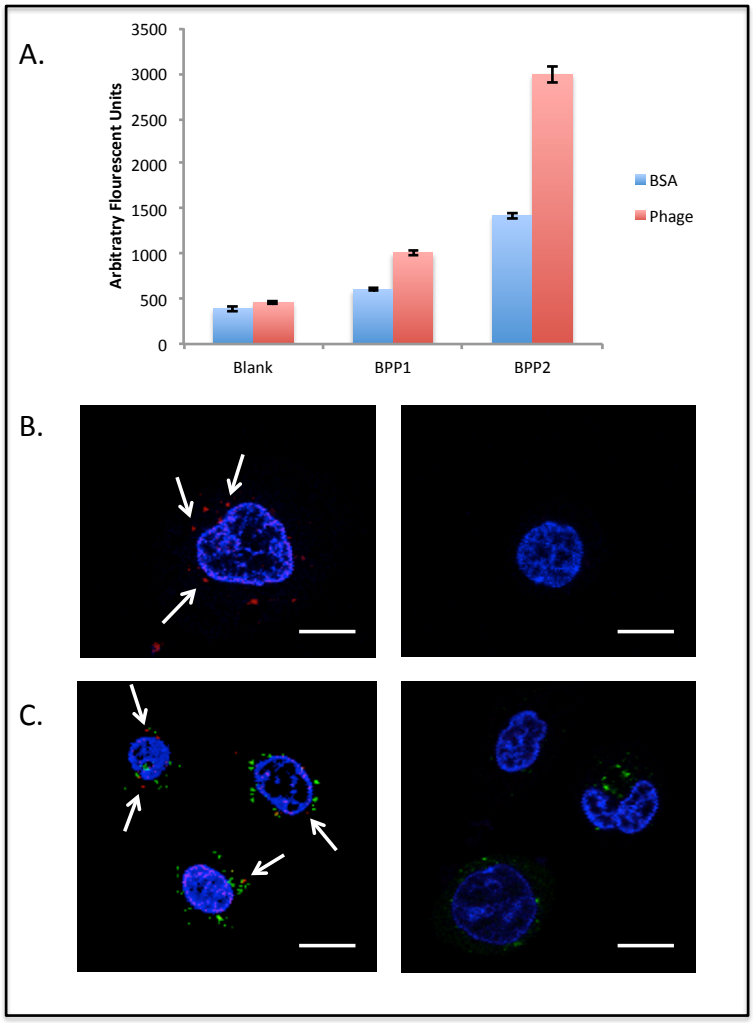

Figure 17. BPP2 Utilization as Live Cell, Phage Detection Reagent. A) ELISA using blank phage or BSA immobilized on Maxisorp plates. Peptide Dimer is labeled with SA-IRCW800 dye then added to the plate. Fluorescents is read using Lycor odyssey. **B)** 15.2 phage is pre-mixed with BPP2-AF546 (Red) then incubated with H1993 cells. Cells are then acid washed and stained with Hoechst 33342 (Blue) and imaged alive using laser scanning confocal microscopy. Right is a control image of cells mixed with BPP2-AF546 without phage. **C)** H1993 cells imaged as in B but also expressing LCB3-GFP (Green). Scale bars represent 20 µm.

DISSCUSSION:

Here we present a novel method for identification of targeting ligands that preferentially internalize into a cancer cells and accumulate in a desired subcellular location. We demonstrate coupling two rounds of panning on H1993 cells with a secondary screening for selecting phage that accumulate in a diffuse perinuclear pattern resulted in the ability to isolate a lysosomal accumulating targeting peptide that differentially accumulates in a panel of NSCLC cell lines compared to normal cell line control.

Current methods allow for the selection of binding and internalizing peptides; however this protocol also allows for direct selection of phage based on a subcellular location.[1,28,29,62-65,74,79,80,87,95,106,116,131,132,149] While we demonstrated selection of lysosomal accumulation in this study, these methods could be applied to other organelles of interest, for example, the Golgi. Future studies utilizing organelle markers in addition to phage staining may allow for easier identification and scoring of wells using a co-localization score that can be calculated from each image to identify hits in a quantitative fashion.[12,14,28,41,80,84,87,134,135,140] As proof of concept for this principle we demonstrate the identification of a novel peptide reagent that can be used in a live imaging format.

Our group recently published a study using modulation of endocytic pathways coupled with selection to identify peptides that selectively internalize into cancer cells via a defined mechanism of endocytosis (please see chapter 2).[22,24,28,40,41,47,86,89,100,121,126-128,142,143,154] This protocol is the evolution of this idea as it allows for direct selection of phage that accumulate in a desired subcellular localization. Thus, both these protocols offer

methods that can be employed to identify targeting ligands for use in rationally designed drug conjugate and delivery strategies.

Modulation of endocytosis during panning or coupling a selection with a secondary screen allows for identification of targeting ligands that accumulate in desired subcellular locations via a receptor-mediated endocytosis mechanism. In contrast, a method developed by Pasqualini et al. also allows for the identification of phage that accumulate in sub cellular organelles, but in their procedure phage internalize via a non-selective mechanism mediated by a Tat derived peptide then accumulate in a subcellular location rather than utilizing a receptor-mediated mechanism of endocytosis.[39,106,120,126] Receptor-mediated endocytosis may allow for larger therapeutic windows for the drug conjugates selected via these methods as they may demonstrate preferential internalization in cellular populations mediated through the targeting ligand.

The secondary screening method for identifying targeting ligands has many benefits including ability to capitalize on the selection to both reduce complexity of the library and maintain high selectivity of ligand internalization in the target cells often observed with phage display biopanning protocols. In addition, direct identification of location of subcellular accumulation may allow for more rapid design of efficacious drug conjugates using rational design based on knowledge from the screen. However, certain aspects of the current protocol could be optimized to enhance ease of use and reliability in the future. Specifically, staining cells with organelle markers would greatly enhance the quantification and confidence in determining the subcellular localization as the analysis could be performed in a completely automated fashion. Also, this study required tyramide amplification to

observe phage accumulation via microscopy. Higher quality antibodies that do not require amplification for viewing may allow for more uniform and cleaner phage staining. Finally, this study observed a relatively small fraction of the phage population (0.2%). Enhancing the number of phage screened may allow for identification of phage that have higher affinity for the target cells or accumulate in more exotic subcellular locations such as nucleus.

H1993.1 appears to demonstrate a potentially large therapeutic window derived from preferential accumulation in cancer cells. The mechanism of H1993.1 internalization appears to be receptor-mediated as the peptide exhibits differential accumulation in cell lines, saturability, and requires membrane fluidity for internalization. However, we currently do not know either the receptor on the cancer cells that mediate endocytosis or the mechanism of endocytosis that is utilized during internalization. We do observe approximately 250-fold difference in internalization of H1993.1 in H1993 NSCLC cells compared to HBEC3, a normal epithelium cell line, and a 100-fold difference in mean internalization into the panel of NSCLC cell lines compared to HBEC3 (13a). Further, H1993.1 appears to accumulate in lysosomes as measured by co-localization with Lamp-1 and a low pH indicator dye. It is desireadble for certain drug conjugates to accumulate in lysosomes, as these organelles have a low pH and contain specific proteases that can be exploited in the design of labile linkers with excellent release profiles.[6,31,41,47,74,102,111,166] In this study we utilized an acid-labile, hydrazone linker to conjugate H1993.1 dimeric peptide to doxorubicin. This conjugate is less than ideal for this situation as hydrazone cleavage is relatively inefficient (~50% cleavage at pH 4 in 4 hours)[14,31,38,62,120] and the BMPH linker does not result in traceless release of non-modified doxorubicin. However, we did observe approximately a two-fold reduction in IC_{50}

of an H1993.1 targeted doxorubicin conjugate compared to free doxorubicin in an in vitro setting (Figure 15). While this is a relatively modest decrease, in IC_{50}, we and others have observed that similar fold changes in in vitro decrease of IC_{50} in doxorubicin conjugates compared to free doxorubicin translate to efficacious treatments in an in vivo setting.[41,52,58,71,106,111]

In addition we observe a reversal in phenotype when H460 cells are treated with H1993.1 conjugate. We observe a 9-fold increase in IC_{50} between H1993.1 conjugate treated H460 cells compared to free doxorubicin. H1993.1 peptide does internalize slightly into H460 cells (albeit 10-fold less than H2009) implying there maybe a threshold that must be surpassed in order to observe killing with H1993.1 conjugate. These data maybe due in part to the sub-optimal release of doxorubicin by BMPH, or due to differing sensitivity to doxorubicin between H2009 and H460 cells. Future studies using H1993.1 conjugates on additional cell lines or in an in vivo setting may offer a better insight as to the therapeutic benefits of this conjugate. In addition, future studies utilizing traceless linkers that are rapidly cleaved in the lysosome such as cathepsin B cleavable linker with a self-immolative drug conjugation and higher activity drug payloads such as Auristatin E may result in highly efficacious drug conjugates utilizing H1993.1 as a targeting moiety.[14,39,87,108,120]

In conclusion, this study presents a novel protocol to isolate targeting ligands by coupling together a phage display biopanning selection with a secondary immunoflourescent screen to identify targeting ligands that both preferentially internalize into cancer cells as well as accumulate in a desired subcellular location. In addition, we utilized this protocol to isolate a targeting peptide H1993.1 that specifically internalizes into a panel of NSCLC cells

line and accumulates in lysosomes. Thus, this method may allow for rapidly identifying targeting ligands that are compatible with known types of linkers and payloads to generate efficacious drug conjugates.

CHAPTER FOUR

Introduction of Plasmid Encoding for Rare tRNA Reduces Amplification Bias in Phage Display Biopanning

INTRODUCTION:

Phage display panning is a versatile tool to identify peptides that bind to desired targets. Large libraries of ligands can be generated as fusions to bacteriophage and used to discover binding agents for a variety of targets including inorganic compounds, proteins, cells, and tissues [6,50,56,87,92,126,131,147,157]. However, most phage display experiments suffer from amplification bias, i.e. bias that occurs from differential replication of phage inside E. coli [1,24,28,29,38,63-65,79,80,87,106,111,131,132,149]. Small differences in growth rate can have substantial impact on the overall diversity of the library. As such, good binders can be lost in the reiterative process of phage amplification that occurs after each round of binding.

Several methods exist to minimize amplification bias including growing phage on plates, in emulsion droplets, or microfluidic devices [28,41,49,80,81,84,88,97,134,135,140]. Deep sequencing in early rounds of panning has been used to identify potential binding phage clones while eliminating or reducing the number of phage amplification steps. However, this results in a high number of false positive clones that must be sifted out. We sought to develop a simple method to reduce amplification bias while minimally perturbing existing phage display protocols.

One potential source of amplification bias arises from codon bias. Codon bias occurs from non-equivalent expression of tRNAs which effects translation rates and overall protein levels,

potentially impacting the production rate of particular phage clones [31,40,78,86,88,121,142,150,166]. Peptide phage display libraries consist of random peptides genetically encoded onto one of the coat proteins [20,29,32,77,117,120,126]. Thus it is difficult to generate large random libraries as well as account for codon bias [32,42,46,74,86,97,111]. Preassembled trinucleotides can be used instead of single nucleotides during library construction to minimize rare codon use [27,38,62,81,88,97,120,131]. However, co-transformation of plasmids encoding for rare tRNAs as well as the expression plasmid can also minimize the impact of codon bias in non-optimized protein expression systems [51,52,58,97,111].

METHODS AND MATERIALS:

pRare Isolation: pRARE was extracted from Rosetta cells and transformed K91 cells to make K91+ cells. These cells are then directly used for phage amplification. The plasmid is maintained by the addition of chloramphenicol during growth and amplification protocols (in addition to currently utilized selection markers for selecting pilus or phage containing bacteria).

Site Directed Mutagenesis: The coding sequence for the Arg switched was switched for each phage clone using site-directed mutagenesis according to manufacture's protocol (Stratgene). The primers used were FTS forward: CACTCCTTTACGAGTCGGAATGCTCATACTG FTS reverse: CAGTATGAGCATTCCGACTCGTAAAGGAGTG SLE forward: GGAGGAGATGAAGAGGACGGGGGGGAAG SLE reverse:

CTTCCCCCCCCGTCCTCTTCATCTCCTCC plasmid DNA isolated from K91 cells containing FTS or SLE was used for template.

Phage Titering: Titering is performed by inoculating 100-fold phage dilutions into E. coli cultures in log phase growth (0.4-0.6 OD_{600}), incubating at 37°C without shaking, and then plating on YT-tet or YT-tet+cam plates followed by overnight incubation at 37°C. Colonies are counted and CFU/mL is calculated using standard formula[14,39,51,87,144].

Phage Extraction from Single Colonies: Single K91 colonies of differing sizes were picked into 25 μL of PBS and incubated at RT with gentle shaking for 20 minutes. The E. coli were then spun down and the supernatant containing phage was harvested then heat inactivated at 65°C for 15 minutes. The phage were spun again and supernatant was harvested and titered according to protocol outlined above.

Phage Competition Assay: 250 FTS and SLE phage are incubated with E. coli at 37°C for 10 minutes then plated on 150 cm YT-tet or YT-tet+cam plates. The following day 12 colonies are picked to monitor phage population then the phage is extracted using standard protocol[86,87,131]. The same procedure is repeated for each iterative round with 500 phage particles from the previous round of amplification carried forward.

RESULTS:

We transformed the pRARE plasmid (Rosetta Cells, 70953 Millipore, San Diego CA USA) into chemically competent K91 cells (Hfr-Cavalli thi). Cells recovered in M9 proline dropout media, to maintain F-pilus expression, and then the cells were plated in M9 proline dropout plates with chloramphenicol (CAM, 30μg/mL)(Alfa Aesar, Heysham, England). Presence of

pRARE plasmid was confirmed using colony PCR (data not shown). These clones retained the ability to internalize phage and thus were termed K91+ cells.

We utilized a library created from the M13 derived, Fd-TET construct that encodes a non-lytic phage which imparts tetracycline resistance to the host E. coli. A 20mer peptide is displayed on the pIII coat protein encoded by ligation of random NNK oligonucleotides [24,38,86,87,111,144]. Due to the library's design, it contains the rare AGG codon for Arginine whose tRNA is encoded by the pRARE plasmid. From this library we identified a phage clone termed FTS that contained an Arginine encoded by the AGG codon. Amplification of FTS in K91+ cells results in a 2-fold higher production of phage than compared to the parental K91 cells ($p<0.05$) (Figure 18). The titer of a second phage clone, termed SLE, that contains an Arg encoded by CGG did not significantly differ between the K91 and K91+ strains. Site directed mutagenesis was used to change the FTS Arg codon from AGG to CGG and the SLE Arg codon from CGG to AGG (Table 6). The apparent titer of SLE (AGG) is significantly different between K91 and K91+ cells (~1.7-fold increase, $p<0.05$). The apparent titer of FTS (CGG) did not significantly differ between K91 and K91+ cells.

Next, we determined the effect of rare codons in iterative amplification. Equal amounts of FTS and SLE were inoculated into either K91 or K91+ cultures then amplified on YT-tet plates or YT-tet+cam plates, respectively. Twelve colonies from each round were sequenced to monitor phage population (McLab, San Francisco, CA USA) Within 3 rounds in K91, the FTS clone (containing the rare codon AGG) diminished from 6/12 clones (50%)

to 1/12 clones (8%). The FTS clone was also lost in the K91+ amplified group but to a lesser extent; at round 3, 33% clones were FTS compared to 50% initially (Figure 18). In sum, these data support the importance of codon usage in phage amplification and suggest that replication of phage using rare codons is enhanced in the presence of pRARE.

A feature we have observed is a wide range of colony sizes upon plating of phage infected K91 cells. However, we noticed that infected K91+ cells demonstrated a significant reduction in variation of colony size compared to the K91 group. In addition, the mean size of colonies is reduced. This is particularly striking for the FTS phage clone containing AGG codon; the variation in colony size between FTS amplified in K91 versus K91+ is significantly different ($p<0.001$) and the average colony size is reduced by 60%. SLE colony variation did not significantly differ ($p=0.09$) but the colony size is also reduced by 60%. Amplification of the phage library also results in significant colony size variation which collapses in the K91+ cells ($p<0.01$) (Table 7). Variation in colony size results in significant differences in phage production (Figure 19); not surprisingly, larger colonies result in more phage production. Thus, reducing the variability of colony size can improve overall diversity of the library and minimizes the effects of a phage clone overcoming the population simply due to growth rate. It is unlikely that the vast variability in colony sizes stems solely from codon usage; regardless the K91+ cells mitigate this colony size amplification bias.

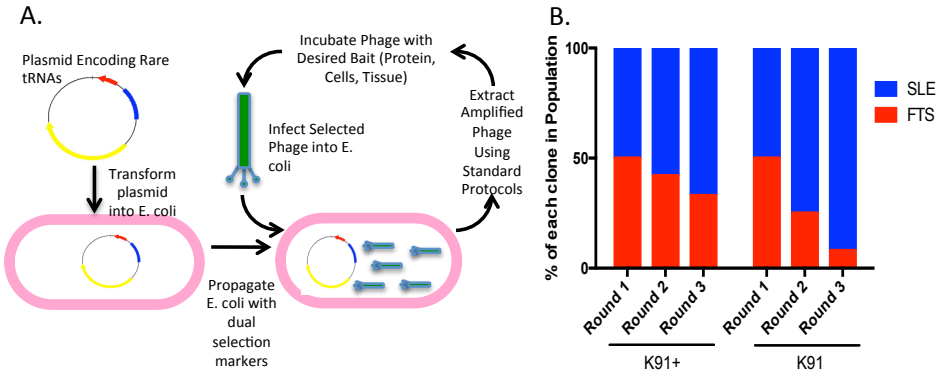

C.

Phage	Peptide Sequence	R Codon	(K91+Titer)/(K91 Titer)
SLE	SLEEEMK**R**TGGKPVSVGGVA	CGG	1.02 ± 0.011
FTS	FTS**R**NAHTEPSEAETNSVQA	AGG	1.90 ± 0.006
SLE	SLEEEMK**R**TGGKPVSVGGVA	AGG	1.71 ± 0.072
FTS	FTS**R**NAHTEPSEAETNSVQA	CGG	1.04 ± 0.049

Figure 18. Transformation of K91 cells with pRARE increase amplification of a phage clone that contains a rare codon A) Scheme outlining the method to reduce phage amplification bias. K91 E coli are transformed with pRARE which encodes for expression of 6 rare tRNAs and imparts chloramphenicol resistance. Once the cells are transformed, phage amplification occurs by standard protocols using chloramphenicol and tetracycline as section markers. **B)** Amino acid sequences of 20mer phage clones SLE and FTS. Arg are highlight in red to indicate the nucleotide sequence that encodes for the amino acid. The coding sequence for the Arg switched was switched for each phage clone using site-directed mutagenisis. Quantification of fold changes in titer difference between phage clones amplified in K91+ compared to K91 cells [(K91+ Titer)/(K91 titer)]. Mean fold change with STD is presented (n=3, $p<0.05$). **C)** Percentage of FTS clones (R encoded by AGG) in iterative rounds of amplification in competition with SLE (R encoded by CGG) (n=2).

Table 6. Nucleotide Sequence of Original and R Mutated Phage Clones

Phage Clone	Nucleotide Sequence*
FTS (original)	TTCTACTCTCACTCCTTTACGAGTAGGAATGCTCATACTGAGCCGTCGGAGGCTGAGACGAA TTCGGTTCAGGCTGCAAGT
FTS (mutated)	TTCTACTCTCACTCCTTTACGAGTCGGAATGCTCATACTGAGCCGTCGGAGGCTGAGACGAA TTCGGTTCAGGCTGCAAGT
SLE (original)	TTCTACTCTCACTCCAGTCTTGAGGAGGAGATGAAGCGGACGGGGGGGGAAGCCGGTGAGTGT GGGGGGGGTTGCGGCAAGT
SLE (mutated)	TTCTACTCTCACTCCAGTCTTGAGGAGGAGATGAAGAGGACGGGGGGGGAAGCCGGTGAGTGT GGGGGGGGTTGCGGCAAGT

*Sequenced using FD-Tet-F_1 primer

Table 7.
Characterization of Colonies of Phage Infected K91 and K91+ Cells

Phage		K91	K91+
FTS	Mean Size Units	1100	690
	Median Size Units	930	640
	Range Size Units	300-3300	400-1100
	Colony Count	110	200
SLE	Mean Size Units	1000	560
	Median Size Units	1000	510
	Range Size Units	500-1500	200-1000
	Colony Count	260	250
Library	Mean Size Units	2100	730
	Median Size Units	1900	710
	Range Size Units	200-5000	400-1200
	Colony Count	150	180

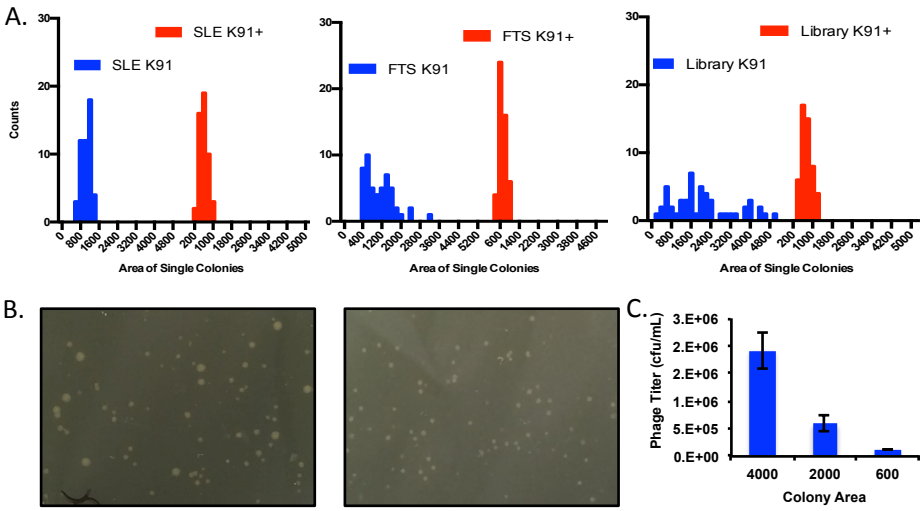

Figure 19. K91+ Cells Demonstrate Significant Increase in Uniformity of Phage Amplification. A) Histograms quantifying reduced variation in colony size in K91+ cells compared to K91 cells (50 colonies). Reduced variability in colony size indicates reduced overall phage amplification bias. X-axis represents arbitrary colony area as quantified in Image J. Detailed analysis of the data is included in Table 7. Panel 1, colony size of K91 and K91+ infected with phage SLE ($p=0.08$); Panel 2, colony size of K91 and K91+ infected with FTS ($p<0.01$); Panel 3, colony size of K91 and K91+ infected with complete library ($p<0.001$). **B)** Representative image of a complete 20mer pIII displayed phage library amplified in K91 and K91+ cells shows the range of colony sizes. **C)** Quantification of phage production by a single colony was determined to relate colony size to phage production (n=3).

DISCUSSION:

Our data suggest that transforming pRARE into K91 cells relieves a block in producing phage containing the AGG codon. This is critical as statistically, 47% of the phage clones in the initial library should contain at least one AGG codon. Poor production of these phage clones will collapse the diversity of the library and binding phage clones may be lost in the panning process. Additionally, each amplification of the starting library for further use will reduce diversity. There are certainly other factors that cause amplification bias but our approach can mitigate some loss of diversity.

Use of K91+ cells has another unexpected advantage that reduces amplification bias: reduction in colony size variability. Phage production is proportional to colony size, thus colonies with a growth advantage will produce more phage particles allowing a clone to dominate the pool over time. Small changes in growth rate between colonies can manifest in large differences in colony size. Phage infected K91+ cells have fewer "super-size" colonies that are larger than the mean. The reason for reduction in colony size in K91+ is not known but may be due to the expression and/or presence of 6 additional tRNAs or due to the addition of the second selection marker.

Antibody phage display protocols utilizing phagemid vectors may also benefit from amplification in E coli containing pRARE. Typical phagemid vectors derived from the pUC system (pCANTAB or pHEN) utilize ampicillin as a selection marker thus pRARE can be utilized directly in these systems by addition CAM; however, phagemid vector that utilize CAM as selection marker would require swapping of antibiotic resistance in pRARE or phagemid before use.

Here we present a simple method to reduce amplification bias in phage display protocols by addition of a plasmid coding for rare tRNAs. The protocol presented here requires only commercially available plasmids and the addition of a second antibiotic to decrease amplification bias. Although we transformed the pRARE plasmid into K91 E. coli it is feasible to transform the pRARE or similar plasmids into ER2738, TG1, or other E. coli commonly used in phage display. Future studies into mechanism of reduced amplification bias as well as creation of new libraries with K91+ are underway.

CHAPTER FIVE

Development of a Novel Immunotherapy for Cancer Based on H1299.3

INTRODUCTION:

Cell-mediated (CM) immunotherapies for cancer treatment are designed to activate the body's adaptive immune responses against a malignant growth.[14,49,81,86-88,97] Generally, the goal of a CM response is to activate a cytotoxic T-cell response against a tumor to eliminate cancer cells. The principle of these treatments is straightforward, yet current work studying the complexity of the tumor micro-environment[24,31,40,78,87,88,114,150,166] as well as methods that attempt to directly activate T cells against tumor antigens[20,29,32,77,87,114,117] demonstrate the difficulty associated generating an immune response against a tumor.

Several CM cancer immunotherapies exist today. Major examples include PD-1 inhibitors, injection of live virus or viral particles into tumors, and adoptive T-cell therapies.[32,40,42,46,86,87,97] However, concerns regarding efficacy, safety, and/or cost have limited the use of many of these treatments. Table 8 outlines the current major classes of immunotherapies underdevelopment as well as demonstrates the strengths and weaknesses of each class. To address the weaknesses identified in table 8, we sought to develop a novel treatment based on developing a fully synthetic, minimal delivery system that facilitates presentation of HLA class I restricted immunogenic peptides specifically on cancer cells without using live virus, viral subunits, or biologically derived material.

Table 8. Comparison of Current CM Immunotherapies

	Cancer Vaccines	Adoptive T cell Therapies	Immuno-modulators & Checkpoint Inhibitors	Viral Therapies	H1299.3 Targeted Immunoliposomes
No ex vivo manipulation of cells or patient derived materials			✓	✓	✓
Activates a rapid CTL immune response		✓	✓	✓	✓
Generates/Activates an antigen specific immune response	✓	✓		✓	✓
Targets a strong "non-self" antigen				✓	✓
Effective for cancers with low mutational loads (pediatric cancers)				✓	✓
Avoids the use of biologically derived materials					✓
Amenable to scalable chemical synthesis					✓

Based on these requirements, we developed a liposomal-based agent consisting of a neutral, stealth liposome that encapsulates a synthetically manufactured immunogenic HLA class I restricted peptide derived from measles virus.[27,81,87,88,97,131,146] In addition, the liposome has a targeting peptide on the external surface that both specifically accumulates in cancer cells and facilitates presentation of the immunogenic peptide in HLA class I molecules (Figure 20a). Thus, this treatment is designed to generate a secondary CM immune response specifically against the tumor if the patient was previously vaccinated against or infected with measles.

In this proof of concept study, we synthesized a liposome that encapsulates H250,[37,51,87,97] an immunogenic HLA class 1 restricted peptide identified from measles hemagglutinin protein. The liposome is designed to specifically internalize in cancer cells by displaying the recently identified targeting peptide H1299.3 on the exterior surface (Figure 20b).[14,21,51,72,87,144] H1299.3 is a 20mer, cancer-specific targeting peptide that was recently identified by our group (please see chapter 2). The peptide was identified using a novel phage display technique that allows for selection of cancer-specific targeting peptides that preferentially internalize in cancer cells via a defined mechanism of endocytosis. This peptide was dimerized on a lysine core and is fully functional outside the context of the phage particle. The H1299.3 peptide accumulates specifically in a panel of NSCLC cell lines compared to a normal bronchial epithelial cell control cell line via a clathrin-dependent mechanism of endocytosis. In this study we demonstrate that H1299.3 facilitates functional presentation of an immunogenic antigen in both MHC and HLA class I molecules as indicated by $CD8^+$ specific IFNγ secretion. In addition, H1299.3 facilitated presentation

utilizes an autophagy-dependent mechanism. Finally, treatment with H1299.3 targeted liposomes containing H250 substantially reduces the growth rate of subcutaneous LLC1 tumors implanted in vaccinated C57BL/6 mice compared to treatment with vehicle control.

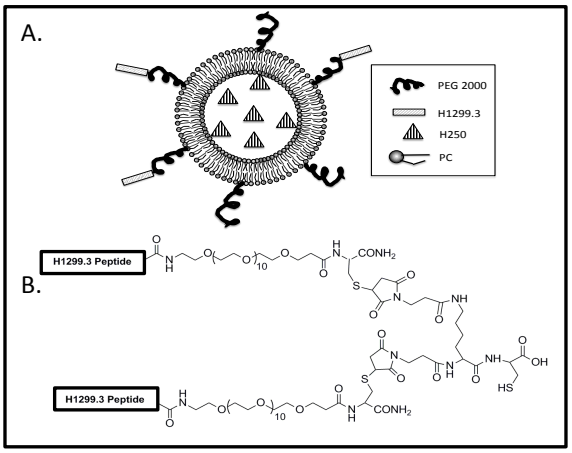

Figure 20. The Minimal Antigen Delivery System Consists of Three Components. A) PEGylated stealth liposomes are loaded with an immunogenic HLA class 1 restricted peptide derived from measles virus, named H250. The surface of the liposome is modified with a cancer-specific targeting peptide, referred to as H1299.3, which mediates binding and internalization of the liposome into the target cell. **B)** The structure of the H1299.3 peptide dimer. A unique thiol, indicated by the box, is incorporated into the lysine core for downstream conjugation to the liposome. Selection and characterization of the H1299.3 peptide is discussed in the Introduction Section and reported in reference 122.

MATERIALS AND METHODS:

Cell Culture and Animal Studies: Cells were cultured according to standard protocols.[40,71,86,144] NSCLC cells were generously provided by the Hamon Center for Therapeutic Oncology (UT Southwestern). LLC1 cells were purchased from ATCC (CRL-1642 lot 3067177). LLC1 cells were grown in RPMI 1640+Glutamate+Pen/strep + Sodium pyruvate + NEAA + 10% FBS (10% PBMC media). Both cell lines were regularly tested for *mycoplasma* contamination. Animal protocols were approved by the Institutional Animal Care and Use Committee at UT Southwestern Medical Center and SRI International. The protocols adhere to standards set forth by the Animal Welfare Act and the US government principals regarding the care and use of laboratory animals.

Peptide Synthesis: Peptides were manufactured using standard FMOC techniques. H1299.3 was manufactured according to previously published protocol.[71,86,144] H1299.3 sequence is LQWRRDDNVHNFGVWARYRL-(PEG_{10})-C- NH_2 and scrambled H1299.3 is QRYGDFNARWHLVRLNWRVD-(PEG_{10})-C-NH_2. The expected/observed masses for each sequence were 3,305.06/3,305.07 and 3,306.01/3,305.07 respectively. The peptides were dimerized on a mono-lysine core as previously reported.[14,36,86,87] The core contains a unique thiol for conjugation to the liposome. SMYRVFEVGV (H250) was also manufactured using FMOC techniques using Valine Wang resin. H250 was purified to greater than 99% purity using reverse phase HPLC. The expected/observed masses were 1,186.367/1,186.743, measured by MALDI TOF. For peptide loading assays H250 was reacted with AF488 functionalized with NHS ester (Life Technologies) according to manufacturer's protocol and purified to greater than 99% purity using rpHPLC.

Liposome Synthesis: Liposomes were manufactured using slightly modified protocol.[24,40,87,114,123,148,151] The liposomes contain 65% phosphatidylcholine, 32% cholesterol, 1.8% DSPE-PEG2000 and 1.2% DSPE-PEG2000 maleimide (Avanti). Lipids were dissolved in 2:1 mixture of chloroform:methanol. 2.5 mg of 1,1'-Dioctadecyl-3,3,3',3'-Tetramethylindotricarbocyanine Iodide (DiR, Molecular Probes) and 1 mg of H250 per 200mg of lipid were added to the lipids dissolved in solvent (Table 9a). Lipophilic DiR was used to track liposomes as well as to quantify relative lipid dosing. This mixture was evaporated under a stream of N_2 at 40-45°C to form a lipid film. Films were rehydrated in phosphate buffer (13mM KH_2PO_4, 54 mM$NaPO_4$, pH=7.4) and emulsified by vortexing. To facilitate peptide loading the emulsion was subjected to 3-4 freeze/thaw cycles alternating between liquid N_2 and 40°C water bath. The lipid solution was sonicated for 1 hr. and extruded 7-10 times through a 0.1 μm filter at 45°C to form uniform liposomes. Liposome size was measured via dynamic light scattering (DLS) using a Zetasizer (Malvern). Following liposome formation the buffer was exchanged to PBS using PD-10 gel filtration columns (GE Heathcare) and then concentrated using 50,000 Dalton MWCO filter (Millipore). For the peptide loading experiments a small amount of H250-AF488 was added to the solvent while manufacturing the lipid film. The input and output fluorescent signals were used to calculate liposome loading according to standard protocol.[40,86,87,114,123] We observed 58% loading of SMYRVFEVGV using SMYRVFEVGV-AF488 (Table 9b). H1299.3 dimer was attached to the liposome with cysteine maleimide chemistry, using fresh lyophilized H1299.3 stored at -20°C for each assay. After labeling potentially unreacted maleimide moieties on the liposomes were quenched using β-mercaptoethanol.[40,86,87,138]

Lymphocytes Isolation: Lymph nodes were harvested from vaccinated C57BL/6 mice then mashed through 70 μm cell strainer. Flow through cells were washed 2 times then frozen in FBS supplemented with 10% DMSO. Before use in assays frozen lymphocytes were thawed and re-suspended in RPMI 1640 +Glutamate + Pen/strep + Sodium pyruvate + NEAA + 10% FBS (10 % PBMC media). These cultures were then supplemented with 10 μM H250 and 200 units IL-2 and expanded for 12 h at 37°C, 5% CO_2. Lymphocytes were then washed 3 times, re-suspended in 10% PBMC media, and then used in co-culture experiments described in the next section.

Isolation and characterization of human PBMCs: We harvested PBMCs from anonymous donor blood clones according to IRB regulations. PBMCs were isolated using Ficoll-Paque Plus method (GE Healthcare).[40,51,87,146] PBMCs were frozen in FBS+10% DMSO and thawed fresh for each assay. PCR based HLA typing was performed according to previously published studies.[3,37,87,91,97,115] PBMCs from donors were cultured with 1μM of H250 for 72 hrs. and levels of IFNγ in the supernatant were quantified by ELISA. Prior to use in co-culture assays PBMCs were thawed, re-suspended in 5% PBMC media supplemented with 200 units of IL-2 and 10 μM H250, and expanded for 12 hrs. at 37°C, 5% CO_2. PBMCs were then washed 3 times before use in co-culture assays.

Co-culture Experiments: Antigen presenting cells (APCs) were seeded at either 1,000 or 10,000 for H1993 or LLC1 cells, respectively, into 96 well round bottom plates then cultured O.N. The next day cells were treated with 5 μL of liposomes (~1,500 AFU using ex/em = 540/590nm to quantify the amount of DiR as surrogate measure for lipid) for 3 hr. in complete media. Cells were then washed 3-times, 5 minutes/wash. Due to semi-adherent

nature the LLC1 cells, these cells were spun down for 5 minute at 2,000 rpm between washes whereas this procedure was unnecessary for H1993 cells. Murine lymphocytes (5×10^5) were added to LLC1 cells that were treated with targeted liposomes containing immunogenic peptide.

For H1993 APCs previously treated with targeted liposomes containing immunogenic peptide, 1×10^6 human PBMC were added. Both cell types were incubated together for 72 hrs. before supernatants were harvested and analyzed for IFNγ or TNFα secretion via ELISA using manufacture's protocol (Becton Dickerson).

CD8 depletion: For $CD8^+$ cell depletion human or murine anti-$CD8^+$ antibody was immobilized on magnetic bead via NHS ester linkage (Thermo Pierce). Post expansion, PBMCs or mouse lymphocytes were incubated with beads at RT with gentle rocking for 30 minutes. Beads were separated using a magnet and the supernatant was collected. The beads were washed 3 times and the residual leukocytes were counted and used in $CD8^-$ assays.

Pharmacological inhibitor assays: LLC1 cell were pre-incubated with pharmacological inhibitors for 30 minutes. We used 100 μM chlorpromazine, 20 μM Nystatin, 55 μg/mL Chloroquine, and 200 nM Wortmannin. After 30 minutes, 5 μL of H1299.3 targeted liposomes containing H250 (~1,500 AFU) was added and incubated for 3 h still in the presence of inhibitor. After 3 h cells were washed 3 times followed by continued incubation with inhibitor for an additional 12 hrs. Under these conditions we observed minimal cytotoxicity at 15.5 hrs. post initial treatment with inhibitors (Data not shown). LLC1 APCs were then fixed in 3.7% formaldehyde and washed 1 time before being co-cultured with lymphocytes using the above protocol.

siRNA Treated APCs: LLC1 or H1993 cells were treated for 4 hrs. with 1 μL of 20 μM siRNA oligo against ATG7 or a control siRNA using RNAi Max (Life Technologies) transfection reagent in RPMI 1640 according to manufacturer's protocol. The cells were incubated for an additional 72 hrs. then used for western blot analysis to quantify protein levels of ATG7 using rabbit primary Ab (Cell Signaling – (D12B11) Rabbit mAb #8558) and anti-rabbit secondary Ab (Biorad)[14,21,72,86,87], or cells were plated for the co-culture assay described above.

Confocal Microscopy for co-localization: Live cell confocal microscopy was performed using a Nikon TE200-E laser scanning confocal microscope, through a 30μm pinhole visualizing the blue, green, and red channels using 408 nm, 488 nm, and 543 nm lasers for excitation, respectively using 60x objective. H1299.3 and scrambled H1299.3 dimers were covalently attached to AF546 C_5 Maleimide (Life Technologies) using cysteine maleimide chemistry as previously published.[40,71,86,144] Equal concentrations of H1299.3 and scrH1299.3 were used in all microscopy assays. H1299.3 was dimerized and covalently attached to AF546 as previously published.[12,71,86,97,144] For Lamp-1 co-localization studies, H1993 or LLC1 cells were treated with BacMam 2.0 system (encoding for Lamp1-GFP 24 hrs. prior to imaging and plated on poly-d-lysine coated dishes (Mattek). H1299.3 or scrH1299.3 –AF546 was added in complete media to cells to a final concentration of 100 nM and incubated for 1 hr. Hoechst 33342 was added for 10 minutes prior to imaging to visual nuclei. For LC3B assays, H1993 and LLC1 cells were transfected with a GFP-LC3B lentiviral construct (Courtesy of Dr. Luis Franco) then sorted based on GFP fluorescence using MoFlo system.

GFP-LC3B cells were treated with 100 nM of H1299.3 or scrH1299.3 –AF546 for 1 hr. then imaged using parameters outlined above.

Murine vaccinations: Wild-type C57BL/6 mice lack the Slam receptor (CD150) that facilitates internalization of measles virus. Therefore to vaccinate these mice against the immunogenic measles peptide of interest we adopted a peptide in adjuvant based approach. We synthesized the highest predicted MHC class 2 binding peptide that contained the SMYRVFEVGV sequence using SYEPEITHI software, PSMYRVFEVGVIRNP, using standard FMOC chemistry. We emulsified PSMYRVFEVGVIRNP in Complete Freund's Adjuvant and vaccinated subcutaneously over the scapular draining lymph nodes (100 μL/mouse, 50 μg of PSMYRVFEVGVIRNP/mouse). Two weeks post first vaccination, the vaccination was repeated using Incomplete Freund's Adjuvant. At 4 and 5 weeks post vaccination, lymph nodes were harvested, processed and stimulated with the MHC class 1 restricted peptide SMYRVFEVGV (H250). After 72 hrs. of incubation, levels of secreted IFNγ were measured using ELISA. An increase in IFNγ secretion was observed at both 4 and 5 weeks post-vaccination compared to control cultures not treated with H250 as well as control mice vaccinated with adjuvant but not PSMYRVFEVGVIRNP peptide (Figure 21d).

Subcutaneous tumor growth assay. C57BL/6 were vaccinated according to the method outlined above. At 3-4 weeks post initial vaccination mice were implanted with 5*10^5 LLC1 cells in the hind flank. LLC1 tumors were allowed to grow for one week until easily palpable (~150 mm^3). Five mice in each group were then treated every other day with H1299.3 targeted liposomes +/- immunogenic peptide I.V. (~10,000 AFU 100 μL, tail vein). Mouse weights and tumor volume measurement were made every other day using scales and

calipers, respectively by a blinded measurer. Tumor volumes were calculated using the formula V= π/6*(L*W)^(3/2).[36,86,144] At the study endpoint LLC1 tumors were explanted and weighed.

Ex vivo H250 presentation assay: Non-vaccinated C57BL/6 female mice bearing subcutaneous LLC1 tumors were injected I.V. 3 times, every other day with either H1299.3 targeted liposomes containing H250 or vehicle control lacking H250. Tumor and liver from each group was harvested into cold RMPI, mashed using a syringe plunger then incubated with collagenase (3mg/mL Sigma) for 1 hr. at 37°C. Cells were then passed through 70 µm cell strainer. Cells were washed 2 times with 5% PBMC media and counted. 10,000 tumor or hepatocyte cells were then incubated with 5*10^5 PBLs from vaccinated C57BL/6 mice for 72 hrs. at 37°C, 5%CO_2. IFNγ secretion was measured in co-culture supernatants via manufacture's protocol (Becton Dickinson)

Liver Toxicity Assays: Non-vaccinated C57BL/6 female mice bearing subcutaneous LLC1 tumors were bled prior to treatment using submandibular technique and serum was separated via a collection tube. Animals were then injected I.V. 3 times every other day with either H1299.3 targeted liposomes containing H250 or Vehicle control lacking H250. Eight hours post last injection Animals were bled again serum was isolated using collection tube. Serum samples were analyzed for AST and ALT at the SRI Clinical Analysis Laboratory.

Sectioning and imaging LLC1 tissue: LLC1 tumors at the study end point were explanted then flash frozen in liquid N_2 in OCT cutting medium. Tumor were sectioned on a Leica cryostat (8 µm slices) and mounted onto glass microscope slides. The slides were fixed in cold 80% acetone then stained with murine anti-CD8 antibody conjugated to FITC according

to manufacturer's protocol. Slides were then treated with vectashield fluorescence mounting medium containing DAPI. 20x images were then taken on a Leica DMI6000 inverted fluorescent microscope using blue and green channels. $CD8^+$ cells present in the control and treated tumors were quantified. Five representative fields were counted from each group spanning from tumor periphery to the center of each tumor.

Organs, sectioned to observe gross organ abnormalities, were harvested and flash frozen in LN_2. Embedding, frozen sectioning, and H&E staining were performed via standard protocol at the University of Virginia Research Histology Core. 20x representative images are displayed.

Statistics: Statistics were performed using Excel or Graphpad. For ELISA data a minimum of three replicates were performed in each experiment with a minimum of two independent experiments for each condition. Data is represented as means with standard error of the mean. Two sided T-tests were used to determine significant differences with a p-value ≤ 0.05 considered significant. For subcutaneous tumor growth assays 5 animals were measured in each group. Paired T-tests were used to determine significance with p-value ≤ 0.05 considered significant. Data is presented as mean tumor volume for each group with standard deviation. A single * is used to denote p-value < 0.05 while ** is used to denote p-value < 0.01.

RESULTS:

Generating a Targeted Liposome for Viral-Antigen Presentation Specifically in Cancer Cells. The first goal of this study is to create a synthetic delivery system that is suitable for

specific delivery of antigenic cargo into cancer cells. The vehicle needs to have high payload capacity and shield the immunogenic peptide cargo without modification as presentation in HLA class I molecules is restricted by size and position of amino acid residues.[28,86,123,148,151] Therefore we decided to utilize liposomes. Liposomes are readily manufactured from synthetic material, easily loaded with synthetic peptide, and amenable to modification with targeting ligands.[40,71,86,123] Further, liposomes accumulate passively in tumors based on the enhanced permeability and retention (EPR) effect, potentially enhancing the specificity of the treatment.[59,86,138] We manufactured 100 nm stealth liposomes that encapsulate a synthetically manufactured 9mer immunogenic peptide, H250 with a loading efficiency of approximately 60 % (Table 9, Figure 22). DSPE PEG2000 modified with maleimide is incorporated into the lipid formulation to allow for conjugation of a thiol containing targeting ligand to the liposome (Table 9).[40,51,71,72,144]

Table 9. Characteristics of Immunoliposomes

A.

Liposome Composition
65% Phosphatidylcholine (Soy)
32% Cholesterol
1.8% DSPE – PEG2000
1.2% DSPE – PEG2000 Malemide

B.

Loading of HLA Class 1 Restricted Peptides*		
58%	SMYRVFEVGV	H250

*Measured by Doping in Fluorescently Labeled Peptide

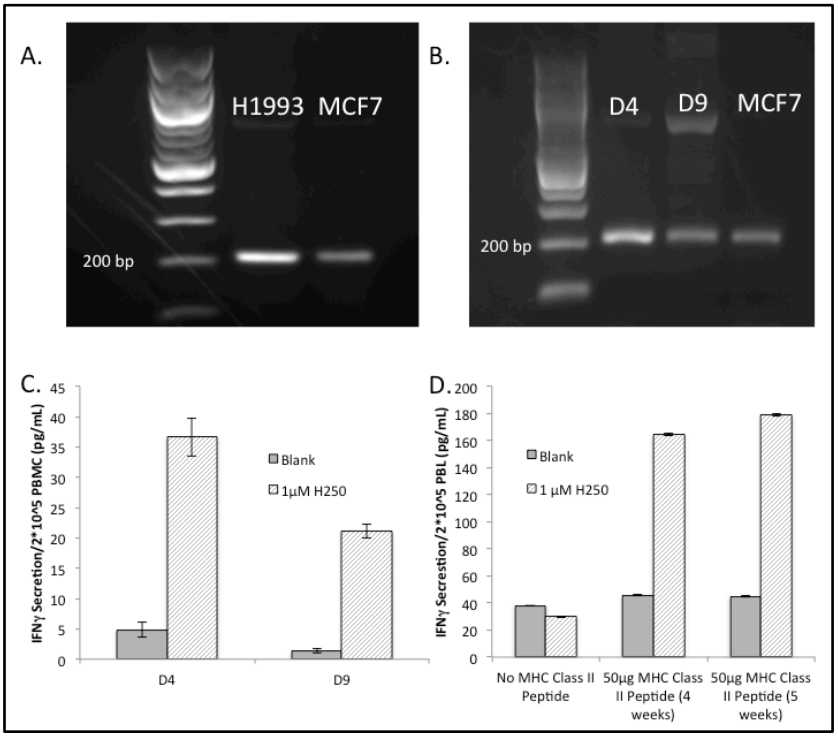

Figure 21. Characterization of Human and Murine Immune and Antigen Presenting Cells. **A**) Results of PCR based HLA typing to identify H1993 as a NSCLC human cell line that is HLA A*02 positive to serve as APC. **B**) Results of PCR based HLA typing to identify human PBMCs that are HLA A*02 positive to use in co-culture assays. **C)** IFNγ secretion of D4 and D9 PBMCs when cultured with 1 μM of H250 peptide or without addition of H250 (Blank). **D)** C57BL/6 mice were vaccinated with 50 μg of PSMYRVFEVGVIRNP (termed MHC Class II Peptide) in CFA followed by boast at 2 weeks of 50 μg peptide in IFA. Lymphocytes harvested from vaccinated mice at 4 and 5 weeks post vaccination generated robust IFNγ response from lymphocytes stimulated with HLA Class 1 restricted H250 peptide compared to lymphocytes not cultured with H250 peptide (Blank).

A.

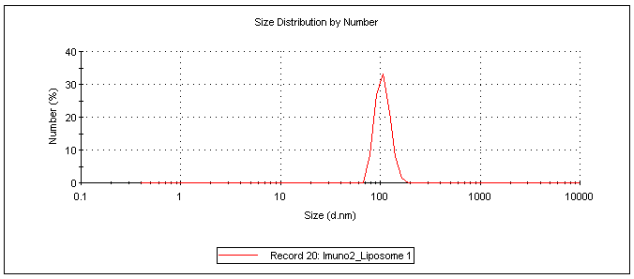

B.

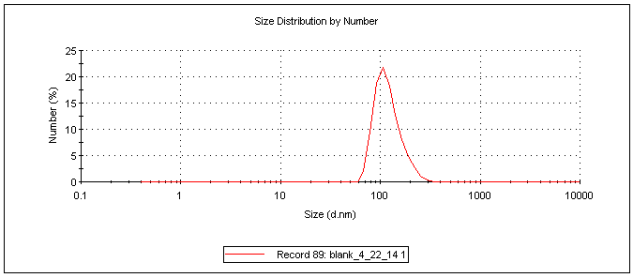

Figure 22. Liposome Size. Liposome size and distribution is measured by DLS using Zetasizer of both **A)** H250 loaded and **B)** Non-loaded liposomes.

The H1299.3 Targeting Ligand Specifically Accumulates in Cancer and Facilitates HLA Class I Presentation. In order to quantify the ability of the liposomal formulation to facilitate presentation of H250 immunogenic peptide, we first needed to develop a system to determine if H250 is present in the cleft of HLA class I molecules. H250 is an immunogenic peptide identified from sequencing peptides present in HLA A*0201 molecules following measles infection.[3,4,13,91,97,115] Thus we identified PBMCs from anonymous donors that were HLA A*02 positive (Figure 21b), and determined if these donors were vaccinated against measles by culturing donor PBMCs with free H250 peptide and measuring IFNγ secretion (Figure 21c). We successfully identified 2 donors that were HLA A*02 positive and had previously been vaccinated against measles virus. PBMCs from these two donors, D4 and D9, were used in the subsequent assays to identify and characterize a cancer specific targeting peptide that can facilitate HLA class 1 presentation. Similarly, an appropriate cancer cell line was needed to serve as the antigen presenting cells. For this, we utilized the human NSCLC cell line, H1993, which we determined to be HLA A*02 positive (Figure 21a).

Next, we screened known cancer-specific targeting peptides to identify a targeting peptide that can facilitate presentation of H250 from the targeted liposomal formulation in HLA class I on the external surface of the cell. Panels of cancer targeting peptides have been identified by our group and others; therefore we identified three different cancer-specific targeting peptides that internalize into H1993 that have been previously published: H1299.2, H2009.1, and H1299.3. Each of these peptides specifically internalize in NSCLC cell lines compared to normal bronchial epithelial cells (Figure 23).[21,86,150] The peptides were

conjugated to the surface of the liposome by a thiol-ester linkage resulting from a Michael addition of a single sulfhydryl group on the targeting peptide to the maleimide present on the liposome. A peptide that does not internalize into H1993 cells, H460.1, was utilized a control.[40,45,57,68,75,86,94]

To screen each targeting peptide, H1993 cells were treated with H1299.2, H2009.1, H460.1, or H1299.3 targeted liposomes containing H250 for three hours. The cells were then washed to eliminate non-internalized/bound liposomes and then co-cultured with donor PBMCs (outlined above) for 72 hrs. Cell culture supernatants were harvested and analyzed for IFNγ secretion via ELISA as a measure of T cell activation. Free H250 peptide served as a positive control in this assay. As demonstrated in Figure 24a, only the H1299.3 targeted liposomes containing H250 resulted in a significant increase in IFNγ secretion compared to controls ($p<0.05$). Liposomes targeted to H1993 cells with H1299.2 or H2009.1 peptides were unable to induce IFNγ secretion in these co-culture experiments despite their ability to internalize the liposome. These data identify H1299.3 as a candidate targeting peptide as well as imply internalization of the antigenic peptide containing liposomes is not sufficient for presentation; the targeting peptide must deliver H250 to an intracellular location that intersects with the HLA class I presentation pathway.

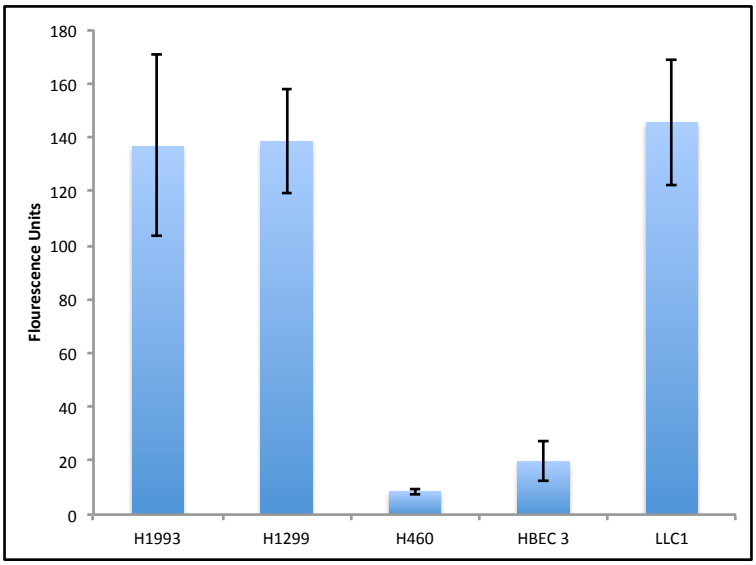

Figure 23. H1299.3 peptide significantly accumulates in both NSCLC H1993 cells as well as murine Lung cancer line LLC1. Fluorescently labeled H1299.3 peptide accumulates in Non-small cell lung cancer (NSCLC) cell lines H1299 and H1993 as well as murine lung cancer line LLC1. We observe minimal accumulation in NSCLC H460 as well as bronchial epithelial line HBEC3 that serves at "normal tissue" control.

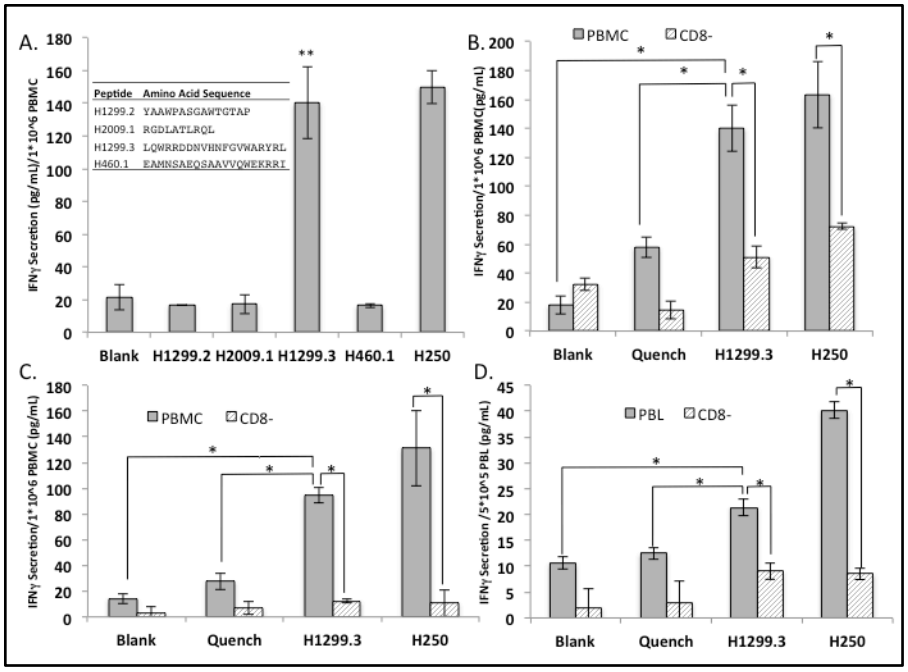

Figure 24. H1299.3 Targeting Peptide Facilitates Presentation of Encapsulated H250 Immunogenic Peptide in MHC and HLA Class I Molecules. **A)** H1993 cells were treated with liposomes containing H250 targeted by previously established cancer specific targeting peptides that internalize into H1993 (H1299.2, H2009.1, and H1299.3) and one non-internalizing ligand (H460.1) as indicated on the X-axis. Treated H1993 cells were then co-cultured with D4 PBMCs (described in Figure 2b,c) and culture supernatants were analyzed for IFNγ secretion. Free H250 peptide (5 μM) is used as positive control (H250 labeled group). The inset table contains amino acid sequence of the targeting peptides used in this figure. **B)** H1993 cells treated with Blank liposomes (lacking both H250 and H1299.3), Quenched liposomes (containing H250 but lacking H12299.3 targeting peptide), or H1299.3 targeted liposomes containing H250. Post treatment, H1993 cells were then co-cultured with D4 PBMCs and culture supernatants were analyzed for IFNγ secretion. Free H250 peptide (5 μM) is used as positive control. CD8- group indicate co-culture with CD8+ depleted PBMCs. **C**) Repeat of assay presented in B. using second human donor PBMCs, termed D9. **D)** LLC1 cells treated with same groups as presented in B., then co-cultured with lymphocytes from H250 vaccinated C57BL/6 mice and analyzed for IFNγ secretion. CD8- group indicates co-culture with CD8 depleted PBLs. Single * indicates a p-value < 0.05, and ** indicates p-value < 0.01.

HLA and MHC Class I Presentation is H1299.3 Dependent. To confirm H1299.3 targeting peptide facilitates HLA class 1 presentation, H1993 cells were treated with liposomes devoid of both targeting and immunogenic H250 peptides (Blank) or H250 loaded liposomes that lack the H1299.3 targeting peptide (Quench) and compared to the H1299.3 targeted liposomes containing H250 (H1299.3). Treated H1993 cells were co-cultured with donor PBMC as described above. Once again, as demonstrated in Figure 24b, only H1299.3 targeted liposomes containing H250 resulted in a significant increase in IFNγ secretion ($p<0.05$). These data provide further support that presentation is dependent on both the H250 antigenic peptide and H1299.3 targeting peptide. These results were duplicated using a second PBMC donor, D9, demonstrating presentation is not patient specific (Figure 24c). Depleting CD8+ T cells from the PBMC cultures results in loss of IFNγ secretion in both human samples ($p<0.05$) (Figure 24b,c). These data indicates that H250 is present in HLA class I molecules and the H1299.3 targeted liposomes containing H250 facilitate activation of a CD8+ memory T cell response in individuals previously vaccinated against measles.

To further characterize the immune response generated by this treatment, we quantified the levels of secreted TNFα in co-culture supernatants. Similar to the above mentioned data, we observed a significant increase in TNFα secretion in H1993 cells treated with H1299.3 targeted liposomes containing H250 relative to H1993 cells treated with blank liposomes in both human donors (Figure 25a,b, $p<0.05$). Upon CD8+ depletion, a reduction in TNFα secretion is observed following treatment of H1993 cells with H1299.3 targeted liposomes containing H250 (Figure 25a, $p<0.05$).

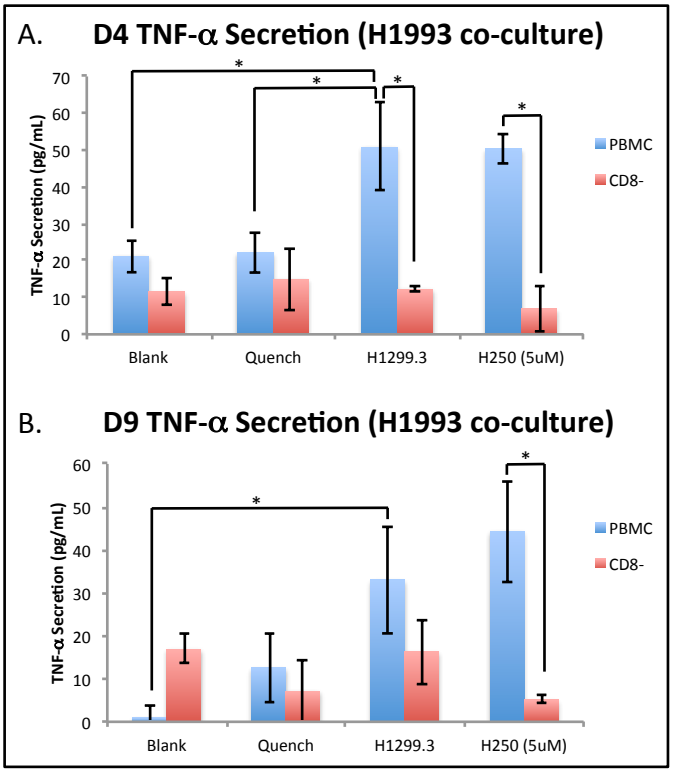

Figure 25. TNFα Secretion from Human co-Culture Assays. A) H1993 cells treated with Blank liposomes (lacking both H250 and H1299.3), Quenched liposomes (containing H250 but lacking H12299.3 targeting peptide), or H1299.3 targeted liposomes containing H250. Post treatment, H1993 cells were co-cultured with D4 PBMCs and analyzed for TNFα secretion. Free H250 peptide (5 μM) is used as positive control. CD8- group indicate co-culture with CD8+ depleted PBMCs. **B)** Repeat of assay presented in A. using second human donor PBMCs, termed D9. Single * indicates a p-value < 0.05.

To extend the breath of these studies we identified a murine lung cancer cell line derived from C57BL/6 mice, Lewis Lung Carcinoma 1 (LLC1) that internalizes the H1299.3 targeting peptide (Figure 23). We then generated murine $CD8^+$ T cells with TCR that recognizes MHC class I loaded H250[11,12,38,54,97,110,111,120] by vaccinating C57BL/6 mice with an extended version of H250 and subsequently harvesting lymphocytes as a source of $CD8^+$ T cells (Figure 21d). LLC1 cells were treated with control or H1299.3 targeted liposomes containing H250, washed, and then incubated with mouse lymphocytes in a similar manner to the human co-culture assay presented above. Similar to the human data, treatment with H1299.3 targeted liposomes containing H250 resulted in a significant increase in IFNγ secretion compared to controls ($p<0.05$, Figure 24d). Depleting $CD8^+$ T cells from the lymphocyte pool resulted in significant loss of IFNγ secretion similar to the human data ($p<0.05$). Thus, the H1299.3 targeted liposome system is able to deliver H250 for functional presentation in both MHC and HLA class I molecules.

H1299.3 Facilitated HLA class I Presentation Requires Autophagy. To determine the mechanism by which H1299.3 facilitates presentation of H250 in HLA class I molecules, we characterized the subcellular accumulation of the H1299.3 peptide. Previous data indicated the newly identified H1299.3 peptide co-localizes with Lamp-1[29,76,77,85,86,144] whereas the other cancer specific targeting ligands H1299.2 and H2009.1 accumulate in perinuclear regions.[23,28,86,101] Therefore we reasoned that the subcellular trafficking pattern is crucial to H1299.3 facilitated presentation.[28,59,71,86,93] Similar to previous results, H1299.3 and Lamp-1 co-localize in both H1993 and LLC1 cell lines as determined by live cell laser scanning confocal microscopy (Figure 26e and g). However, these data do not offer a clear explanation

for mechanism of presentation. Lamp1 is a marker of both lysosomes and autolysosomes[59,109,110] raising the possibility that autophagy plays a role in this process. To test this hypothesis the imaging experiments were repeated using LLC1 and H1993 cells that contain a GFP-LC3B construct which is a marker for autophagosomes. Clear co-localization with LC3B puncti is observed in both cell lines indicating H1299.3 accumulates autolysomes (Figure 26a,c). Importantly, treatment of the corresponding cells with a scrambled sequence version of H1299.3 results in no significant peptide internalization and consequently, no co-localization with either Lamp-1 or LC3B (Figure 26b, d, f, and h). Together, the data show sequence dependent co-localization of the H1299.3 peptide in autophagosomes.

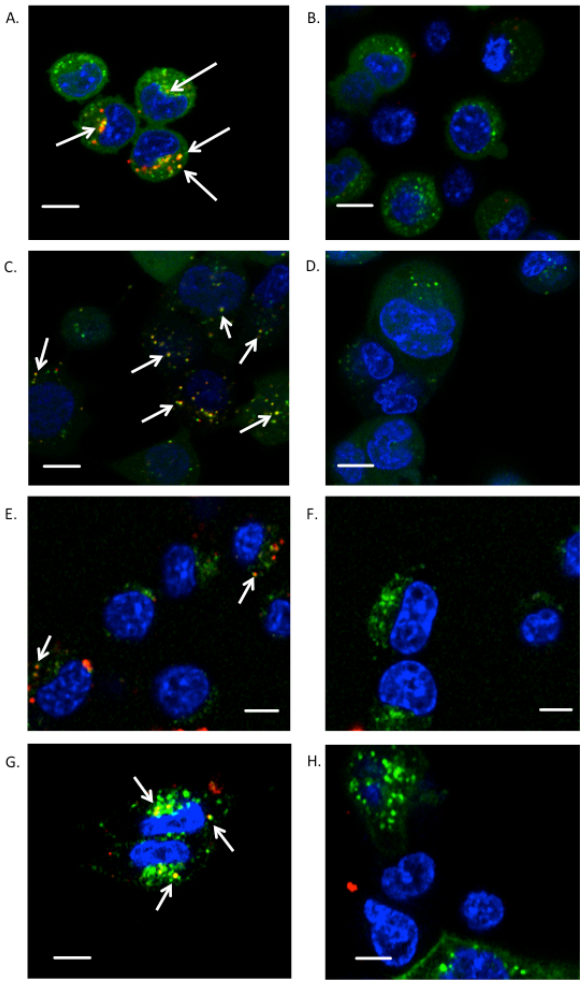

Figure 26. H1299.3 Co-localizes with Autophagic Vesicles. **A)** LLC1 cells expressing GFP-LC3B (green) are incubated with 100 nM of H1299.3-AF546 (red). Cells are imaged using live cell confocal microscopy. Blue represents nuclei stained with Hoechst 33342. White arrows indicate co-localization of the peptide and LC3B. **B)** LLC1 cells expressing GFP-LC3B treated with 100 nM scrambled H1299.3-AF546. **C)** H1993 cells expressing GFP-LC3B treated with 100 nM of H1299.3-AF546; white arrows indicate co-localization. **D)** H1993 cells expressing GFP-LC3B treated with 100 nM of scrambled H1299.3-AF546. **E)** LLC1 cells expressing Lamp1-GFP (green) via Bacmam 2.0 system. Cells are then treated with 100 nM of H1299.3-AF546 (Red) then imaged using live cell confocal microscopy. Blue indicates nuclei stained with Hoechst 33342. White arrows indicate co-localization. **F)** LLC1 cells expressing Lamp1-GFP treated with 100 nM scrambled H1299.3-AF546. **G)** H1993 cells expressing Lamp1-GFP using Bacmam 2.0 system, treated with 100 nM H1299.3-AF546. White arrows indicate co-localization. **H)** H199.3 cells expressing Lamp1-GFP treated with 100 nM scrambled H1299.3-AF546. Scale bars = 20 µm.

If H1299.3 accumulates in autophagic vesicles, perturbing autophagy should result in loss of H250 presentation in MHC class I molecules following treatment with H1299.3 targeted liposomes. LLC1 cells were treated with H1299.3 targeted liposomes containing H250 in the presence of the inhibitors, chloroquine, chlorpromazine, nystatin, and wortmannin. After allowing trafficking of the peptides to occur, the LLC1 cells were fixed and co-cultured with lymphocytes as previously described. Treatment with known inhibitors of autophagy, including wortmannin and chloroquine, resulted in significant reduction in IFNγ secretion compared to controls ($p<0.05$, 27a). Chlorpromazine, an inhibitor of clathrin-mediated endocytosis, reduced presentation. This is consistent with our previous results demonstrating that the H1299.3 peptide is internalized by a clathrin-mediated mechanism, and cellular uptake of the peptide is reduced in the presence of chlorpromazine.[86,144] Nystatin, an inhibitor of cholesterol dependent endocytosis exhibits no effect.

To further validate the role of autophagy in H1299.3 facilitated presentation, LLC1 cells were treated with siRNA targeting autophagy related protein 7 (ATG7). ATG7 specific knockdown in LLC1 cells by siRNA is quantified via western blot using β-actin as loading control (Figure 27c). Treatment with ATG7 specific oligos resulted in ~80% reduction in ATG7 protein levels whereas minimal decrease in ATG7 levels are observed using a control siRNA hairpin.[97,98,115] Knockdown of ATG7 significantly reduced IFNγ secretion in LLC1 cells incubated with H1299.3 targeting liposomes containing H250 compared to LLC1 cells not treated with siRNA or LLC1 cells treated control siRNA ($p<0.05$, Figure 27b). We repeated ATG7 knockdown assays in H1993 cells. Similar to LLC1 cells, we observed ~80% reduction in ATG7 protein levels in H1993 cells treated with siRNA oligos targeting ATG7

via western blot (Figure 27e). Treatment with control siRNA did not affect ATG7 levels. ATG7 knockdown in H1993 cells resulted a significant decrease in IFNγ secretion following treatment with H1299.3 targeted liposomes containing H250 and co-culture with D9 PBMCs compared to controls ($p<0.05$. Figure 27d). Thus, the microscopy and phenotype data imply that H1299.3 facilitates presentation of H250 via an autophagy dependent mechanism.

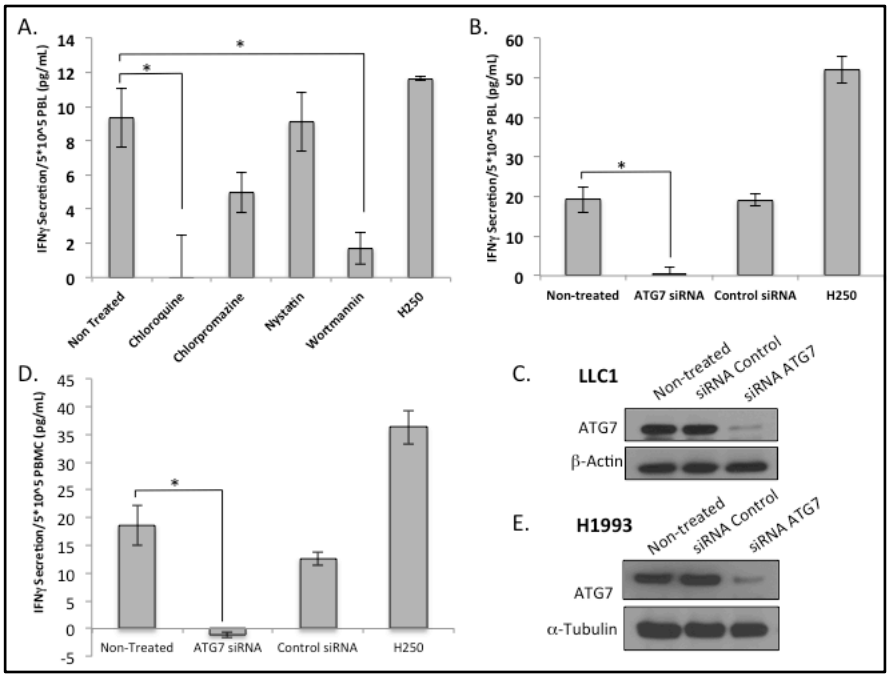

Figure 27. Pharmacological and Genetic Perturbation of Autophagy Results in Loss H1299.3 Facilitated Presentation. A) LLC1 cells are treated with H1299.3 targeted liposomes containing H250 in the presences of pharmacological inhibitors, fixed, washed and subjected to co-culture with PBLs. Co-culture supernatants were analyzed for IFNγ secretion. Fixed LLC1 cells incubated with free H250 peptide (5μM) served as positive control (labeled H250). **B)** ATG7 or control siRNA treated LLC1 are subjected to H1299.3 targeted liposomes containing H250 then co-cultured with lymphocytes and analyzed for IFNγ secretion. Free H250 peptide (5μM) is used as positive control. **C)** Western blot quantifying ATG7 levels in LLC1 cells treated with siRNA. β-actin levels are presented as loading control. **D)** IFNγ secretion from H1993 treated with siRNA against ATG7 then treated with H1299.3 targeted liposomes. D9 PBMCs were used in the co-culture assay and culture supernatant is analyzed for IFNγ secretion. Free H250 peptide (5μM) is used as positive control. **E)** Western blot quantifying ATG7 protein levels in H1993 cells treated with siRNA. A western blot demonstrating α-tubulin levels is presented as loading control. A single * indicates p-value < 0.05.

H1299.3 Targeted Liposomes Encapsulating H250 Reduce Tumor Burden In Vivo. Next we utilized H1299.3 targeted liposomes containing H250 in a murine model to determine efficacy of this platform as a CM immunotherapy. C57BL/6 mice were vaccinated against H250, as described above, then LLC1 cells were implanted subcutaneously into the hind flank. LLC1 tumors were grown until palpable (~150 mm^3) at which point mice were treated six times I.V. with H1299.3 targeted liposomes containing H250 or vehicle that lacked the H250 immunogenic peptide. We observed a significant decrease in LLC1 tumor growth rate in the treated group following the third treatment ($p<0.01$, Figure 28a). After explanting the tumors we observed >2-fold reduction in tumor weight and volume ($p<0.05$, Figures 28c, e, and Figure 29c).

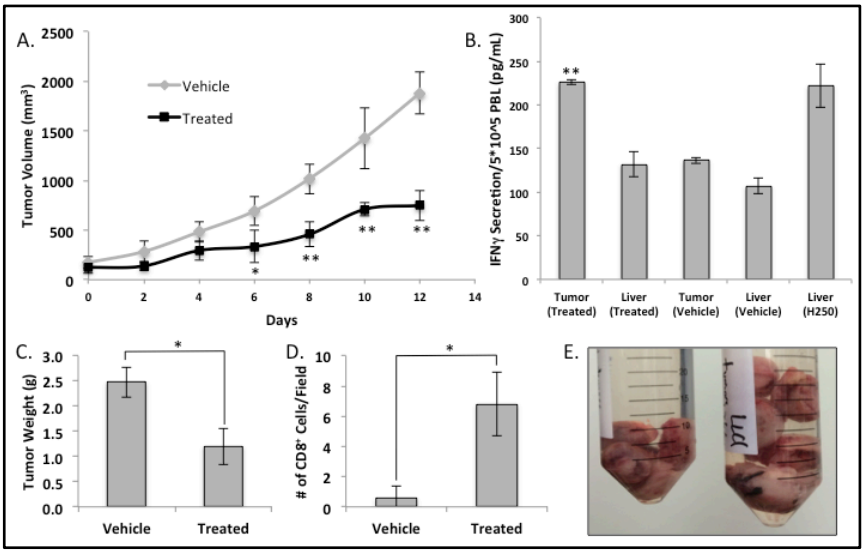

Figure 28. Treatment with H1299.3 targeted liposomes containing H250 results in significant reduction in LLC1 tumor growth in vaccinated C57BL/6 mice. **A)** Subcutaneous LLC1 tumor growth rate in C56BL/6 mice vaccinated against H250 that are treated every other day I.V. with H1299.3 targeted liposomes containing H250 as treatment group or lacking H250 as vehicle control (n=5). **B)** Ex vivo IFNγ secretion from tumor and liver cells derived from non-vaccinated C57BL/6 mice treated 3 times I.V. with either H1299.3 targeted liposomes containing H250 or vehicle control lacking H250. Isolated, in vivo treated cells, are cultured with PBLs from vaccinated C57BL/6 mice and IFNγ levels are quantified from co-culture supernatants. Free H250 peptide (5 μM) is used as positive control (labeled H250). **C)** Mean weights of explanted tumors separated by group. **D)** Quantification of $CD8^+$ cells present in tumor sections from either treated or control groups. Five fields were counted from each group. **E)** Picture of explanted LLC1 tumors with treated group on the left and vehicle group on the right. A single * indicates p-value < 0.05 while ** indicates p-value < 0.01.

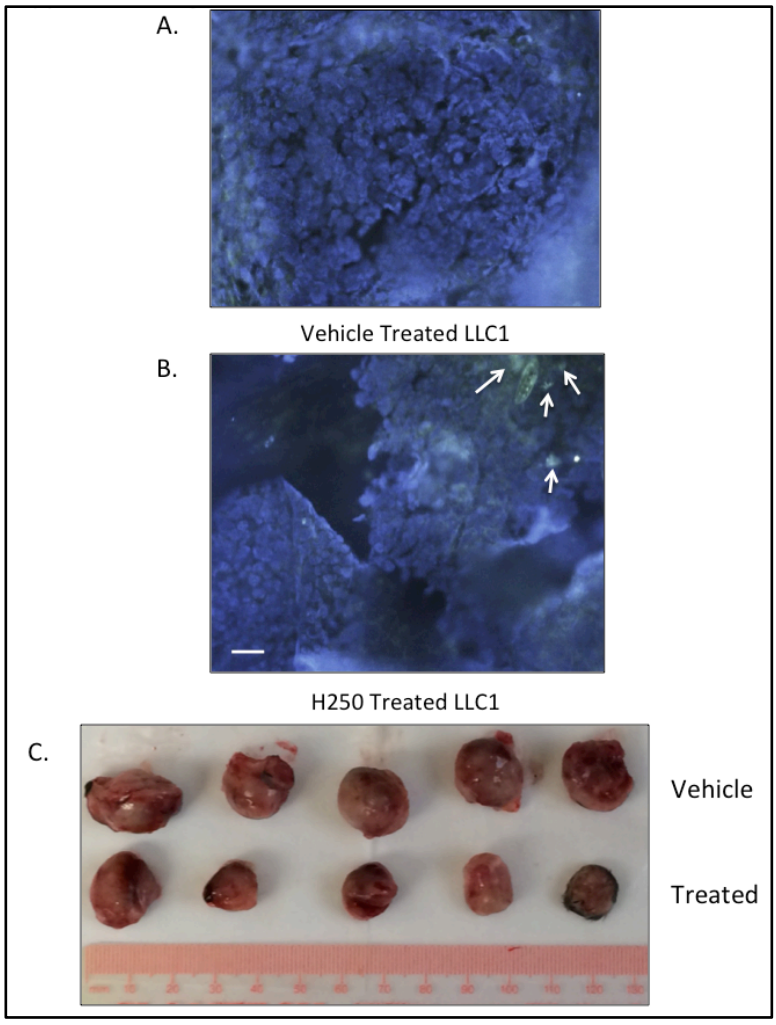

Figure 29. LLC1 tumor Characteristics. Representative Tumor Sections of LLC1 tumors stained with mCD8⁺ antibody. **A)** Tumor section from mice treated with vehicle. **B)** Tumor section from mice treated with H1299.3 targeted liposomes containing H250. White arrows indicate regions of CD8⁺ cell infiltration. Scale bar = 100 µm **C)** Picture demonstrating size of tumors explanted from C57BL/6

During the tumor efficacy studies, no significant difference in animal weight is observed between groups (Figure 30), and the animals demonstrate no weight loss. Together, these data suggest the animals suffer no gross toxicity from the treatment. None-the-less, liposomes are cleared via the liver raising the possibility of liver toxicity. As such, we quantified serum levels of AST and ALT in non-vaccinated mice containing subcutaneous LLC1 tumors following three treatments with either H1299.3 targeted liposomes containing H250 or vehicle control (Table 10). All values are within normal ranges indicting limited liver toxicity. Further, liver, kidney, heart and lung tissues were harvested, sectioned, and stained with H&E. Sections from these organs identified no gross abnormalities in either the treated or vehicle groups (Figure 31).

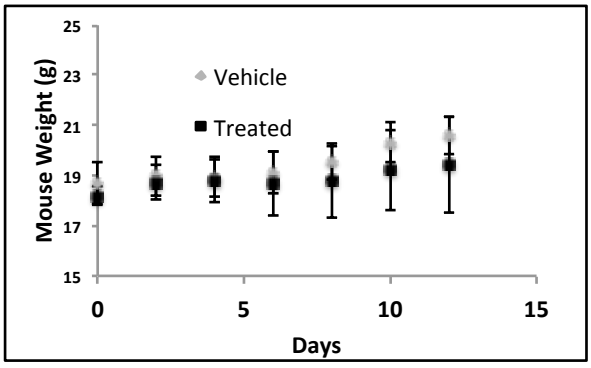

Figure 30. Toxicity Profile of H1299.3 Targeted Liposome containing H250 treatment. Murine weights from vaccinated C57BL/6 mice, bearing subcutaneous LLC1 tumors, treated with 6 doses of H1299.3 targeted liposomes containing H250 or vehicle control lacking H250.

Table 10. Livery Toxicity Profile of H1299.3 Targeted Liposome containing H250 Treatment

	Pre-Treatment	Treated	Vehicle
AST (U/L)	113	84	143
ALT (U/L)	33	28	40

*Normal Values from Charles Rivers for C57BL/6 mice
AST (U/L) = 127.58 ± 142.05
ALT (U/L) = 66.48 ± 184.87

Serum levels AST and ALT from non-vaccinated mice bearing subcutaneous LLC1 tumor treated with 3 doses of H1299.3 targeted liposomes containing H250 or vehicle control lacking H250.

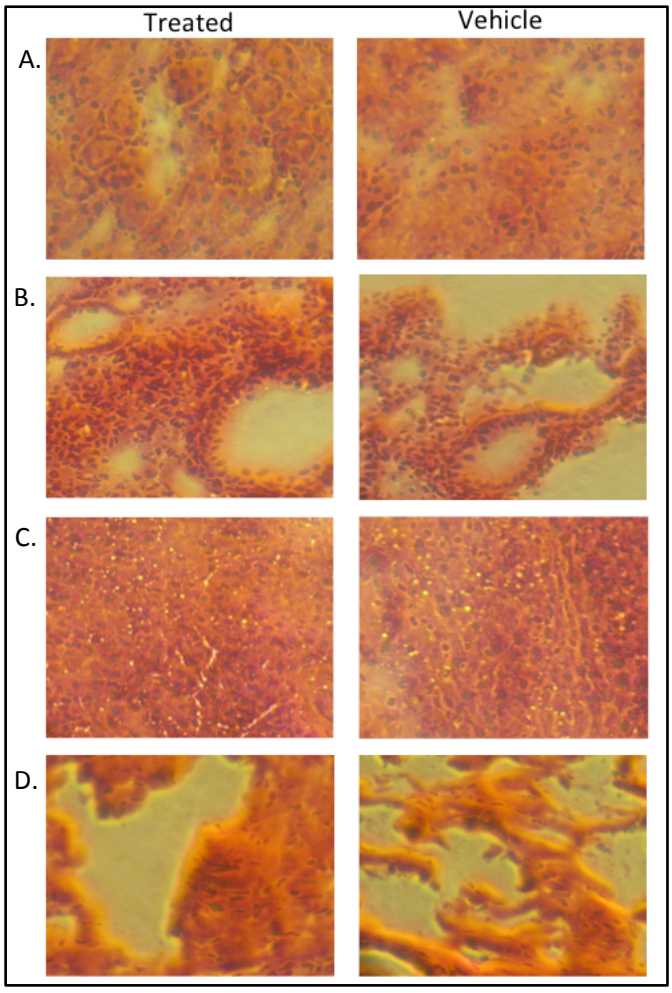

Figure 31. Histology of Organs Following Immunotherapy Treatment. A) Kidney tissue sectioned and stained with H&E from non-vaccinated mice bearing subcutaneous LLC1 tumor treated with 3 doses of H1299.3 targeted liposomes containing H250 (Treated)(Left) or vehicle control lacking H250 (Vehicle)(Right). **B)** Lung sections treated as in A. **C)** Liver sections treated and presented as in A. **D)** Heart sections treated and presented as in A.

Finally, to connect the in vitro data to the in vivo data tumors were sectioned and stained for $CD8^+$ cells. A 10-fold increase of $CD8^+$ cells is observed in tumors treated with H1299.3 targeted liposomes compared to vehicle treated tumors consistent with the in vitro data demonstrating a $CD8^+$ T cell response ($p<0.05$, Figures 29a,b, 23d). To further support that the H1299.3-targeted liposome delivers H250 in vivo, non-vaccinated mice containing subcutaneous LLC1 tumors were treated three times with either H1299.3 targeted liposomes containing H250 or vehicle control. The tumor and liver tissues from these mice were then harvested and single cell suspensions of tumor cells and hepatocytes were generated. These primary cells were directly utilized as APCs in the co-culture assays outlined above using lymphocytes from vaccinated C57BL/6 mice. Tumor cells treated with H1299.3 targeted liposomes containing H250 induced a significant increase in IFNγ secretion compared to vehicle treated tumor cells ($p<0.01$, Figure 28b). Thus, the H1299.3 liposomal formulation is able to deliver H250 to tumors and the H250 peptide is presented in MHC class I molecules on the tumor in vivo. By comparison, using the hepatocytes as the APC, there was no difference in IFNγ secretion levels in either group (Figure 28b). Thus, even if the liposomes accumulate in the liver, H250 is not presented in MHC class I as measured by the lack CM immune response generated against the liver cells. In sum, these data imply treatment with H1299.3 targeted liposomes containing H250 is non-toxic and H1299.3 can facilitate presentation of H250 preferentially in a tumor in vivo.

DISCUSSION:

Here we present a novel cancer immunotherapy based on developing a minimal delivery system to facilitate presentation of HLA class 1 restricted immunogenic peptide in cancer cells, resulting in a secondary immune response against a tumor. This approach bypasses the need to identify tumor-associated antigens or to generate a primary immune response against the tumor, which are major hurdles in cancer vaccine development. Unlike immunomodulators, the immune response generated by our liposomal delivery approach is antigen specific and does not involve an overall general activation of the immune response. This minimizes problems with auto-immune and off-target effects. This protocol also differs from current viral based immunotherapies, as viral products or live viruses are not employed, reducing safety concerns associated with these types of therapies. A potential downside with our approach is it is unlikely to generate inflammatory conditions that occur with viral infections, potentially reducing the potency of the immune response. In part, this problem is mitigated by utilizing a secondary immune response that requires less inflammatory inputs to generate an immune response. Furthermore, evidence exists that the tumor microenvironment exhibit inflammatory conditions in which case our therapy maybe using this condition for cytokine inputs.[16,150]

Utilizing a delivery ligand to facilitate HLA class I presentation has previously been achieved using Cholera or Shiga toxins fused to class 1 restricted immunogenic peptides.[45,68,94,124] Yet, these toxins accumulate indiscriminately in cells and are not targeted specifically to cancer cells. H1299.3 selectively accumulates in cancer cells and demonstrates limited binding to normal human bronchial epithelial cells thus potentially providing a greater therapeutic treatment window (Figure 23).[7,32,46,54,110,117] Furthermore, manufacturing

Cholera or Shiga toxin requires biological synthesis and concerns remain about immunogenicity of the toxin-carriers. In addition, this work, differs from hapten painting or antibody-recruiting strategies in which a targeting agent delivers a hapten to the cell surface, resulting in antibody recruitment. The therapy presented in this manuscript is designed to directly activate T cells via specific presentation of HLA class I restricted antigens in cancer cells via an internalization mechanism rather than generating antibody-dependent cellular cytotoxicity from hapten immobilization on the cell surface.[66,76,85]

H1299.3 utilizes an autophagy dependent mechanism to facilitate presentation of immunogenic peptides. Coupled with previous data, H1299.3 appears to internalize via clathrin-mediated endocytosis and traffic to lysosomes or autolysosomes. Autophagy plays an interesting role in cancer progression and metastasis and its role is still being elucidated. However it is clear that certain subsets of cancer up regulate autophagy. Thus it is possible we observe an additional level of selectivity (the first being selective internalization mediated by H1299.2) to restrict presentation of immunogenic antigen to cancer cells as our data indicates that the liposome containing immunogenic class 1 antigen both needs to internalize and be processed in autophagic vesicles. Autophagy is appreciated to be involved in classical class II presentation but its role in class I antigen presentation is still emerging. Our data here along with recent reports suggest that autophagy can also participate in class I presentation.[23,101] We hypothesize that H250 peptide is recycled back into the cytosol along with contents of the autolysosome thereby allowing for transport by TAP into the ER and subsequent presentation (Figure 32).[59,93] However, we cannot rule out other trafficking pathways that could facilitate antigen presentation. Data from this study including

microscopy, pharmacological inhibitors and siRNA experiments imply the necessity of autophagy but it is unclear the precise role of autophagy in the process of H1299.3 facilitated antigen presentation. Future studies may further elucidate the precise subcellular trafficking resulting in antigen presentation.

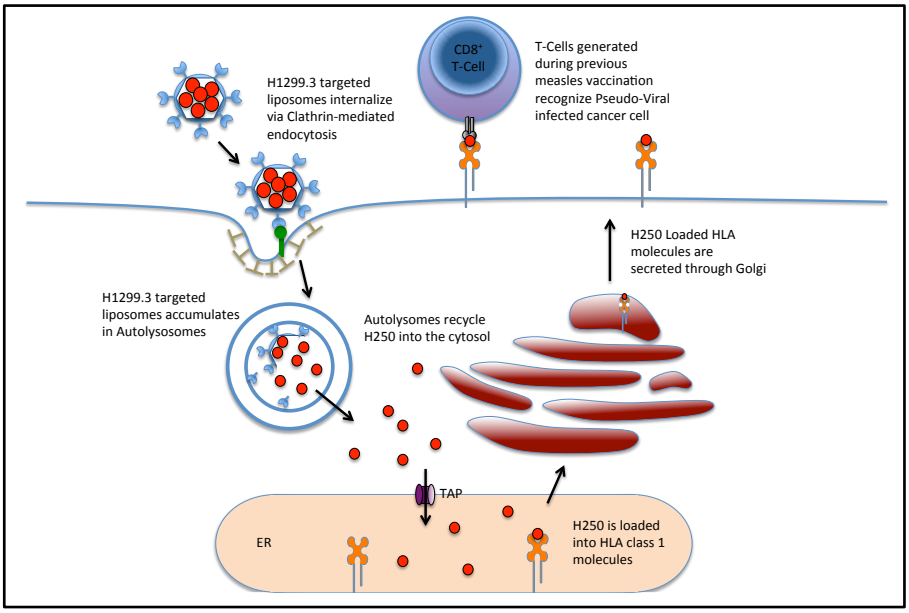

Figure 32. Theoretical model of H1299.3 facilitated HLA class 1 presentation

Multiple subcellular locations feed into the HLA class I pathway including cytosol, endoplasmic reticulum and secretory network. Of note, the previously mentioned Cholera toxin B presentation strategy uses the Golgi secretory network.[109,110] This implies that ligands which traffic to multiple subcellular location maybe suitable for use in this CM immunotherapy. However, our data suggests the immunogenic peptide needs to feed into the HLA class 1 presentation pathway to be effective. Case in point, other NSCLC-targeting peptides that bind to and are internalized into H1993 cells did not facilitate presentation (Figure 24a).[86] These peptides accumulate and remain sequestered in a perinuclear compartment; thus intracellular delivery of the antigenic peptide does not necessarily result in presentation of the antigen.

This treatment is designed to elicit a secondary immune response that allows for a more rapid and potentially efficacious immune response against the tumor. However, it also necessitates that the therapy is both HLA type and vaccination status dependent.[97,98] HLA typing is standardized in clinical practice; however, immunogenic peptides that bind to different HLA types will need to be identified. In addition, although ~95% of the United States is vaccinated against measles for many patients that may have been years ago implying the need to quantitate immune response to measles virus for efficacious treatment.[16] Although this treatment is dependent on several variables, it is also modular in nature. Thus, it is feasible to optimize the targeting and/or immunogenic peptide to expand the utility and breadth of this approach. For example, other HLA class I restricted peptides could be encapsulated in the liposome. This treatment is dependent on expression of HLA class 1 which is down regulated in certain cancers. Interestingly, the mathematical models indicate

that as few as 5 HLA molecules can activate an effector T cell.[124] Thus, while down regulation may affect the treatment, complete abrogation of HLA class 1 would be required to completely negate the benefits of this treatment. Complete abrogation of HLA class 1 is a classic activation marker for NK cells which would still result in cancer cell cytotoxicity. Thus, while down regulation of HLA class 1 may affect the efficacy of this treatment it is improbable that it will negate all therapeutic benefit. Future studies to assess the effect of differing levels of HLA class 1 expression will be needed to fully elucidate the effect of HLA class 1 down regulation on treatment with H1299.2 targeted immunoliposomes.

Treatment of vaccinated mice with H1299.3 targeted liposomes containing H250 resulted in a significant reduction in LLC1 subcutaneous tumor growth compared to H1299.3 targeted liposomes lacking H250. This is an aggressive cancer line indicating the strong potential of an efficacious therapy. Increased presence of $CD8^+$ T cells in tumor section and ex vivo activation of CD8+ T cells using APCs from mice treated with H1299.3 targeted liposomes containing H250 implies that this treatment works by generating a cytotoxic T cell response against the LLC1 tumor cells in vivo and is consistent with the in vitro murine and human data presented. Other CM therapies that generate Th1-like responses and increase levels of $CD8^+$ infiltrates have demonstrated efficacy in both animal and human trials.[7,32,46,117] Thus, the therapy presented here potentially achieves similar beneficial immune activation in a safer and cost effective manner compared to current CM therapies.

In conclusion, this study presents a novel cancer immunotherapy based on developing the minimal delivery platform to generate pseudo-infected cancer cells. We demonstrate proof of principle that a targeting liposome containing immunogenic peptide can facilitate

presentation in HLA class 1 molecules, and that this treatment may be efficacious as a novel cancer immunotherapy. It remains to be determined if the anti-cancer effect of this immunotherapy can be augmented with adjuvant chemotherapy.

CHAPTER SIX
Conclusions and Recommendations

Subcellular Targeting Ligands:

Our group and other recognize the importance of subcellular accumulation when utilizing targeting ligands.[66] However, methods that identify these types of ligands are largely absent from the literature. Thus, providing simple methods based on existing protocols such as phage display are crucial to identify the next generation of targeting ligands. Prior to these types of methods, subcellular trafficking of targeting ligands was largely either ignored or relied on large post-hoc studies to identify the subcellular trafficking after the ligand was already identified as a punitive hit based on other properties such as selective internalization into a given subtype of cells.[75,96,120,159] These empiric approaches, while at times effective, require large amount of resources and time to identify a targeting ligand with all the desired properties. The methods outlined in this proposal have the potential to substantially reduce the time and effort required to identify ligands by directly accounting for subcellular trafficking during initial identification of the targeting ligand. In addition the methods presented in this study are widely generalizable to different types of phage display applications such as antibodies or darpin libraries as well as different baits. While we utilized cancer cells as a model for these studies, these types of panning experiments could be performed using a variety of cell types or even whole tissue. In particular the secondary immunofluorescent protocol could be readily applied to whole tissue applications and identify hits that preferentially accumulate in the cells or ECM of tumors for example. Thus,

the methods presented in these studies have the potential to expand the number of targeting ligands available to the field by allowing ease of identification and characterization of the targeting ligand subcellular trafficking patterns during the initial phase of identifying a targeting ligand.

One of the interesting problems related to this particular field is how to employ newly identified subcellular targeting ligands. In our hands, the more complex trafficking ligands also often exhibit lower binding affinity for the target cells (H1299.3 demonstrates ~ 5 fold reduction in internalization compared to H2009.1 at matched concentrations). This implies the ligands may not actually function well in a traditional direct drug conjugate fashion. Instead additional strategies might be required to locate the ligand to the tissue of interest. For example in the immunotherapy study presented in chapter 5, it is probable that the liposome mediates accumulation in the tumor via the EPR effect then once out of circulation H1299.3 mediates internalization and subsequent subcellular trafficking. While a nanoparticle is an obvious way to alter tissue distribution other methods such as coupling together a ligand with high affinity to a tissue specific ligand that is not internalized with a subcellular targeting ligand may allow for tissue accumulation as well as internalization and trafficking to the desired subcellular location. Thus affinity of the subcellular targeting ligand should be accounted for in the end application of each ligand to achieve the optimal delivery of a cargo into a subset of cells in a desired subcellular location.

Use of Ligands in Drug Conjugates

This study is particularly focused on identifying targeting ligands for drug conjugate applications. This is simply because of the high and direct importance of subcellular trafficking plays in development of efficacious drug conjugates.[12,56,83,89] By using targeting ligands identified via the methods presented in this study, drug conjugates could be rationally designed resulting in quicker generation of efficacious drug conjugates. This study is designed to augment the current work on linkers and drug optimization that have dominated the field of drug conjugates.[8,78,83,139] Given the substantial number of liable, traceless linkers presented in the literature we believe that these methods will allow for the rational design of any number of conjugates based on the subcellular trafficking of the targeting ligand. For example, catB cleavable linkers can be used for targeting ligands to lysosomes where as furin linkers could be used with targeting peptides that accumulate in the Golgi.[10,31,66,89,111,120,152,153,161] In addition the subcellular trafficking is defined at or near the time of targeting ligand identification thus allowing ligands to be rapidly moved from identification to efficacy testing without large empirical studies to identify the optimal combination of linker and drug to match with the ligand. Thus, the ligands identified in these studies as well as novel ligands identified via the methods outlined in this manuscript will directly impact the field of direct conjugates.

One of the significant problems with the approach outlined in these studies is the inherent restriction of drug classes suitable for these types of ligands. Essentially ligands developed using the methods outlined in this study are suitable only for two classes of drugs. First, are drugs that have a mechanism of action in the same subcellular location as selected, for example, using geloinin with a Golgi accumulating ligands. Second, membrane

permeable drugs that once the linker is cleaved the drug can diffuse freely through the vesicle membrane and interact with molecular target to induce cytotoxicity. These limitations are primarily due to the lack of vesicle escape properties present in these peptides. The methods outlined in this study can offer precision targeting to an organelle but not necessarily release from said organelle into cytosol. This greatly affects the types of cargo that are suitable for ligands identified using these methods. Future methods that allow for live cell tracking of phage and peptide as outlined in the future directions section of chapter 3 may overcome this barrier in part because we can elucidate which organelles the ligand traffics through to achieve its final point of accumulation as well as offer insights as to how the ligand is removed from the cell. Selecting based on these additional parameters may expand the suitable applications for ligands selected using the methods outlined in this study. For example we currently hypothesize that the immunotherapy presented in chapter 5 functions by recycling of autophagic contents back into the cytosol to achieve HLA class 1 presentation. Thus methods to better define trafficking patterns of targeting ligands in vitro and in vivo may greatly expand the applications for targeting ligands.

Use of Ligands in Delivery Systems

The targeting ligands identified in these studies are also applicable to targeting larger scale delivery systems. Previous work by our group and others demonstrate the ability of peptide targeting ligands to dictate subcellular accumulation patterns of nanoscale delivery vehicles.[14,70,86,122,139] Thus, targeting peptides identified via the methods outlined in this study maybe directly applicable to wide range of vehicles. However, similar to discussion outlined

in the drug conjugate section, the targeting ligand still needs to be paired with the vehicle to achieve optimal function. For example the H1299.3 and H1993.1 peptide are known to accumulate in a low pH compartment and thus maybe directly useful in $CaPO_4$ containing liposomes as low pH is desirable to induce precipitation of the $CaPO_4$ complexes to enhance transfection of siRNA oligos and plasmid DNA in only a subset of cells.[31,67,104,166] Further peptides that accumulate in low pH compartments may be directly useful to pH sensitive polymers that lose structure at low pH resulting in cargo delivery. Finally, low pH accumulating targeting ligands may be directly applicable to endosomal bursting peptides that require low pH to insert into a membrane and form pores, thereby allowing contents of the delivery vehicle access to the cytosol. Thus, knowledge of subcellular trafficking patterns of targeting ligands may be useful in designing certain types of delivery systems. In contrast, utilizing delivery vehicles containing, for example, an non-pH dependent endosomal bursting peptide would be relatively insensitive to subcellular trafficking patterns.[38,72,103,133,158] For this type of delivery vehicle simply identifying peptides that internalize via a receptor-mediated mechanism is potentially sufficient. Thus while certain delivery vehicles may benefit from conjugation of a targeting peptide with defined subcellular trafficking this benefit may not extend to all types of delivery vehicles to the same extent as subcellular trafficking effects drug conjugates.

Immunotherapies based on subcellular localization

The role of subcellular accumulation is still being appreciated in designing immunotherapies. Most current immunotherapies are designed around ex vivo expansion of a patient cells or

treatment with immunomodulating antibodies targeting surface ligands (PD-1 CTLA4 etc).[46,67,107] However, the strategy presented in this study based on subcellular trafficking of a targeting ligands to promote antigen in HLA class I molecules achieves similar results to current immunotherapies in a cost effective manner without ex vivo manipulation of patient material.

The therapy presented in chapter 5 relies on liposomal trafficking into autophagic vesicles to facilitate presentation of antigen. This strategy appears efficacious and outlines a novel use of autophagy to facilitate antigen presentation. Interestingly previous studies demonstrate targeting antigen to the Golgi can also facilitate presentation.[45,94,137,155,156] While these early subcellular studies utilized cholera and shiga toxin that lack the cell specificity necessary to translate them into efficacious therapies, they do demonstrate the value of subcellular trafficking of targeting ligands in facilitating HLA class I presentation. Further studies that identify addition ligands that facilitate HLA class I presentation will solidify the ability of utilizing ligands with defined subcellular trafficking patterns to control antigenicity and modulate immune responses as a novel form of adjuvant.

The novel immunotherapy presented in this study may also be useful in conjunction with current standard of care immunotherapies. Particular it may synergize with immunomodulators and cytokine therapies that while currently successful have only approximately 30% response rate in a patient population. This barrier is currently overcome in the laboratory by combining these treatments with dendritic cell vaccines and CAR-T cell therapies that are extremely expensive and patient specific. Thus, it maybe possible to couple our liposomal therapy with existing, cost effective immunotherapies in order to achieve

higher response rates while maintaining costs at a rate that is affordable across the entire patient population.

Conclusions:

In conclusion, subcellular trafficking of targeting ligands has the potential to modulate the efficacy of a large number of pharmacological applications. In this study we identified two methods to identify ligands that preferentially internalize into cancer cells and accumulate in defined subcellular locations. In addition I demonstrate the efficacy of these protocols by identifying proof of principle targeting peptides that preferentially internalize into NSCLC cells lines and accumulate in lysosomes. We utilize these peptides both in traditional drug conjugate applications as well as a novel immunotherapy to demonstrate the utility of understanding subcellular trafficking patterns to generating efficacious therapies

BIBLIOGRAPHY

1. 't Hoen, P.A.C. *et al.* Phage display screening without repetitious selection rounds. *Anal. Biochem.* 421:622–631, 2012.

2. Abu Ajaj, K., M.L. Biniossek, and F. Kratz. Development of protein-binding bifunctional linkers for a new generation of dual-acting prodrugs. *Bioconjugate Chem.* 20:390–396, 2009.

3. Aguet, F., C.N. Antonescu, M. Mettlen, S.L. Schmid, and G. Danuser. Advances in analysis of low signal-to-noise images link dynamin and AP2 to the functions of an endocytic checkpoint. *Dev. Cell* 26:279–291, 2013.

4. Ames, R.S., T.A. Kost, and J.P. Condreay. BacMam technology and its application to drug discovery. *Expert Opin Drug Discov* 2:1669–1681, 2007.

5. Azzoli, C.G., S. Temin, and G. Giaccone. 2011 Focused Update of 2009 American Society of Clinical Oncology Clinical Practice Guideline Update on Chemotherapy for Stage IV Non-Small-Cell Lung Cancer. *J Oncol Pract* 8:63–66, 2012.

6. Bassindale, A.R., A. Codina-Barrios, N. Frascione, and P.G. Taylor. An improved phage display methodology for inorganic nanoparticle fabrication. *Chem. Commun. (Camb.)* 2956–2958, 2007.

7. Bauzon, M., and T. Hermiston. Armed therapeutic viruses - a disruptive therapy on the horizon of cancer immunotherapy. *Front Immunol* 5:74, 2014.

8. Bernardes, G.J.L., M. Steiner, I. Hartmann, D. Neri, and G. Casi. Site-specific chemical modification of antibody fragments using traceless cleavable linkers. *Nat Protoc* 8:2079–2089, 2013.

9. Berstad, M.B. *et al.* Design of an EGFR-targeting toxin for photochemical delivery: in vitro and in vivo selectivity and efficacy. *Oncogene*, 2015.

10. Biswas, A. *et al.* Endoprotease-mediated intracellular protein delivery using nanocapsules. *ACS Nano* 5:1385–1394, 2011.

11. Biswas, S., and V.P. Torchilin. Nanopreparations for Organelle-Specific Delivery in Cancer. *Adv. Drug Deliv. Rev.*, 2013.

12. Bolte, S., and F.P. Cordelières. A guided tour into subcellular colocalization analysis in light microscopy. *J Microsc* 224:213–232, 2006.

13. Boyce, F.M., and N.L. Bucher. Baculovirus-mediated gene transfer into mammalian

cells. *Proc. Natl. Acad. Sci. U.S.A.* 93:2348–2352, 1996.

14. Brown, K.C. Peptidic tumor targeting agents: the road from phage display peptide selections to clinical applications. *Curr. Pharm. Des.* 16:1040–1054, 2010.

15. Carnemolla, B. *et al.* Enhancement of the antitumor properties of interleukin-2 by its targeted delivery to the tumor blood vessel extracellular matrix. *Blood* 99:1659–1665, 2002.

16. Centers for Disease Control and Prevention (CDC). Vaccination coverage among children in kindergarten--United States, 2011-12 school year. *MMWR Morb. Mortal. Wkly. Rep.* 61:647–652, 2012.

17. Chaudhary, N. *et al.* Endocytic crosstalk: cavins, caveolins, and caveolae regulate clathrin-independent endocytosis. *PLoS Biol.* 12:e1001832, 2014.

18. Chen, Q.-X., W.-P. Wang, S. Zeng, S. Urayama, and A.-M. Yu. A general approach to high-yield biosynthesis of chimeric RNAs bearing various types of functional small RNAs for broad applications. *Nucleic Acids Res.* 43:3857–3869, 2015.

19. Chen, X., J.L. Zaro, and W.-C. Shen. Fusion protein linkers: property, design and functionality. *Adv. Drug Deliv. Rev.* 65:1357–1369, 2013.

20. Chiocca, E.A., and S.D. Rabkin. Oncolytic viruses and their application to cancer immunotherapy. *Cancer Immunol Res* 2:295–300, 2014.

21. Chung, C.-Y., S.V. Madhunapantula, D. Desai, S. Amin, and G.P. Robertson. Melanoma prevention using topical PBISe. *Cancer Prev Res (Phila)* 4:935–948, 2011.

22. Conrad, U., and J. Scheller. Considerations on antibody-phage display methodology. *Comb. Chem. High Throughput Screen.* 8:117–126, 2005.

23. Crotzer, V.L., and J.S. Blum. Autophagy and its role in MHC-mediated antigen presentation. *J. Immunol.* 182:3335–3341, 2009.

24. Cwirla, S.E., E.A. Peters, R.W. Barrett, and W.J. Dower. Peptides on phage: a vast library of peptides for identifying ligands. *Proc. Natl. Acad. Sci. U.S.A.* 87:6378–6382, 1990.

25. D'Arcangelo, M., and F.R. Hirsch. Clinical and comparative utility of afatinib in non-small cell lung cancer. *Biologics* 8:183–192, 2014.

26. Dal Corso, A., L. Pignataro, L. Belvisi, and C. Gennari. αvβ3 Integrin-Targeted Peptide/Peptidomimetic-Drug Conjugates: In-Depth Analysis of the Linker Technology. *Curr Top Med Chem*, 2015.

27. Dass, C.R. Drug delivery in cancer using liposomes. *Methods Mol. Biol.* 437:177–182, 2008.

28. Derda, R., S.K.Y. Tang, S.C. Li, S. Ng, W. Matochko, and M.R. Jafari. Diversity of phage-displayed libraries of peptides during panning and amplification. *Molecules* 16:1776–1803, 2011.

29. Dominska, M., and D.M. Dykxhoorn. Breaking down the barriers: siRNA delivery and endosome escape. *J. Cell. Sci.* 123:1183–1189, 2010.

30. Dorywalska, M. *et al.* Effect of attachment site on stability of cleavable antibody drug conjugates. *Bioconjugate Chem.* 26:650–659, 2015.

31. Dubowchik, G.M. *et al.* Cathepsin B-labile dipeptide linkers for lysosomal release of doxorubicin from internalizing immunoconjugates: model studies of enzymatic drug release and antigen-specific in vitro anticancer activity. *Bioconjugate Chem.* 13:855–869, 2002.

32. Dudley, M.E. *et al.* Cancer regression and autoimmunity in patients after clonal repopulation with antitumor lymphocytes. *Science* 298:850–854, 2002.

33. Ellington, A.D., and J.W. Szostak. In vitro selection of RNA molecules that bind specific ligands. *Nature* 346:818–822, 1990.

34. Erickson, H.K. *et al.* Tumor delivery and in vivo processing of disulfide-linked and thioether-linked antibody-maytansinoid conjugates. *Bioconjugate Chem.* 21:84–92, 2010.

35. Famulok, M., and G. Mayer. Aptamers and SELEX in Chemistry & Biology. *Chem. Biol.* 21:1055–1058, 2014.

36. Feldman, J.P., R. Goldwasser, and S. Mark. A mathematical model for tumor volume evaluation using two-dimensions. *J Appl Quant …*, 2009.

37. Fernandez-Viña, M.A., M. Falco, Y. Sun, and P. Stastny. DNA typing for HLA class I alleles: I. Subsets of HLA-A2 and of -A28. *Hum. Immunol.* 33:163–173, 1992.

38. Flygare, J.A., T.H. Pillow, and P. Aristoff. Antibody-drug conjugates for the treatment of cancer. *Chem Biol Drug Des* 81:113–121, 2013.

39. Gray, B.P., and K.C. Brown. Combinatorial peptide libraries: mining for cell-binding peptides. *Chem. Rev.* 114:1020–1081, 2014.

40. Gray, B.P., M.J. McGuire, and K.C. Brown. A liposomal drug platform overrides peptide ligand targeting to a cancer biomarker, irrespective of ligand affinity or density. *PLoS ONE* 8:e72938, 2013.

41. Gray, B.P., S. Li, and K.C. Brown. From phage display to nanoparticle delivery: functionalizing liposomes with multivalent peptides improves targeting to a cancer biomarker. *Bioconjugate Chem.* 24:85–96, 2013.

42. Guillerme, J.-B. *et al.* Measles virus vaccine-infected tumor cells induce tumor antigen cross-presentation by human plasmacytoid dendritic cells. *Clin. Cancer Res.* 19:1147–1158, 2013.

43. Guo, P. RNA nanotechnology: engineering, assembly and applications in detection, gene delivery and therapy. *J Nanosci Nanotechnol* 5:1964–1982, 2005.

44. Gutbrodt, K.L. *et al.* Antibody-based delivery of interleukin-2 to neovasculature has potent activity against acute myeloid leukemia. *Sci Transl Med* 5:201ra118, 2013.

45. Haicheur, N. *et al.* The B subunit of Shiga toxin fused to a tumor antigen elicits CTL and targets dendritic cells to allow MHC class I-restricted presentation of peptides derived from exogenous antigens. *J. Immunol.* 165:3301–3308, 2000.

46. Hamid, O. *et al.* Safety and tumor responses with lambrolizumab (anti-PD-1) in melanoma. *N. Engl. J. Med.* 369:134–144, 2013.

47. Hammers, C.M., and J.R. Stanley. Antibody phage display: technique and applications. *J. Invest. Dermatol.* 134:e17, 2014.

48. Henriksen, L., M.V. Grandal, S.L.J. Knudsen, B. van Deurs, and L.M. Grøvdal. Internalization mechanisms of the epidermal growth factor receptor after activation with different ligands. *PLoS ONE* 8:e58148, 2013.

49. Hu, C.-T., J.-R. Wu, and W.-S. Wu. The role of endosomal signaling triggered by metastatic growth factors in tumor progression. *Cell. Signal.* 25:1539–1545, 2013.

50. Hu, Q. *et al.* Intracellular pathways and nuclear localization signal peptide-mediated gene transfection by cationic polymeric nanovectors. *Biomaterials* 33:1135–1145, 2012.

51. Ivanov, A.I. Pharmacological inhibition of endocytic pathways: is it specific enough to be useful? *Methods Mol. Biol.* 440:15–33, 2008.

52. Ivanov, A.V. *et al.* Development of the system ensuring a high-level expression of hepatitis C virus nonstructural NS5B and NS5A proteins. *Protein Expr. Purif.* 48:14–23, 2006.

53. Jensen, K.B., and P. Kristensen. Isolation of recombinant phage-displayed antibodies recognizing skin keratinocytes. *Methods Mol. Biol.* 289:359–370, 2005.

54. Johannes, L., and W. Römer. Shiga toxins--from cell biology to biomedical applications. *Nat. Rev. Microbiol.* 8:105–116, 2010.

55. Junutula, J.R. *et al.* Site-specific conjugation of a cytotoxic drug to an antibody improves the therapeutic index. *Nat. Biotechnol.* 26:925–932, 2008.

56. Khalil, I.A., K. Kogure, H. Akita, and H. Harashima. Uptake pathways and subsequent intracellular trafficking in nonviral gene delivery. *Pharmacol. Rev.* 58:32–45, 2006.

57. Kim, Y. *et al.* Targeting heat shock proteins on cancer cells: selection, characterization, and cell-penetrating properties of a peptidic GRP78 ligand. *Biochemistry* 45:9434–9444, 2006.

58. Kirienko, N.V., K.A. Lepikhov, L.A. Zheleznaya, and N.I. Matvienko. Significance of codon usage and irregularities of rare codon distribution in genes for expression of BspLU11III methyltransferases. *Biochemistry Mosc.* 69:527–535, 2004.

59. Klionsky, D.J. Autophagy: from phenomenology to molecular understanding in less than a decade. *Nat. Rev. Mol. Cell Biol.*, 2007.

60. Klussman, K., B.J. Mixan, C.G. Cerveny, D.L. Meyer, P.D. Senter, and A.F. Wahl. Secondary mAb--vcMMAE conjugates are highly sensitive reporters of antibody internalization via the lysosome pathway. *Bioconjugate Chem.* 15:765–773, 2004.

61. Kornberger, P., and A. Skerra. Sortase-catalyzed in vitro functionalization of a HER2-specific recombinant Fab for tumor targeting of the plant cytotoxin gelonin. *MAbs* 6:354–366, 2014.

62. Krumpe, L.R.H., K.M. Schumacher, J.B. McMahon, L. Makowski, and T. Mori. Trinucleotide cassettes increase diversity of T7 phage-displayed peptide library. *BMC Biotechnol.* 7:65, 2007.

63. Kuzmicheva, G.A., P.K. Jayanna, I.B. Sorokulova, and V.A. Petrenko. Diversity and censoring of landscape phage libraries. *Protein Eng. Des. Sel.* 22:9–18, 2009.

64. Lackey, C.A., O.W. Press, A.S. Hoffman, and P.S. Stayton. A biomimetic pH-responsive polymer directs endosomal release and intracellular delivery of an endocytosed antibody complex. *Bioconjugate Chem.* 13:996–1001, 2002.

65. Lajunen, T. *et al.* Light induced cytosolic drug delivery from liposomes with gold nanoparticles. *J Control Release* 203C:85–98, 2015.

66. Lambert, J.M. Antibody-Drug Conjugates (ADCs): Magic Bullets at Last! *Mol. Pharm.* 12:1701–1702, 2015.

67. Lee, J.-H., K. Na, S.-C. Song, J. Lee, and H.-J. Kuh. The distribution and retention of paclitaxel and doxorubicin in multicellular layer cultures. *Oncol. Rep.* 27:995–1002,

2012.

68. Lee, R.S. *et al.* Major histocompatibility complex class I presentation of exogenous soluble tumor antigen fused to the B-fragment of Shiga toxin. *Eur. J. Immunol.* 28:2726–2737, 1998.

69. Leriche, G. *et al.* Spiro Diorthoester (SpiDo), a Human Plasma Stable Acid-Sensitive Cleavable Linker for Lysosomal Release. *Bioconjugate Chem.*, 2015.

70. Li, D. *et al.* DCDT2980S, an anti-CD22-monomethyl auristatin E antibody-drug conjugate, is a potential treatment for non-Hodgkin lymphoma. *Mol Cancer Ther* 12:1255–1265, 2013.

71. Li, S. *et al.* Synthesis and characterization of a high-affinity {alpha}v{beta}6-specific ligand for in vitro and in vivo applications. *Mol Cancer Ther* 8:1239–1249, 2009.

72. Li, S., B.P. Gray, M.J. McGuire, and K.C. Brown. Synthesis and biological evaluation of a peptide-paclitaxel conjugate which targets the integrin $\alpha v\beta_6$. *Bioorg. Med. Chem.* 19:5480–5489, 2011.

73. Li, X. *et al.* Site-Specific Dual Antibody Conjugation via Engineered Cysteine and Selenocysteine Residues. *Bioconjugate Chem.*, 2015.

74. Lindner, T., H. Kolmar, U. Haberkorn, and W. Mier. DNA libraries for the construction of phage libraries: statistical and structural requirements and synthetic methods. *Molecules* 16:1625–1641, 2011.

75. Liu, Y., S.C.J. Steiniger, Y. Kim, G.F. Kaufmann, B. Felding-Habermann, and K.D. Janda. Mechanistic studies of a peptidic GRP78 ligand for cancer cell-specific drug delivery. *Mol. Pharm.* 4:435–447, 2007.

76. Lu, Y., and P.S. Low. Folate targeting of haptens to cancer cell surfaces mediates immunotherapy of syngeneic murine tumors. *Cancer Immunol. Immunother.* 51:153–162, 2002.

77. Lyu, M.-A., Y.J. Cao, K.A. Mohamedali, and M.G. Rosenblum. Cell-targeting fusion constructs containing recombinant gelonin. *Meth. Enzymol.* 502:167–214, 2012.

78. Maier, K., and E. Wagner. Acid-labile traceless click linker for protein transduction. *J. Am. Chem. Soc.* 134:10169–10173, 2012.

79. Matochko, W.L., S. Cory Li, S.K.Y. Tang, and R. Derda. Prospective identification of parasitic sequences in phage display screens. *Nucleic Acids Res.* 42:1784–1798, 2014.

80. Matochko, W.L., S. Ng, M.R. Jafari, J. Romaniuk, S.K.Y. Tang, and R. Derda.

Uniform amplification of phage display libraries in monodisperse emulsions. *Methods* 58:18–27, 2012.

81. Mayor, S., R.G. Parton, and J.G. Donaldson. Clathrin-Independent Pathways of Endocytosis. *Cold Spring Harb Perspect Biol* 6, 2014.

82. Mårlind, J. *et al.* Antibody-mediated delivery of interleukin-2 to the stroma of breast cancer strongly enhances the potency of chemotherapy. *Clin. Cancer Res.* 14:6515–6524, 2008.

83. McCombs, J.R., and S.C. Owen. Antibody drug conjugates: design and selection of linker, payload and conjugation chemistry. *AAPS J* 17:339–351, 2015.

84. McConnell, S.J., A.J. Uveges, and D.G. Spinella. Comparison of plate versus liquid amplification of M13 phage display libraries. *Biotech.* 18:803–4– 806, 1995.

85. McEnaney, P.J., C.G. Parker, A.X. Zhang, and D.A. Spiegel. Antibody-recruiting molecules: an emerging paradigm for engaging immune function in treating human disease. *ACS Chem. Biol.* 7:1139–1151, 2012.

86. McGuire, M.J. *et al.* Identification and characterization of a suite of tumor targeting peptides for non-small cell lung cancer. *Sci Rep* 4:4480, 2014.

87. McGuire, M.J., S. Li, and K.C. Brown. Biopanning of phage displayed peptide libraries for the isolation of cell-specific ligands. *Methods Mol. Biol.* 504:291–321, 2009.

88. Mellman, I., G. Coukos, and G. Dranoff. Cancer immunotherapy comes of age. *Nature* 480:480–489, 2011.

89. Merten, H., F. Brandl, A. Plückthun, and U. Zangemeister-Wittke. Antibody-Drug Conjugates for Tumor Targeting-Novel Conjugation Chemistries and the Promise of non-IgG Binding Proteins. *Bioconjugate Chem.*, 2015.

90. Minami, T. *et al.* HER2 as Therapeutic Target for Overcoming ATP-binding Cassette Transporter-Mediated Chemoresistance in Small Cell Lung Cancer. *Mol Cancer Ther*, 2012.

91. Motley, A., N.A. Bright, M.N.J. Seaman, and M.S. Robinson. Clathrin-mediated endocytosis in AP-2-depleted cells. *J. Cell Biol.* 162:909–918, 2003.

92. Ni, M., Y. Zhang, and A.S. Lee. Beyond the endoplasmic reticulum: atypical GRP78 in cell viability, signalling and therapeutic targeting. *Biochem. J.* 434:181–188, 2011.

93. Nixon, R.A. The role of autophagy in neurodegenerative disease. *Nature medicine*, 2013.

94. Noakes, K.L., H.T. Teisserenc, J.M. Lord, P.R. Dunbar, V. Cerundolo, and L.M. Roberts. Exploiting retrograde transport of Shiga-like toxin 1 for the delivery of exogenous antigens into the MHC class I presentation pathway. *FEBS Lett.* 453:95–99, 1999.

95. Noren, K.A., and C.J. Noren. Construction of high-complexity combinatorial phage display peptide libraries. *Methods* 23:169–178, 2001.

96. Okeley, N.M., S.C. Alley, and P.D. Senter. Advancing antibody drug conjugation: from the laboratory to a clinically approved anticancer drug. *Hematol. Oncol. Clin. North Am.* 28:13–25, 2014.

97. Ota, M.O. *et al.* Hemagglutinin protein is a primary target of the measles virus-specific HLA-A2-restricted CD8+ T cell response during measles and after vaccination. *J. Infect. Dis.* 195:1799–1807, 2007.

98. Ovsyannikova, I.G., K.L. Johnson, H.R. Bergen, and G.A. Poland. Mass spectrometry and peptide-based vaccine development. *Clin. Pharmacol. Ther.* 82:644–652, 2007.

99. Oyama, T., K.F. Sykes, K.N. Samli, J.D. Minna, S.A. Johnston, and K.C. Brown. Isolation of lung tumor specific peptides from a random peptide library: generation of diagnostic and cell-targeting reagents. *Cancer Lett.* 202:219–230, 2003.

100. Pansri, P., N. Jaruseranee, K. Rangnoi, P. Kristensen, and M. Yamabhai. A compact phage display human scFv library for selection of antibodies to a wide variety of antigens. *BMC Biotechnol.* 9:6, 2009.

101. Patterson, N.L., and J.D. Mintern. Intersection of autophagy with pathways of antigen presentation. *Protein Cell* 3:911–920, 2012.

102. Pini, A. *et al.* Design and use of a phage display library. Human antibodies with subnanomolar affinity against a marker of angiogenesis eluted from a two-dimensional gel. *J. Biol. Chem.* 273:21769–21776, 1998.

103. Pirie, C.M., D.V. Liu, and K.D. Wittrup. Targeted cytolysins synergistically potentiate cytoplasmic delivery of gelonin immunotoxin. *Mol Cancer Ther* 12:1774–1782, 2013.

104. Ramishetti, S., and L. Huang. Intelligent design of multifunctional lipid-coated nanoparticle platforms for cancer therapy. *Ther Deliv* 3:1429–1445, 2012.

105. Rangel, R. *et al.* Combinatorial targeting and discovery of ligand-receptors in organelles of mammalian cells. *Nat Commun* 3:788, 2012.

106. Rangel, R. *et al.* Targeting mammalian organelles with internalizing phage (iPhage)

libraries. *Nat Protoc* 8:1916–1939, 2013.

107. Rao N, V., S.R. Mane, A. Kishore, J. Das Sarma, and R. Shunmugam. Norbornene derived doxorubicin copolymers as drug carriers with pH responsive hydrazone linker. *Biomacromolecules* 13:221–230, 2012.

108. Rejman, J., V. Oberle, I.S. Zuhorn, and D. Hoekstra. Size-dependent internalization of particles via the pathways of clathrin- and caveolae-mediated endocytosis. *Biochem. J.* 377:159–169, 2004.

109. Sandvig, K., and B. van Deurs. Membrane traffic exploited by protein toxins. *Annu. Rev. Cell Dev. Biol.* 18:1–24, 2002.

110. Sandvig, K., B. Spilsberg, S.U. Lauvrak, M.L. Torgersen, T.-G. Iversen, and B. van Deurs. Pathways followed by protein toxins into cells. *Int. J. Med. Microbiol.* 293:483–490, 2004.

111. Sassoon, I., and V. Blanc. Antibody-drug conjugate (ADC) clinical pipeline: a review. *Methods Mol. Biol.* 1045:1–27, 2013.

112. Satsangi, A., S.S. Roy, R.K. Satsangi, R.K. Vadlamudi, and J.L. Ong. Design of a paclitaxel prodrug conjugate for active targeting of an enzyme upregulated in breast cancer cells. *Mol. Pharm.* 11:1906–1918, 2014.

113. Schneider, E.L., L. Robinson, R. Reid, G.W. Ashley, and D.V. Santi. β-Eliminative releasable linkers adapted for bioconjugation of macromolecules to phenols. *Bioconjugate Chem.* 24:1990–1997, 2013.

114. Schwendener, R.A., B. Ludewig, A. Cerny, and O. Engler. Liposome-based vaccines. *Methods Mol. Biol.* 605:163–175, 2010.

115. Shah, J.K., H.R. Garner, M.A. White, D.S. Shames, and J.D. Minna. sIR: siRNA Information Resource, a web-based tool for siRNA sequence design and analysis and an open access siRNA database. *BMC Bioinformatics* 8:178, 2007.

116. Shahsavarian, M.A. *et al.* Exploitation of rolling circle amplification for the construction of large phage-display antibody libraries. *J. Immunol. Methods* 407:26–34, 2014.

117. Shiao, S.L., A.P. Ganesan, H.S. Rugo, and L.M. Coussens. Immune microenvironments in solid tumors: new targets for therapy. *Genes & Development* 25:2559–2572, 2011.

118. Shin, M.C. *et al.* Combination of antibody targeting and PTD-mediated intracellular toxin delivery for colorectal cancer therapy. *J Control Release* 194:197–210, 2014.

119. Shin, M.C. *et al.* Recombinant TAT-gelonin fusion toxin: synthesis and characterization of heparin/protamine-regulated cell transduction. *J Biomed Mater Res A* 103:409–419, 2015.

120. Sievers, E.L., and P.D. Senter. Antibody-drug conjugates in cancer therapy. *Annu. Rev. Med.* 64:15–29, 2013.

121. Singh, A.N. *et al.* Dimerization of a Phage-Display Selected Peptide for Imaging of αvβ6- Integrin: Two Approaches to the Multivalent Effect. *Theranostics* 4:745–760, 2014.

122. Singh, R., and H.K. Erickson. Antibody-cytotoxic agent conjugates: preparation and characterization. *Methods Mol. Biol.* 525:445–67– xiv, 2009.

123. Singh, R.D., V. Puri, J.T. Valiyaveettil, D.L. Marks, R. Bittman, and R.E. Pagano. Selective caveolin-1-dependent endocytosis of glycosphingolipids. *Mol. Biol. Cell* 14:3254–3265, 2003.

124. Singleton, K.L. *et al.* Itk controls the spatiotemporal organization of T cell activation. *Sci Signal* 4:ra66, 2011.

125. Smith, G.P., and J.K. Scott. Libraries of peptides and proteins displayed on filamentous phage. *Meth. Enzymol.*, 1992.

126. Smith, G.P., and V.A. Petrenko. Phage Display. *Chem. Rev.* American Chemical Society, 97:391–410, 1997.

127. Stefan, N., P. Martin-Killias, S. Wyss-Stoeckle, A. Honegger, U. Zangemeister-Wittke, and A. Plückthun. DARPins recognizing the tumor-associated antigen EpCAM selected by phage and ribosome display and engineered for multivalency. *J. Mol. Biol.* 413:826–843, 2011.

128. Steiner, D., P. Forrer, and A. Plückthun. Efficient selection of DARPins with sub-nanomolar affinities using SRP phage display. *J. Mol. Biol.* 382:1211–1227, 2008.

129. Stinchcombe, T.E., and M.A. Socinski. Considerations for second-line therapy of non-small cell lung cancer. *Oncologist* 13 Suppl 1:28–36, 2008.

130. Stoltenburg, R., C. Reinemann, and B. Strehlitz. SELEX--a (r)evolutionary method to generate high-affinity nucleic acid ligands. *Biomol. Eng.* 24:381–403, 2007.

131. Stoneham, C.A., M. Hollinshead, and A. Hajitou. Clathrin-mediated endocytosis and subsequent endo-lysosomal trafficking of adeno-associated virus/phage. *J. Biol. Chem.* 287:35849–35859, 2012.

132. Su, X., N. Yang, K.D. Wittrup, and D.J. Irvine. Synergistic antitumor activity from

two-stage delivery of targeted toxins and endosome-disrupting nanoparticles. *Biomacromolecules* 14:1093–1102, 2013.

133. Suzawa, T. *et al.* Enhanced tumor cell selectivity of adriamycin-monoclonal antibody conjugate via a poly(ethylene glycol)-based cleavable linker. *J Control Release* 79:229–242, 2002.

134. Suzuki, R., and K. Maruyama. Effective in vitro and in vivo gene delivery by the combination of liposomal bubbles (bubble liposomes) and ultrasound exposure. *Methods Mol. Biol.* 605:473–486, 2010.

135. Suzuki, R., T. Takizawa, Y. Negishi, N. Utoguchi, and K. Maruyama. Effective gene delivery with liposomal bubbles and ultrasound as novel non-viral system. *J Drug Target* 15:531–537, 2007.

136. Sørensen, M.D., I.E. Agerholm, B. Christensen, S. Kølvraa, and P. Kristensen. Microselection--affinity selecting antibodies against a single rare cell in a heterogeneous population. *J. Cell. Mol. Med.* 14:1953–1961, 2010.

137. Tan, W., M.J. Donovan, and J. Jiang. Aptamers from cell-based selection for bioanalytical applications. *Chem. Rev.* 113:2842–2862, 2013.

138. Taurin, S., H. Nehoff, and K. Greish. Anticancer nanomedicine and tumor vascular permeability; Where is the missing link? *J Control Release* 164:265–275, 2012.

139. Tian, F. *et al.* A general approach to site-specific antibody drug conjugates. *Proc. Natl. Acad. Sci. U.S.A.* 111:1766–1771, 2014.

140. Torchilin, V.P. Lipid-core micelles for targeted drug delivery. *Curr Drug Deliv* 2:319–327, 2005.

141. Tuerk, C., and L. Gold. Systematic evolution of ligands by exponential enrichment: RNA ligands to bacteriophage T4 DNA polymerase. *Science* 249:505–510, 1990.

142. Tuller, T., Y.Y. Waldman, M. Kupiec, and E. Ruppin. Translation efficiency is determined by both codon bias and folding energy. *Proc. Natl. Acad. Sci. U.S.A.* 107:3645–3650, 2010.

143. Umlauf, B.J., J.S. Mercedes, C.-Y. Chung, and K.C. Brown. Identification of a novel lysosomal trafficking peptide using phage display biopanning coupled with endocytic selection pressure. *Bioconjugate Chem.* 25:1829–1837, 2014.

144. Umlauf, B.J., J.S. Mercedes, C.-Y. Chung, and K.C. Brown. Identification of a Novel Lysosomal Trafficking Peptide using Phage Display Biopanning Coupled with Endocytic Selection Pressure. *Bioconjugate Chem.*

145. Umlauf, B.J., M.J. McGuire, and K.C. Brown. Introduction of plasmid encoding for rare tRNAs reduces amplification bias in phage display biopanning. *Biotech.* 58:81–84, 2015.

146. Umlauf, B.J., N.A. Pinsky, I.G. Ovsyannikova, and G.A. Poland. Detection of vaccinia virus-specific IFNγ and IL-10 secretion from human PBMCs and $CD8^+$ T cells by ELISPOT. *Methods Mol. Biol.* 792:199–218, 2012.

147. Un, K., K. Sakai-Kato, Y. Oshima, T. Kawanishi, and H. Okuda. Intracellular trafficking mechanism, from intracellular uptake to extracellular efflux, for phospholipid/cholesterol liposomes. *Biomaterials*, 2012.

148. van Endert, P.M. Peptide selection for presentation by HLA class I: a role for the human transporter associated with antigen processing? *Immunol. Res.* 15:265–279, 1996.

149. Varkouhi, A.K., M. Scholte, G. Storm, and H.J. Haisma. Endosomal escape pathways for delivery of biologicals. *J Control Release* 151:220–228, 2011.

150. Vitale, M., C. Cantoni, G. Pietra, M.C. Mingari, and L. Moretta. Effect of tumor cells and tumor microenvironment on NK-cell function. *Eur. J. Immunol.* 44:1582–1592, 2014.

151. Watanabe, R., K. Asakura, M. Rodriguez, and R.E. Pagano. Internalization and sorting of plasma membrane sphingolipid analogues in differentiating oligodendrocytes. *J. Neurochem.* 73:1375–1383, 1999.

152. Weldon, J.E. *et al.* A recombinant immunotoxin against the tumor-associated antigen mesothelin reengineered for high activity, low off-target toxicity, and reduced antigenicity. *Mol Cancer Ther* 12:48–57, 2013.

153. Weldon, J.E. *et al.* Designing the Furin-Cleavable Linker in Recombinant Immunotoxins Based on Pseudomonas Exotoxin A. *Bioconjugate Chem.* 26:1120–1128, 2015.

154. Winter, G., A.D. Griffiths, R.E. Hawkins, and H.R. Hoogenboom. Making antibodies by phage display technology. *Annu. Rev. Immunol.* 12:433–455, 1994.

155. Wu, X., J. Chen, M. Wu, and J.X. Zhao. Aptamers: active targeting ligands for cancer diagnosis and therapy. *Theranostics* 5:322–344, 2015.

156. Xiang, D. *et al.* Nucleic acid aptamer-guided cancer therapeutics and diagnostics: the next generation of cancer medicine. *Theranostics* 5:23–42, 2015.

157. Xu, S. Internalization, Trafficking, Intracellular Processing and Actions of Antibody-Drug Conjugates. *Pharm. Res.*, 2015.

158. Yang, N.J., D.V. Liu, D. Sklaviadis, D.Y. Gui, M.G. Vander Heiden, and K.D. Wittrup. Antibody-mediated neutralization of perfringolysin o for intracellular protein delivery. *Mol. Pharm.* 12:1992–2000, 2015.

159. Yoneda, Y. *et al.* A cell-penetrating peptidic GRP78 ligand for tumor cell-specific prodrug therapy. *Bioorg. Med. Chem. Lett.* 18:1632–1636, 2008.

160. Yu, Y.J. *et al.* Boosting brain uptake of a therapeutic antibody by reducing its affinity for a transcytosis target. *Sci Transl Med* 3:84ra44, 2011.

161. Yuan, X., X. Lin, G. Manorek, and S.B. Howell. Challenges associated with the targeted delivery of gelonin to claudin-expressing cancer cells with the use of activatable cell penetrating peptides to enhance potency. *BMC Cancer* 11:61, 2011.

162. Zacher, A.N., III, C.A. Stock, J.W. Golden II, and G.P. Smith. A new filamentous phage cloning vector: fd-tet. *Gene*, 1980.

163. Zeman, S.M., D.R. Phillips, and D.M. Crothers. Characterization of covalent adriamycin-DNA adducts. *Proc. Natl. Acad. Sci. U.S.A.* 95:11561–11565, 1998.

164. Zhang, J., H. Spring, and M. Schwab. Neuroblastoma tumor cell-binding peptides identified through random peptide phage display. *Cancer Lett.* 171:153–164, 2001.

165. Zhang, W.Y., W. Zhang, Z. Liu, C. Li, Z. Zhu, and C.J. Yang. Highly parallel single-molecule amplification approach based on agarose droplet polymerase chain reaction for efficient and cost-effective aptamer selection. *Anal. Chem.* 84:350–355, 2012.

166. Zhong, Y.-J., L.-H. Shao, and Y. Li. Cathepsin B-cleavable doxorubicin prodrugs for targeted cancer therapy (Review). *Int. J. Oncol.* 42:373–383, 2013.

167. Zhu, G., G. Niu, and X. Chen. Aptamer-Drug Conjugates. *Bioconjugate Chem.*, 2015.